DELFT UNIVERSITY OF TECHNOLOGY

MASTER'S THESIS

RECALCITRANT COMPOUNDS FROM THERMALLY HYDROLYSED SEWAGE SLUDGE

Author:
Zhouyuan WANG

Thesis committee:
Prof. Merle DE KREUK
Prof. Wiebren DE JONG
Ir. Javier PAVEZ JARA

External supervisors:
Dr. Jan PELS
Dr. Rian VISSER

A thesis submitted in partial fulfillment of the requirements for the degree of Master of Science

in the

Faculty of Civil Engineering and Geosciences

June 23, 2022

Abstract

Thermal hydrolysis (TH) has been widely applied to sewage sludge treatment to improve downstream anaerobic digestion (AD) by enhancing organic solids hydrolysis and subsequent biogas productivity. However, TH also has several drawbacks, including the formation of recalcitrant compounds, which are anaerobically non-biodegradable and even inhibitory to the downstream AD. Melanoidins produced from the Maillard reaction have been regarded as a representative of such compounds. Theoretically, the production of melanoidins increases with increasing TH temperature.

This study collaborated with TORWASH®, a patented TH technology developed by TNO, aiming to characterise the recalcitrant compounds derived under TORWASH® conditions from 180 - 210 °C. In addition, we investigated the effects of anaerobic pre-digestion on the TH performance, attempting to increase the biogas productivity of digestate. Moreover, we also sought pretreatment methods that could mitigate the production of recalcitrant compounds. By reviewing the studies of Zhang et al. (2020) and other researchers in this field, we found that acidic pretreatments could be the solution. Then, we assumed that the addition of acetic acid and CO_2 gas could limit the progression of the Maillard reaction. A laboratory simulation of the TH process was performed on waste activated sludge (WAS) at 180 - 200 °C and anaerobically pre-digested WAS at 180 - 210 °C. The following TH tests with acidic pretreatments were only conducted on WAS at 190 °C.

We found that the production of recalcitrant compounds (soluble humic substances) increased with increasing reaction temperature, corresponding to increased UVA_{254} and colour formation. Proteins were primarily hydrolysed or denatured during TH, and competition for carbohydrates between the Maillard and caramelisation reactions could occur at 190 °C and above. In addition, TH disintegrated high molecular weight DOM > 1 kDa into low molecular weight DOM < 0.1 kDa, and stronger sludge disintegration occurred at higher reaction temperatures. Moreover, BMP decreased after anaerobic pre-digestion but increased after TH treatment. The liquid fraction of pre-digested WAS could reach an equivalent degree of anaerobic biodegradability as that of WAS when applying a higher reaction temperature.

All acidic pretreatments applied decreased the production of soluble humic substances by 10 %, corresponding to a 13 % decrease in UVA_{254}. CO_2 pressurisation at 10 bar could effectively reduce the formation of fulvic-acid like and humic-acid like matter, compared with the untreated sample. The effect of 20 bar CO_2 was less pronounced than that of 10 bar CO_2, whether or not the samples were pre-added with HAc.

Acknowledgements

I would like to express my deepest appreciation to my thesis committee chair, Professor Merle de Kreuk, who offered me the chance to work on this project. I appreciate her insightful knowledge and valuable guidance on my thesis. I am very grateful that she provided me with enough freedom and a great platform to conduct such incredible research.

I also wish to thank my daily supervisor Javier Pavez Jara. Thank you for always helping me with every problem I encountered during my thesis. He has always been positive, supportive, and encouraging to me, providing suggestions on the experimental design and data analysis. He taught me his valuable experimental skills, which will benefit me in my future study. Without him, it is impossible for this project to reach such a stage.

I would like to express my genuine appreciation to Dr. Jan Pels for offering me the internship at TNO. He provided me with samples for analysis and collected raw samples with me in person. He unconditionally supported me throughout the entire project. It was a great honour to work with such a professional and experienced person.

Besides, I also wish to thank Professor Wiebren de Jong and Dr. Rian Visser for their valuable suggestions to improve my project and report. I also would like to thank the entire WaterLab group for all the help they provided during my project.

In the end, I thank my friend Connie Au and neighbour Xiao Xiu for their company and support during the COVID-19 pandemic. I also express my gratitude and love to my family for their unconditional support and encouragement.

Zhouyuan Wang
Delft, The Netherlands
June 23, 2022

Contents

List of Figures

List of Tables

List of Abbreviations

AD	Anaerobic digestion
ANOVA	Analysis of variance
ARP	Amadori rearrangement products
BIX	Biological index
BMP	Biomethane potential
BOD	Biochemical oxygen demand
BSA	Bovine serum albumin
COD	Chemical oxygen demand
DCOS	Dissolved carbon oxidation state
DOC	Dissolved organic carbon
DOM	Dissolved organic matter
EEM	Excitation emission matrix
Em	Emission
EPS	Extracellular polymeric substances
Ex	Excitation
FI	Fluorescence index
Fn(280)	Protein-like fluorescence parameter
Fn(355)	Humic-like fluorescence parameter
FRI	Fluorescence regional integration
HAc	Acetic acid
HIX	Humification index
HMF	Hydroxymethylfurfural
HPSEC	High performance size-exclusive chromatography
HS	Humic substances
LCFA	Long chain fatty acids
PCA	Principal component analysis
PC	Principal component
Pt-Co	Platinum-Cobalt
SCOD	Soluble chemical oxygen demand
SMA	Specific methanogenic activity
$SUVA_{254}$	Specific ultraviolet absorbance at 254 nm
TCOD	Total chemical oxygen demand
TH	Thermal hydrolysis
TN	Total nitrogen
TS	Total solids
TP	Total phosphorous
URI	Ultraviolet absorbance ratio index
UVA_{210}	UV absorbance at 210 nm
UVA_{254}	UV absorbance at 254 nm
VS	Volatile solids
VFA	Volatile fatty acids
WAS	Waste activated sludge
WWTP	Wastewater treatment plant

Chapter 1

Introduction

1.1 Anaerobic digestion

Anaerobic digestion (AD) is a fermentative process in which biowastes are degraded with biogas production (Mao et al., 2015; van Lier et al., 2020). These biowastes undergo four successive steps during AD: hydrolysis, acidogenesis, acetogenesis, and methanogenesis (**Figure 1.1**). In the first step, fermentative bacteria enzymatically hydrolyse the complex organic matter into soluble monomers: sugars, amino acids, and fatty acids. These monomers are further degraded into volatile fatty acids (VFA), lactic acid, alcohols, ketones, CO_2, and H_2 in the next step, acidogenesis. The third step, acetogenesis, converts the remaining fatty acids from the previous two steps into acetic acid, CO_2, and H_2. In the final methanogenesis step, the products from the last two steps are consumed; acetate, H_2, and CO_2 are converted into methane by aceticlastic and hydrogenotrophic methanogens (van Lier et al., 2020). Among the four steps, hydrolysis is the rate-limiting step, constrained by the free accessible surface area and structure of complex organic matter (van Lier et al., 2020). Therefore, several physicochemical pretreatment methods have been developed to accelerate hydrolysis; according to their working principles, they can be divided into four categories: mechanical, thermal, chemical, and combined, as shown in **Figure 1.2**.

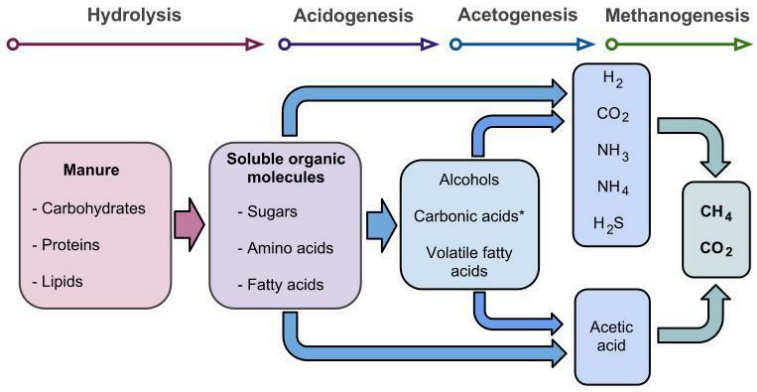

Figure 1.1: AD process scheme (Rea, 2014).

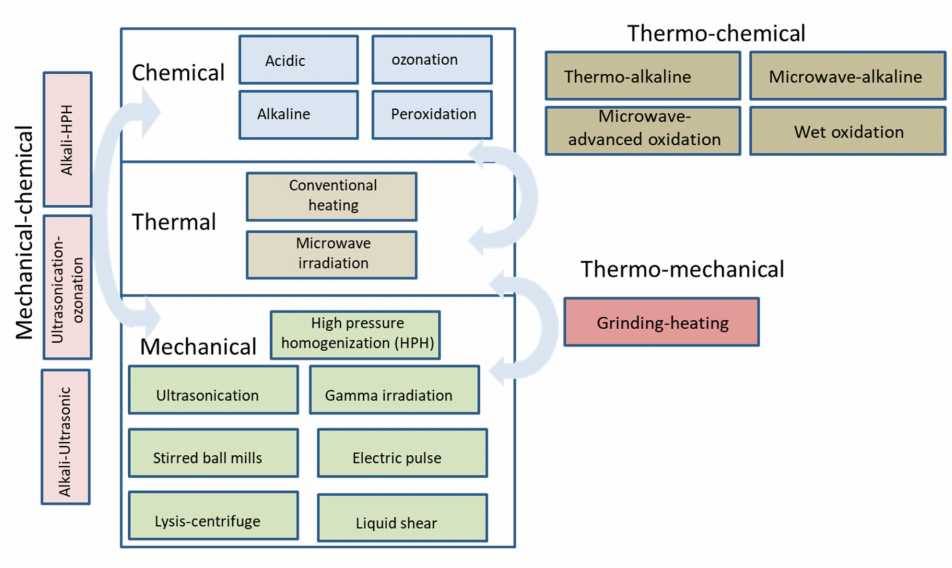

Figure 1.2: Classification of the different substrate pre-treatment methods (González et al., 2018).

1.2 Thermal hydrolysis

Thermal hydrolysis (TH) refers to a process technology that involves physicochemical reactions occurring under high temperature and pressure conditions in the presence of water (Byrappa & Yoshimura, 2012; Hii et al., 2014). TH has been applied extensively to sewage sludge treatment to improve downstream AD, waste stabilisation, sterilisation, and dewaterability (Abelleira-Pereira et al., 2015; Barber, 2016).

1.2.1 TORWASH®

TORWASH® is a continuous TH technology developed by TNO (Netherlands Organisation for Applied Scientific Research), which is currently in the pilot testing stage (Nanou et al., 2020). The design of the pilot installation consists of five sections: feeding, pre-heating, TORWASH® (i.e., TH), cooling, and depressurisation (**Figure 1.3**). During operation, pre-thickened sludge is pumped into the upper inlet of a continuous tubular thermal reactor, entering the pre-heating section. Once the required temperature is reached, the sludge flows into the TORWASH® section with a retention time of around 30 min. Once the TH is finished, the thermally-hydrolysed sludge is cooled and depressurised. Conventionally, the TH-treated sludge is sent to the AD reactor directly as in the design of Cambi® and Bio Thelys™ (Pilli et al., 2015), but TORWASH® uses a filter press to separate the TH-treated sludge into filtrate and press cake; only the filtrate is AD-treated. This separation could make the AD treatment more efficient; according to Bougrier et al. (2008), higher biogas production was achieved in the soluble fraction compared with the particulate fraction for WAS TH-treated at 95 - 170 °C.

The reaction temperature applied in TORWASH® spans from 180 to 210 °C; which is higher than that of conventional industrial-scale TH installations such as Cambi® (150 - 160 °C) and Bio Thelys™ (150 - 180 °C) (Pilli et al., 2015). In this higher temperature range, not only does hydrolysis take place, but mild torrefaction occurs (Nanou et al., 2020). Torrefaction corresponds to a thermal treatment carried out at reaction temperatures

of 200 - 300 °C in the absence of oxygen, which generally improves the fuel properties of biomass (i.e., energy density) by reducing the moisture content in torrefied biomass (Atienza-Martínez et al., 2015).

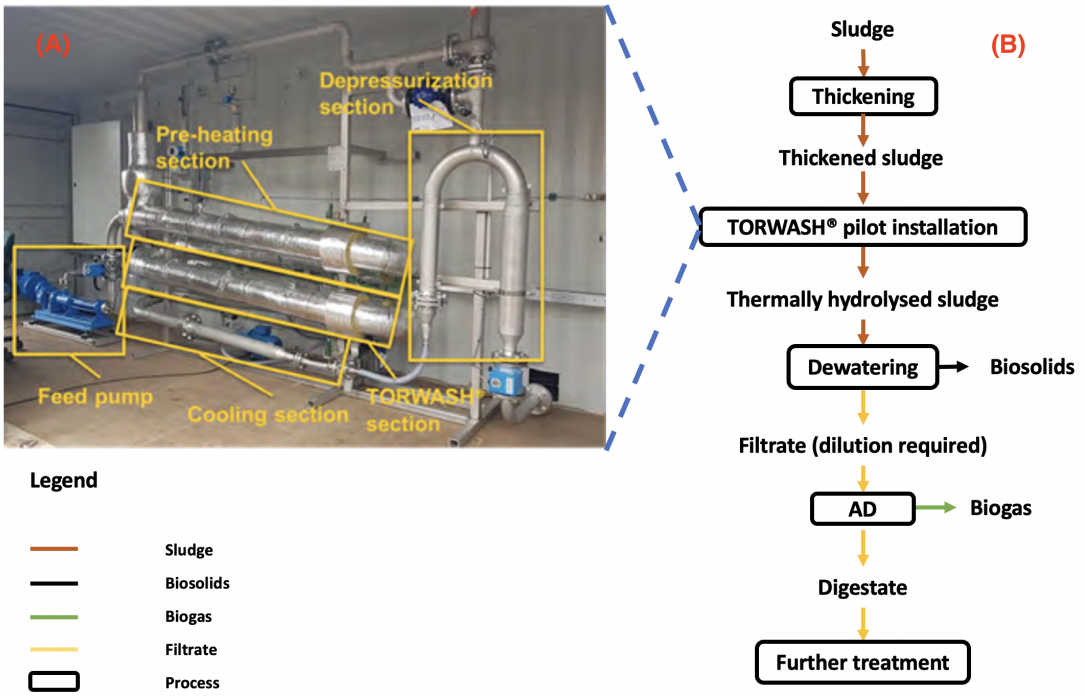

Figure 1.3: TORWASH® pilot installation (A) and flow diagram (B), adapted from Nanou et al. (2020).

1.2.2 Factors affecting TH performance

Reaction temperature

Our study focuses on high-temperature TH conducted at above 100 °C. In this temperature range, Toutian et al. (2020) observed a 21 % increase in soluble COD (SCOD) for lab-scale TH of WAS at 130 - 170 °C compared with untreated WAS. In addition, Wilson and Novak (2009) reported an 8 - 21.4 % increase in COD solubilisation for WAS TH-treated at 130 - 200 °C with respect to raw WAS. However, an increased COD solubilisation at higher reaction temperatures does not always result in higher anaerobic biodegradability (**Figure 1.4**). It has been widely reported that 170 - 190 °C is the optimal temperature range for TH of WAS to reach the highest anaerobic biodegradability, although the concentration of SCOD is still observed to increase at reaction temperatures up to 220°C (Gonzalez et al., 2018; Mottet et al., 2009). This inconsistency between COD solubility and anaerobic biodegradability implies a potential trade-off between the solubilisation of biodegradable matter and the formation of soluble recalcitrant compounds. The biodegradable matter contributes to methane production, but the soluble recalcitrant compounds do not. Therefore, a reaction temperature of 190 °C is postulated as the temperature above which the formation of recalcitrant compounds outcompetes the sludge digestibility improvement, but the exact temperature depends on the composition of the sludge and other factors (Gonzalez et al., 2018).

Furthermore, Wilson and Novak (2009) reported that the relative solubilisation of polysaccharides was higher than that of proteins at 130 - 220 °C. It was hypothesised that most proteins were already solubilised at a temperature > 100 °C, while carbohydrates only started to solubilise at 130 °C (Gonzalez et al., 2018). Therefore, the main effect of TH on carbohydrates blow 220 °C is solubilisation instead of degradation. In contrast, extensive degradation and denaturation of proteins are expected to occur at temperatures of 190 - 220 °C (Wilson & Novak, 2009).

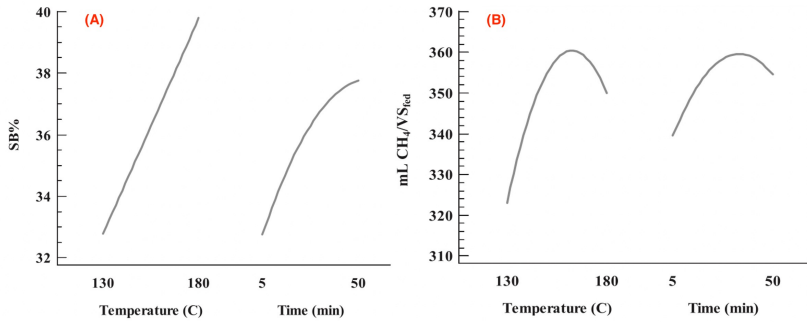

Figure 1.4: Effect of reaction temperature and time evaluated on solubilisation (A) and methane production (B) of TH-treated WAS (Sapkaite et al., 2017). SB is the solubilisation factor.

Reaction time

A longer reaction time leads to an increase in the solubility of compounds. For example, Xue et al. (2015) conducted TH (120 - 180 °C) of high solid sludge for different reaction times (15 - 180 min), which showed the concentrations of SCOD, soluble carbohydrates, and proteins generally increased with a longer reaction time. Furthermore, Aboulfoth et al. (2015) reported that COD solubilisation still improved when the reaction time was prolonged to 240 min for TH of combined sludge (primary and WAS) at 175 °C. However, a higher degree of organic solubilisation achieved by a longer reaction time may not necessarily increase methane production (**Figure 1.4**). Sapkaite et al. (2017) observed a decrease in methane production when the reaction time exceeded 30 min, which can be associated with the formation of soluble recalcitrant compounds (Ngo et al., 2021). Furthermore, based on the consensus, a 30 - 40 min reaction time is considered the optimal condition when WAS is TH-treated at 160 - 180 °C (Barber, 2016). Correspondingly, this time range is also adopted within the industry; Cambi® and Bio Thelys™ processes are currently operated at 20 - 30 min and 30 - 60 min, respectively (Pilli et al., 2015).

Feed source

Various feedstocks, including sewage sludge, slaughterhouse or fatty waste, manure, lignocellulosic biomass, food waste, and algae, can be pre-treated with TH (Carrere et al., 2016). The feedstocks of interest in our study are WAS and anaerobically pre-digested WAS (digestate) for the simulation of both pre- and inter-stage TH pretreatments (i.e., TH-AD and AD-TH-AD). Pre-digestion degrades readily biodegradable substances into biogas and a small portion of complex organic matter; thereby, pre-digested sludge contains less SCOD and VFA but more hardly biodegradable organic matter than raw WAS (X. Liu et al., 2021; Nielsen et al., 2011). In addition, pre-digestion increases pH due to the ammonium produced from protein hydrolysis and VFA depletion (Nielsen et al., 2011). The increase in pH could affect the pathway of recalcitrant compounds formation via the Millard reaction during TH (Hodge, 1953).

1.2.3 TH mechanism

A series of physicochemical reactions occur during TH; they contribute to the morphological change in the gel-like structure of WAS through the destruction of extracellular polymeric substances (EPS) (**Figure 1.5**). EPS are microbial-derived polymers consisting of protein, polysaccharides, lipids, nucleic acids, and humic substances (HS), maintaining the colloidal structure of the sludge aggregates (Guo et al., 2016). Therefore, the destruction of EPS during TH leads to the release of polysaccharides and proteins (Barber, 2016). The mechanisms of EPS degradation and solubilisation of organic macromolecules are based on free radical oxidation and hydrolysis (Yan et al., 2022).

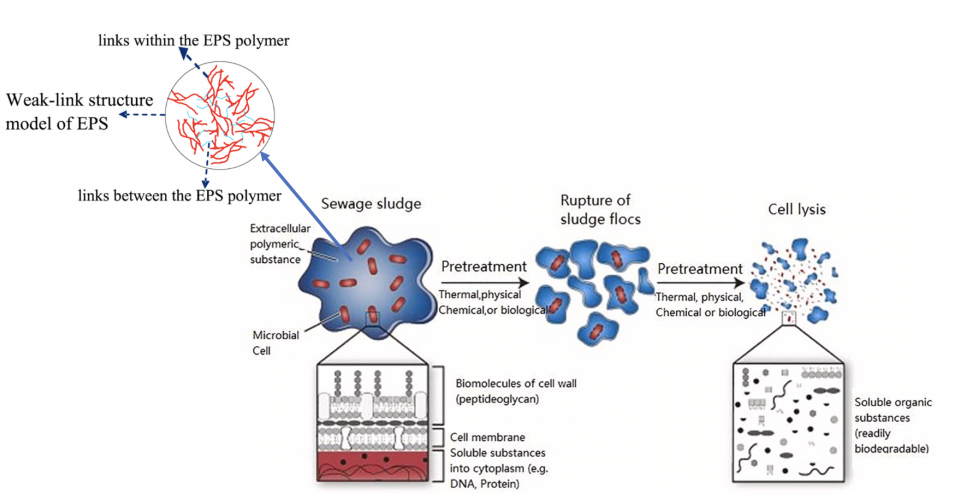

Figure 1.5: Sludge morphology transformation during TH (Yan et al., 2022).

Free radical oxidation

Free radicals are chemical species that contain at least one unpaired valence electron; these unpaired electrons lead to a highly oxidative property (McNaught, 1997). TH provides ideal conditions for their formation. The development of free radicals can be divided into three stages, initiation, propagation, and termination (Togo, 2004). In the first stage, free radicals, including alkyl (R·) and hydrogen (H·) radicals, are produced from the degradation of organics under conditions of high temperature and oxygen deficiency (**Equation 1.2.1**) (Yousefifar et al., 2017). These radicals can further react with stable molecules to form new radicals in the next stage (**Equation 1.2.2**, **Equation 1.2.3**, and **Equation 1.2.4**) to continuously generate more free radicals, such as hydroxyl radicals (HO·), alkyl radicals (R·), and amino radicals ($R_2N\cdot$) (Bachir et al., 2001; Yousefifar et al., 2017). Finally, interactions between free radical species occur and form stable, non-radical adducts, including short-chain alcohols (**Equation 1.2.5** and **Equation 1.2.6**) and carboxylic acids (**Equation 1.2.7**) (Aggrey et al., 2012).

$$RH \rightarrow R\cdot + H\cdot \qquad (Eq.\ 1.2.1)$$

$$H_2O + H\cdot \rightarrow HO\cdot + H_2 \qquad (Eq.\ 1.2.2)$$

$$RH + HO\cdot \rightarrow R\cdot + H_2O \qquad (Eq.\ 1.2.3)$$

$$R_2NH + HO\cdot \rightarrow R_2N\cdot + H_2O \quad (Eq.\ 1.2.4)$$

$$R\cdot + HO\cdot \rightarrow ROH \quad (Eq.\ 1.2.5)$$

$$R_2N\cdot + H_2O \rightarrow NH_4^+ + 2ROH \quad (Eq.\ 1.2.6)$$

$$R\cdot + 2HO\cdot \rightarrow R'COOH \quad (Eq.\ 1.2.7)$$

Hydrolysis
The concept of hydrolysis in TH is different from that in AD. The hydrolysis during TH is driven by increased water reactivity at elevated temperatures and pressures (Yan et al., 2022). In contrast, the hydrolysis during AD is catalysed by exoenzymes produced by hydrolytic bacteria (Carlsson et al., 2012). During TH, complex organics (A-B) are hydrolysed to form low molecular weight hydrolysed products (A-H and B-OH) (**Equation 1.2.8**, Brunner (2009)), which is manifested in COD solubilisation, converting particulate COD (particulate COD = total COD - SCOD) into SCOD (Ngo et al., 2021).

$$A-B + H_2O \rightarrow A-H + B-OH \quad (Eq.\ 1.2.8)$$

1.3 Recalcitrant compounds

This study collaborated with TNO to investigate soluble recalcitrant compounds derived from lab-scale TH experiments under operating conditions similar to those of TORWASH®. The recalcitrant compounds refer to aerobically or anaerobically non-biodegradable dissolved organic matter (DOM) derived from TH. TH-treated sludge contains thousands of different recalcitrant compounds, each in small concentrations, overall adding up to a large concentration (Faixo et al., 2021). Furthermore, the formation of recalcitrant compounds during TH is primarily associated with two reactions, the Maillard and caramelisation reactions (Penaud et al., 2000). Typical products of these two reactions include furfurals, hydroxymethylfurfural (HMF), melanoidins, and caramelans, which might be recalcitrant, toxic, or both to the downstream AD (Bolado-Rodríguez et al., 2016; Monlau et al., 2014). When TH is operated at TORWASH® designated temperature range (180 - 210 °C), both reactions occur concurrently; therefore, it is difficult to differentiate these two reactions as they share the same intermediates (Göncüoğlu Taş & Gökmen, 2017). In addition, acidic pretreatments were applied to WAS as a potential method to mitigate the formation of recalcitrant compounds. To understand how pH can affect the pathways of these two reactions, the mechanism is introduced below.

1.3.1 Maillard reaction

The Maillard reaction is a non-enzymatic browning reaction between aldoses and amino compounds, producing coloured (mainly brownish), UV-absorbing and non-biodegradable polymers (Hodge, 1953). TH of the sewage sludge provides ideal temperature conditions and reactants for the occurrence of Maillard reaction since the sewage sludge contains 20 - 40 % of carbohydrates and 30 - 50 % of proteins (Bemiller, 2018; Jimenez et al., 2013). The Maillard reaction can be divided into three stages (Hodge, 1953) as follows (**Figure 1.6**):

Early stage

During TH, polysaccharides are solubilised and further degraded into mono- and disaccharides (Wilson & Novak, 2009). The carbonyl groups of these saccharides can condense with the amino group of the amino acids, producing N-substituted glycosylamine (RN = CHR'), which then undergoes the Amadori rearrangement, forming the relatively stable and colourless intermediates known as Amadori rearrangement products (ARP). The Amadori rearrangement is generally a non-reversible reaction and can occur spontaneously even at room temperature (Nursten, 2005).

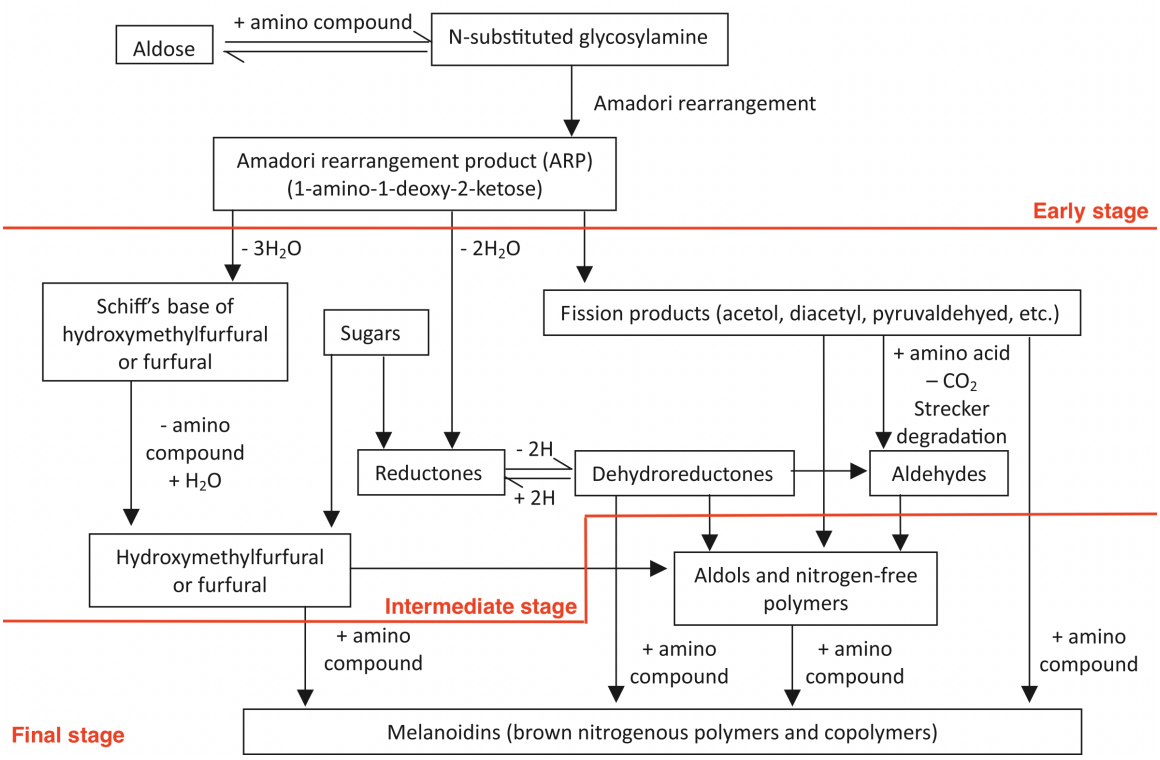

Figure 1.6: Maillard reaction scheme (Hodge, 1953). Horizontal lines divide the reaction scheme into three stages.

Intermediate stage

The intermediate stage corresponds to the breakdown of ARP through dehydration and fragmentation. The dehydration pathways include 1,2-enolisation and 2,3 enolisation, depending on the pH of the reaction system. Under acidic conditions (pH ≤ 7), dehydration occurs primarily via 1,2-enolisation (losing three water molecules), producing furfural (when aldopentoses are involved) or HMF (when aldohexoses are involved) (Bemiller, 2018). Furfural and HMF both have been reported to inhibit the downstream AD process at a concentration above 2.0 g/L (Ghasimi et al., 2016). At pH above 7, dehydration via 2,3 enolisation (losing two water molecules) is favoured to generate reductones (slightly acidic reducing agents), which can be dehydrated into deoxyreductone. In addition, the ARP can also undergo fragmentation, forming fission products with shorter chains, such as carbonyl and dicarbonyl. These fission products can further react with α-amino acid to produce aldehydes and release CO_2 through Strecker degradations (**Equation 1.3.1** (Schönberg & Moubacher, 1952), suggesting the CO_2 partial pressure may influence the progress of this reaction. Besides, COLE (1967) suggested that CO_2 could be used as an indicator of the progression of the Maillard reaction, assuming that CO_2 was formed mainly via the Strecker

degradation. It was reported that CO_2 was the major component (> 90 %) present in the gas sample taken from the TORWASH® reactor during steady operation. The CO_2 formed during TH could react with water and produce carbonic acid as an acid catalyst (F. Liu et al., 2012). In short, the products from the intermediate stage are yellow and UV-absorbing; they are highly reactive and can participate in further reactions in the final stage (Hodge, 1953).

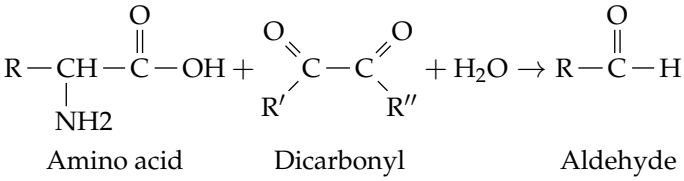

(*Eq. 1.3.1*)

Final stage

The final stage leads to the production of nitrogenous, brown, and UV-absorbing polymers or co-polymers, known as melanoidins, via aldol and aldehyde–amine condensation (Hodge, 1953). The low molecular weight melanoidins are initially formed through the reactions between the intermediates and the amino compounds (O'Brien et al., 1998). Subsequently, low molecular weight melanoidins (< 3.5 kDa) are polymerised or/and cross-linked via α-amino groups to generate high molecular weight melanoidins (> 10 kDa) (Hui et al., 2008; O'Brien et al., 1998). Lü et al. (2015) reported that high molecular weight melanoidins were formed at 140 - 165 °C. Considering the temperature range (above 180 °C) applied in TORWASH®, the production of melanoidins seems unavoidable. Many structures and molecular weights have been found in a variety of melanoidins; generally, melanoidins are postulated to be high molecular weight polymers with repeating units of furans and/or pyrroles (S. Martins & van Boekel, 2003). The empirical formula of melanoidins is $C_{17-18}H_{26-27}O_{10}N$ with a molecular weight of 5 – 40 kDa (Nursten, 2005). In addition, melanoidins are overall resistant to biodegradation due to their high molecular weight, complex structure and xenobiotic nature (Chandra et al., 2008). Hence, melanoidins are difficult to be degraded anaerobically.

1.3.2 Caramelisation

In addition to the Maillard reaction, caramelisation is another non-enzymatic browning reaction occurring at 160 - 170 °C, which further darkens the colour in the liquid fraction of thermally-hydrolysed sludge (Barber, 2016; Gonzalez et al., 2018; Villamiel et al., 2006). Caramelisation is the pyrolysis of sugars, polysaccharides, polyhydroxycarboxylic acids, and reductones into caramelans (Ajandouz et al., 2001; Barber, 2016; Nursten, 2005). Besides, the caramelisation reaction does not involve amides; therefore, caramelisation products are not nitrogenous, which can be distinguished from melanoidins (Gonzalez et al., 2018). The pathway of caramelisation depends on the pH and type of sugar in the reaction system, which begins with Lobry de Bruyn–Van Ekenstein transformation, catalysed by base or acid media. This transformation converts aldoses into ketose isomers (e.g., glucose isomerised to fructose in **Equation 1.3.2**) or vice versa, whilst producing tautomeric enediols as reaction intermediates (Kroh, 1994). These carbohydrates and isomeric carbohydrates can be further dehydrated or fragmented. Under neutral or acidic conditions, dehydration is the dominant reaction, producing HMF from hexoses (**Equation 1.3.3**) and furfural from pentoses. Under alkaline conditions, the dehydration rate is slower than that under neutral or acidic conditions; therefore, fragmentation is the dominant reaction, producing fission products, such as acetol, acetoin and diacetyl (Hui et al., 2008). In addition, caramelisation generally requires a reaction temperature higher than the Maillard reaction. This is in line with the results of Wilson and Novak

(2009) that caramelisation does not appear to contribute to UVA_{254} of sludge hydrolysate at temperatures < 220 °C.

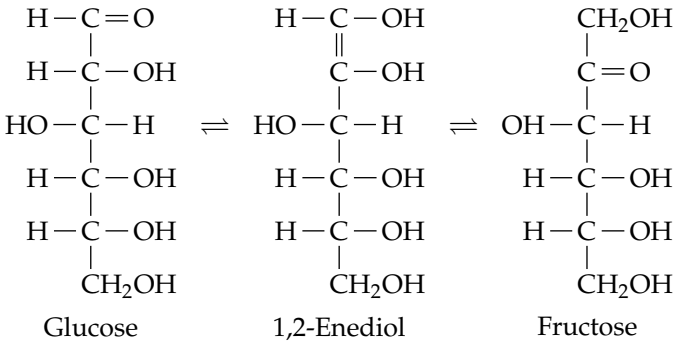

(*Eq. 1.3.2*)

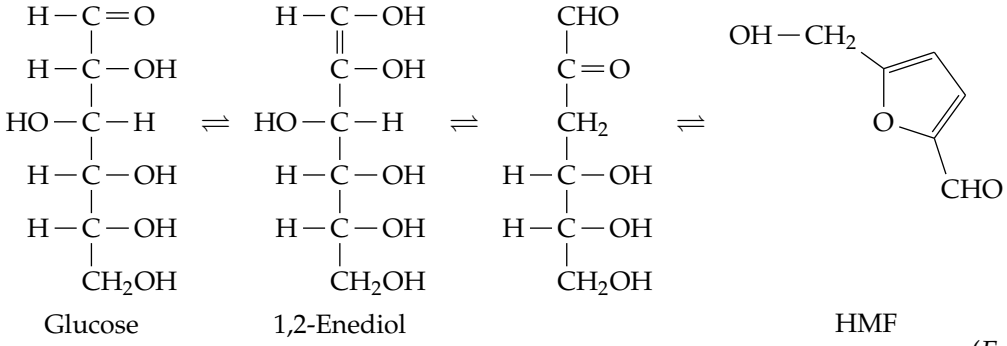

(*Eq. 1.3.3*)

1.3.3 Mitigation of recalcitrant compounds formation

Generally, the reaction rate of the Maillard reaction decreases at a lower pH (Villamiel et al., 2006). In the early stage of the Maillard reaction, the unprotonated amines and the open-chain reducing sugars are considered reactive forms (S. I. Martins et al., 2000). The unprotonated amino groups can actively participate in nucleophilic reactions to condense with open-chain sugars, producing glycosylamine (**Figure 1.7**). The protonation depends on pH and amino groups' acid dissociation constants (see pKa2 in **Table 1.1**). Generally, more unreactive protonated amino acids would present at lower pH. The ratio of unprotonated amino groups is less than 1% at pH < 7 (Van Boekel, 2001). Besides, pH can also influence the configuration of the reducing sugars. The acyclic sugars are more reactive than the cyclic sugars due to their higher reducibility (**Equation 1.3.4**). Lowering the pH can reduce the chain opening rate and the fraction of acyclic sugars (**Table 1.2**) (Bemiller, 2018; Cantor & Peniston, 1940; Zhang et al., 2020). Overall, acidification could lower the concentration of reactive amines and reducing sugars in the early stage of Maillard reactions. Subsequently, fewer intermediates could be formed; Ge and Lee (1997) confirmed that the ARP formation rate is decreased at a lower pH.

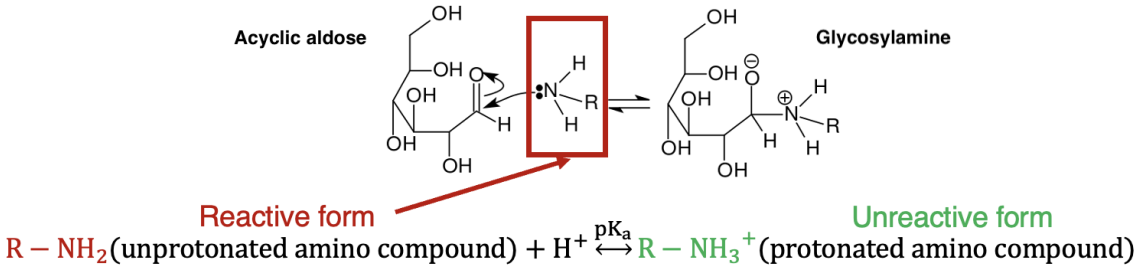

Figure 1.7: Sugar amine condensation and amine protonation.

Table 1.1: Acid dissociation constants of common amino acids

Amino acid	Molecular Formula	pKa1 [1]	pKa2 [2]
Cysteine	$C_3H_7NO_2S$	1.96	10.28
Serine	$C_3H_7NO_3$	2.21	9.15
Threonine	$C_4H_9NO_3$	2.09	9.10
Tyrosine	$C_9H_{11}NO_3$	2.20	9.11
Tryptophan	$C_{11}H_{12}N_2O_2$	2.83	9.39
Arginine	$C_6H_{14}N_4O_2$	2.17	9.04
Lysine	$C_6H_{14}N_2O_2$	2.18	8.95

[1] pKa1 is the negative logarithm of the dissociation constant for the -COOH group.
[2] pKa2 is the negative logarithm of the dissociation constant for the -NH_3 group.

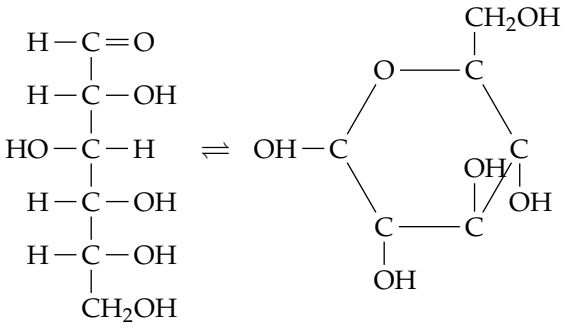

D-Glucose
Acyclic, more reducible

D-Glucopyranose
Cyclic, less reducible

(*Eq. 1.3.4*)

Table 1.2: Variation in percentage of acyclic sugar at pH 6.5, 7.0 and 7.5.

Sugar [1]	pH 6.5	pH 7.0	pH 7.5
D-Lyxose	15 %	18 %	36 %
L-Arabinose	13 %	22 %	46 %
D-Xylose	10 %	13 %	36 %
D-Galactose	7 %	8.5 %	14 %
D-Mannose	4 %	6.2 %	11 %
D-Glucose	1.2 %	2.2 %	4 %

[1] 0.1 M of Sugar at at 25 °C (Cantor & Peniston, 1940).

1.4 Knowledge Gaps and research objectives

According to the literature, several knowledge gaps need further investigation. Studies have been conducted on the design of AD-TH-AD configuration to increase the ultimate methane production, but there is limited effort to address the effects of anaerobic pre-digestion on recalcitrant compounds derived from TH. In addition, intensive studies were carried out to reduce recalcitrant compounds formation and enhance biological performance, such as acidic treatment using sulphuric acid (Takashima & Tanaka, 2010) and the addition of sodium sulfite during alkaline TH of sludge (N. Yang et al., 2022). However, CO_2 pressurisation as a pretreatment method to mitigate the formation of recalcitrant compounds is scarcely reported, and the impact of CO_2 partial pressure on recalcitrant compounds during TH of sludge was unclear.

According to the stated knowledge gaps, the main objectives of this research are as follows:

1. To characterise the recalcitrant compounds derived from thermally-hydrolysed WAS and anaerobically pre-digested WAS at different reaction temperatures.
2. To investigate the effect of CO_2 partial pressure and the addition of acetic acid (HAc) on the formation of generated recalcitrant compounds derived from TH.

1.5 Research questions and approaches

To meet the research objectives, the following research questions are formulated:

1. What are the differences between WAS and pre-digested WAS before and after TH?
2. How can reaction temperature affect the formation of recalcitrant compounds?
3. What are the differences between acidifying TH systems through HAc addition and CO_2 pressurisation?

To answer these research questions, the research approach can be divided into three steps:

1. Characterise WAS and anaerobically pre-digested WAS subjecting to TH at different reaction temperatures.

2. Conduct TH on WAS with the addition of HAc and CO_2 partial pressure for the potential mitigation of recalcitrant compounds production.
3. Qualitatively and pseudo-quantitatively analyse the impacts of reaction temperature and CO_2 partial pressure on the production of recalcitrant compounds.

Chapter 2

Materials and Methods

2.1 Source of sludge

WAS and anaerobically pre-digested WAS samples were obtained from the sludge treatment processes at WWTP Land van Cuijk, The Netherlands, where the WAS was first thickened (in sludge thickener 2) and then anaerobically digested; the digested WAS was temporally stored in buffer tank 1 with the addition of polyelectrolyte to improve the dewaterability in the next step (**Figure 2.1**). Two batches of samples were collected. The first batch of samples included thickened WAS (referred to as WAS-1, taken from the sludge thickener 2) and digested WAS (referred to as DWAS-1, taken from the sludge buffer tank 1) (**Table 2.1**). For the second batch, only thickened WAS was sampled (referred to as "WAS-2"). Collected samples were stored in a refrigerator at 4 °C.

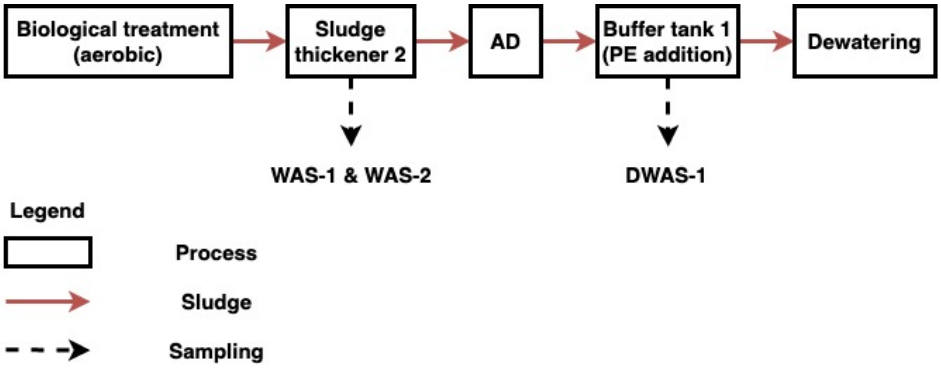

Figure 2.1: Sludge treatment at WWTP Land van Cuijk and sample collection.

Table 2.1: Feedstocks for TH tests.

Parameter	WAS-1	DWAS-1	WAS-2
pH (-)	6.1	7.7	6.3
TS (%)	3.9	3.9	6.8
VS (%)	3.0	2.9	4.9
TCOD (mg O_2/L)	54,200 $\pm$ 300	44,000 $\pm$ 1000	72,000 $\pm$ 1000
TN (mg N/L)	2580 $\pm$ 40	3430 $\pm$ 40	3840 $\pm$ 40
TP (mg P/L)	1260 $\pm$ 40	1240 $\pm$ 20	696 $\pm$ 4

2.2 Experimental design

TH experiments were divided into two parts. The first part was conducted at the biofuels lab of TNO (Petten, The Netherlands) by Dr. Jan Pels to find optimal reaction temperatures for WAS-1 and DWAS-1 based on dewatering tests (**Section 2.2.1**). The second part was to assess the effect of acidic pretreatments on TH of WAS-2 at WaterLab of Delft University of Technology (Delft, The Netherlands) (**Section 2.2.2**).

2.2.1 TH experiment at different reaction temperatures

A multiclave system (Fisher Scientific, USA) with a regular heating/stirring plate was used to perform TH on WAS-1 and DWAS-1. It consisted of several sealed single thermal reactors that allowed samples, each around 80 mL, to proceed concurrently. Multiclave tests on WAS-1 were carried out at temperatures ranging from 180 to 200 °C for 30 min (**Figure 2.2**). After cooling, a Carver hydraulic press was used to test the dewaterability of thermally-hydrolysed WAS-1. First, a reaction temperature of 180 °C was applied to WAS-1, while the produced hydrolysate could not directly pass through the Carver hydraulic press; thus, a centrifuge was used to obtain the supernatant called WAS-1-M180. Furthermore, a similar situation also occurred when the reaction temperature was raised to 185 °C; hence, the centrifuge was used again to collect the supernatant called WAS-1-M185. However, the hydrolysates of WAS-1 generated at 190 and 200 °C could be dewatered through the carver press, and the pressed filtrates were obtained, named as WAS-1-M190 and WAS-1-M200, respectively. The optimal temperature for WAS-1 was defined as the lowest temperature at which the hydrolysed WAS-1 could be dewatered by the carver hydraulic press (i.e., 190 °C). Subsequently, the optimal temperature was then applied in a larger scale TH test in a 20 L autoclave (Fisher Scientific, USA) for 30 min via thermal conduction. The produced hydrolysate was vacuum filtered using a Büchner funnel with a glass fibre filter (pore size 2.7 μm); the filtrate WAS-1-A190 was collected.

Multiclave tests on DWAS-1 were performed at temperatures from 180 to 210 °C for 30 min (**Figure 2.3**). The results of dewatering tests showed that the Carver press could only poorly dewater the samples of thermally-hydrolysed DWAS-1. Therefore, the centrifuge was used to separate the hydrolysates of DWAS-1 heated at 180 and 190 °C. The obtained supernatants were named as DWAS-1-M180 and DWAS-1-M190. The remaining TH tests on DWAS-1 were performed at reaction temperatures of 195, 200, 205, and 210 °C, orderly, and then separated using a glass fibre filter with vacuum suction to obtain the corresponding filtrates DWAS-1-M195, DWAS-1-M200, DWAS-1-M205, and DWAS-1-M210. The filter cakes retained in the glass fibre filters were dewatered through the carver hydraulic press to determine the optimal temperature based on their dewaterability. Following the same principle, it was concluded that 205 °C was the optimal temperature for DWAS-1. In addition, 20 L of DWAS-1 was also thermally hydrolysed at the optimal temperature (205 °C) for 30 min and then vacuum filtered using a glass fibre filter (pore size 2.7 μm); the obtained filtrate was named as DWAS-1-A205.

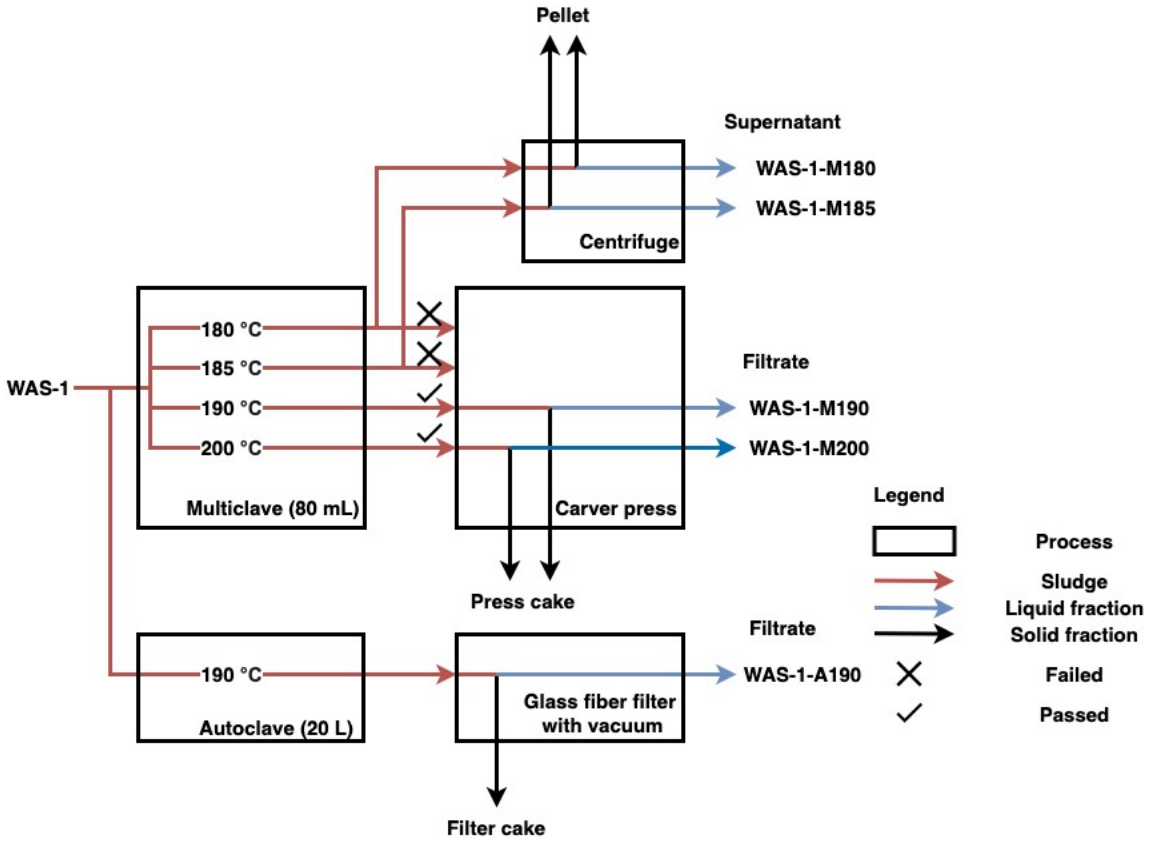

Figure 2.2: Scheme of TH and dewatering tests on WAS-1.

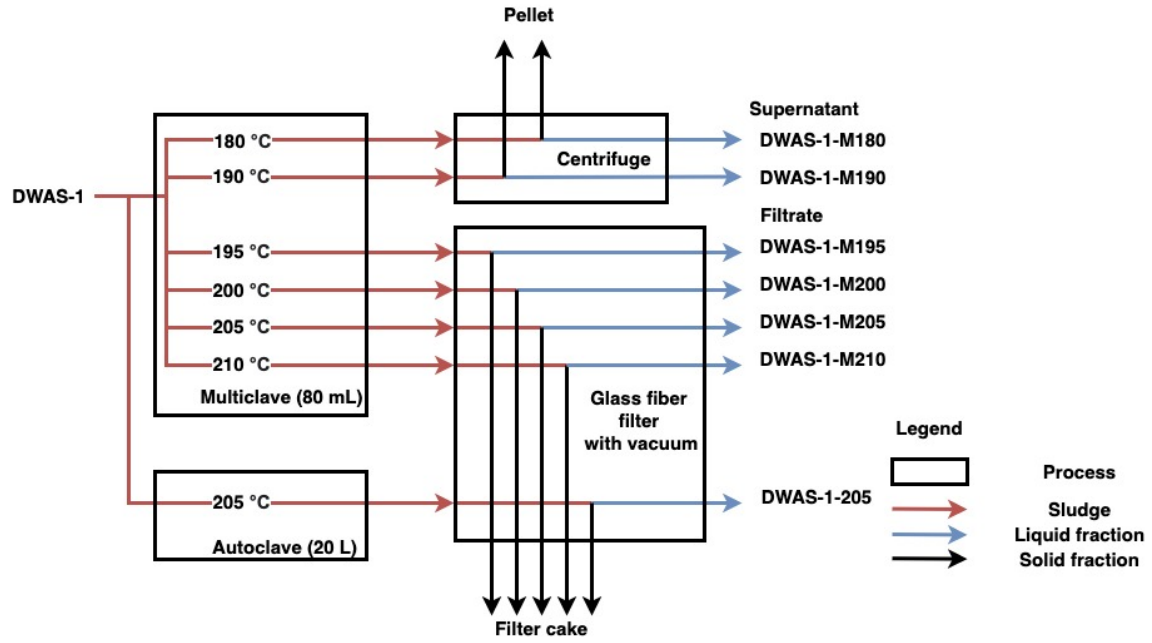

Figure 2.3: Scheme of TH and dewatering tests on DWAS-1.

2.2.2 Acidified TH experiment

Acidified TH experiments on WAS-2 were carried out in an on-stirred Parr No. 4600 pressure vessel system (Illinois, USA). The system consisted of a Parr 4838 temperature controller, a benchtop heater and a 4600-1.9L-HP-VGR vessel (**Figure 2.4**). There were six openings on the head of the reactor vessel, including one inlet valve, two outlet valves, one safety valve, one port for manometer and one thermowell coupled with a thermocouple for temperature measurement (**Figure 2.4 (D)**). Furthermore, steam heating was applied; around 400 mL of demi water (demineralised water) was first added to the reactor vessel. Then an unsealed metal cylindrical container filled with approximately 300 g sample was placed in the centre of the vessel to isolate demi water and sample. The demi water vaporised during heating provided a more uniform convective steam heating than conductive electrical heating applied in multiclave and autoclave.

Before commencing acidified TH experiments, a non-acidified TH of WAS-2, referred to as WAS-2-control, was conducted at 190 °C for 30 min. The 190 °C was concluded from TH tests of WAS-1. After the reaction, the reactor was set aside in a fume hood to cool down at room temperature. When the reading on the temperature controller had dropped below 100 °C, two outlet valves were turned on slowly to release the pressure, accelerating the cooling process. Therefore, the water loss due to evaporation was unavoidable, and a correction factor was calculated based on the mass change of the sludge sample before and after TH. For the acidified TH experiments, three acidic pretreatments were applied, including the addition of acetic acid (HAc) (WAS-2-HAc), CO_2 pressurisation (WAS-2-10CO_2 and WAS-2-20CO_2) and the combination of both (WAS-2-HAc+10CO_2 and WAS-2-HAc+20CO_2), as shown in **Table 2.2**. For WAS-2-HAc, it followed the same operating procedure as WAS-2-Control, but HAc was added to WAS-2 before TH, exceeding part of the buffer capacity of the VFA system (pKa = 4.75) in the sludge by lowering the pH of WAS-2 to 4.3 (Nativ et al., 2021). The operating procedure for WAS-2-10CO_2 and WAS-2-20CO_2 was slightly different from WAS-2-Control and WAS-2-HAc. Before TH, the intake valve of the reactor vessel was connected to a CO_2 tank, and low-pressure CO_2 was injected into the reactor to flush out the residual air in the headspace through the outlet nozzle. Subsequently, the outlet valve was closed, and high-pressure CO_2 continuously flowed into the reactor until reaching the designated pressure, 10 bar for WAS-2-10CO_2 and 20 bar for WAS-2-20CO_2. The pressurised reactor was left standing overnight in the fume hood without any operation to achieve equilibrium of solubility among CO_2, sludge sample and demi-water. The headspace pressure slightly dropped due to the CO_2 dissolution in the liquid phase on the following day; hence, the replenishment of CO_2 was needed before TH tests. The last two TH tests, WAS-2-HAc+10CO_2 and WAS-2-HAc+20CO_2, first dosed WAS-2 with the same amount of HAc as in the TH test of WAS-2-HAc, and then followed the same procedure as TH tests WAS-2-10CO_2 and WAS-2-20CO_2, pressurising the reactor with CO_2: 10 bar for WAS-2-HAc+10CO_2 and 20 bar for WAS-2-HAc+20CO_2.

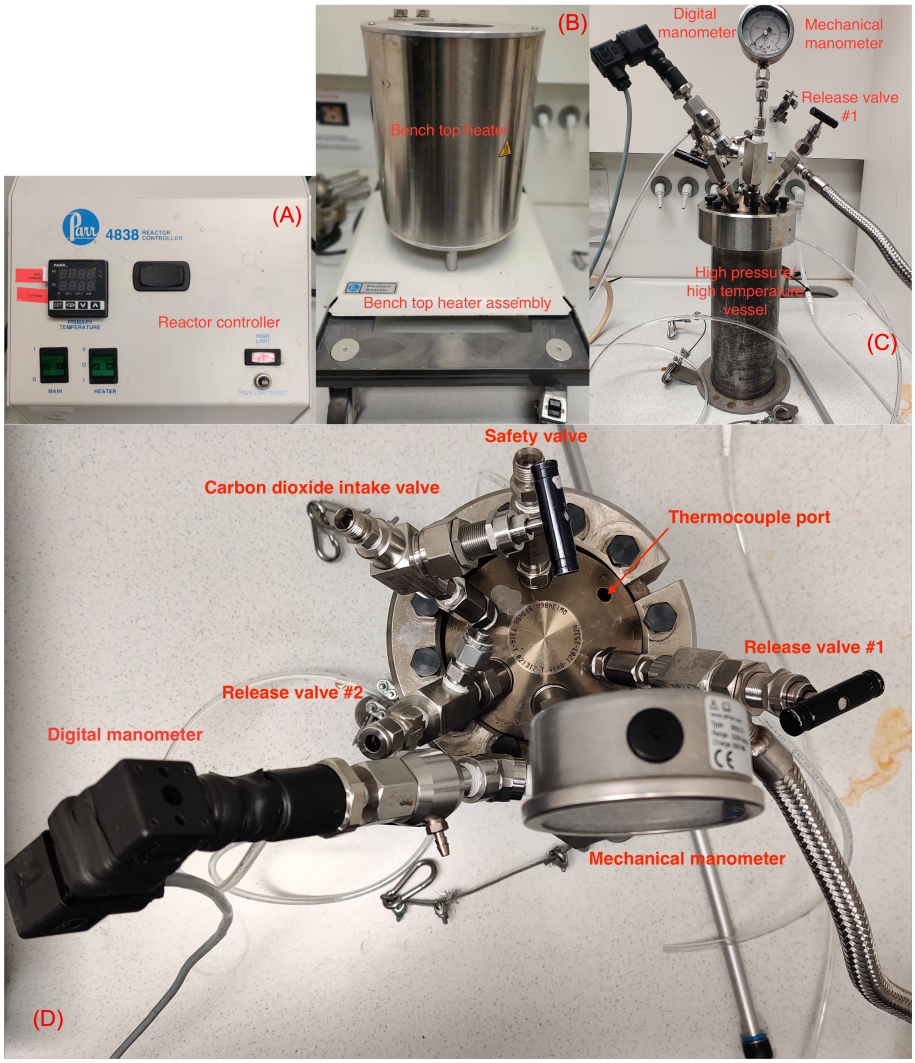

Figure 2.4: Parr No. 4600 pressure vessel system, which consists of a Parr 4838 temperature controller (A), a bench top heater on a base plate (B), and a 4600-1.9L-HP-VGR vessel (side view (C) and top view (D)).

Table 2.2: Acidified TH tests on WAS-2.

Test	Reactor	Reaction temperature (°C)	Time (min)	pH [1] (-)	CO_2 [2] (bar)	HAc (added) [3] (mg/L)
WAS-2-control	Parr No. 4600	190	30	6.3	-	-
WAS-2-HAc	Parr No. 4600	190	30	4.3	-	16,985
WAS-2-10CO_2	Parr No. 4600	190	30	6.3	10	-
WAS-2-20CO_2	Parr No. 4600	190	30	6.3	20	-
WAS-2-HAc+10CO_2	Parr No. 4600	190	30	4.2	10	16,985
WAS-2-HAc+20CO_2	Parr No. 4600	190	30	4.2	20	16,985

[1] The pH of samples measured before TH.
[2] The pressure of CO_2 in the reactor headspace before TH.
[3] The concentration of HAc added in sample.

2.3 Analytical methods

Total solids (TS) and volatile solids (VS) were determined gravimetrically according to standard methods (APHA et al., 1998). pH was measured with a SenTix 940 IDS probe attached to a multimeter (9620 IDS, Xylem Inc., USA), calibrated prior to each use. COD and BOD_5 were measured with photometric test kits, LCK514 and LCK555 (Hach, Germany), respectively. Total phosphorus (TP) and total nitrogen (TN) were determined using photometric test kits, LCK350 and LCK338 (Hach, Germany), respectively. For the dissolved parameters, the sample was centrifuged at 13,000 rpm for 15 min (Sorvall™ ST 16 Centrifuge Series, Thermo Fisher Scientific, USA). The supernatant was filtered with a syringe membrane filter (0.45 μm, CHROMAFIL Xtra RC, Germany). The ammonium, orthophosphate, and dissolved organic carbon (DOC) were measured with test kits, LCK303, LCK350, and LCK387 (Hach, Düsseldorf, Germany), respectively. True colour was determined with a UV-Vis spectrophotometer (GENESYS 6, Thermo Fisher Scientific, USA) at a wavelength of 475 nm using platinum-cobalt (Pt-Co) solutions as standards. UVA_{254} was spectrophotometrically measured in a 1 cm path length quartz cell (K. Y. Park et al., 2019); the results were normalised to the concentration of DOC, giving the value of specific ultraviolet absorbance ($SUVA_{254}$) in units of L/(mg·m). In addition, the mean oxidation state of dissolved organic carbon (DCOS) was calculated using **Equation 2.3.1** (Højris & Lund Skovhus, 2019). For quantification of organic macromolecules, the concentrations of soluble proteins and humic substances (HS) were determined based on the modified Lowry method (B. Frȼlund et al., 1995; B. O. Frȼlund et al., 1996); soluble carbohydrates concentration was determined with the phenol sulfuric acid assay (Dubois et al., 1956), using D-glucose monohydrate solutions as standards. Every sample used for the analyses above was diluted according to the range required by the test kits or corresponding methods, and all analyses above were done in triplicate.

$$DCOS\ (-) = \frac{4 \times (DOC\ (mol\ C/L) - SCOD\ (mol\ O_2/L))}{DOC(mol\ C/L)} \qquad (Eq.\ 2.3.1)$$

2.3.1 Biomethane potential tests

Biomethane potential (BMP) tests were conducted on WAS-1, DWAS-1, WAS-1-A190, and DWAS-1-A205 using the automatic methane potential test system II (AMPTS II, BPC Instruments, Sweden) in 500 mL bottles. **Table 2.3** shows the details of the tests. The bottles were flushed with nitrogen to remove oxygen from the headspace and tightly sealed to maintain anaerobic conditions. AD occurred under mesophilic conditions at 35 °C and was terminated when daily methane production was below 1 % of the accumulated volume of methane for three consecutive days (Holliger et al., 2016). In AMPTS II, CO_2 and H_2S were stripped in a NaOH scrubber, and the volume of the remaining dry pure methane gas was continuously measured by liquid displacement in individual flow cell units for each batch. The BMP was expressed as the volume of dry methane gas under standard conditions (273.15 K and 101.33 kPa) per mass of VS added (NL CH_4/kg VS) (Holliger et al., 2016).

Table 2.3: Details for the BMP tests on WAS-1, DWAS-1, WAS-1-A190, and DWAS-1-A205.

Batch No.	Load (g)	Substrate (g)	Inoculum (g)	Water (mL)	Micronutrients [1] (mL)	Macronutrients [1] (m)	Buffer (100 g $NaHCO_3$/L) (mL)
1, 2, 3	2.32 VS	76.62 (WAS-1)	173.20	143.54	0.24	2.40	4.00
4, 5, 6	2.32 VS	81.28 (DWAS-1)	173.20	138.89	0.24	2.40	4.00
7, 8, 9	2.32 VS	128.86 (WAS-1-A190)	173.20	91.30	0.24	2.40	4.00
10, 11, 12	2.32 VS	220.16 (DWAS-1-A205)	173.20	0.00	0.24	2.40	4.00
13, 14, 15	Control	2.42 (Cellulose [2])	173.20	220.16	0.24	2.40	4.00
16, 17, 18	Blank	-	173.20	220.16	0.24	2.40	4.00

[1] The inoculum characterisation and composition of macronutrient and micronutrient solutions can be found in **Appendix B**.
[2] The VS of cellulose was estimated to be 96.1 %.

2.3.2 Volatile fatty acids

Volatile fatty acids (VFA) were quantified by gas chromatography (Agilent Technology 7890A, USA) with a flame ionisation detector. The column was HP-FFAP 25 m x 320 μm x 0.5 μm (length x internal diameter x film thickness). The temperature of the GC oven was programmed to increase from 80 to 180 °C in 10.5 min. The injector temperature was kept at 80 °C at an injection volume of 1 µL, and gasified VFA were detected at 240 °C. High purity helium was used as a carrier gas at a flow rate of 67 mL/min with a split ratio of 25:1. Prior to GC analysis, 10 mL of sample was first centrifuged at 13,000 rpm for 15 min, and then the supernatant was filtered over a 0.45 μm syringe membrane filter (CHROMAFIL Xtra, Germany). The filtered liquid was diluted 2 to 10 times with pentanol (325.8 mg/L) as an internal standard, and a 1.5 mL diluted sample was transferred to a 1.5 mL vial with an addition of 10 μL of formic acid (purity > 99 %).

2.3.3 Size exclusion chromatography

High-performance size exclusion chromatography (HPSEC) was conducted on the liquid fraction of thermally-hydrolysed samples using a Phenomenex column (YarraTM 3 µm SEC-2000, LC Column 300 × 7.8 mm, Ea) connected to an ultrafast liquid chromatography system (Prominence, Shimadzu). The mobile phase was 25 % acetonitrile in Milli-Q water with 10 mM sodium phosphate buffer (pH = 7). The flow rate of the mobile phase was 1 mL/min, and the injection volume was 50 µL. Separation was achieved at 25 °C after 20 min, and the eluted substances were sequentially detected by UV at 254 and 210 nm. Moreover, the ultraviolet absorbance ratio index (URI) was calculated based on the ratio between UVA_{210} and UVA_{254}.

2.3.4 Fluorescence excitation emission matrix

Fluorescence spectra were measured in standard 1 cm quartz cuvettes using a spectrofluorometer (AQUALOG, HORIBA, USA) equipped with a 150 W xenon arc lamp (excitation source). Three-dimensional EEM spectra were collected at a temperature of 25 °C with subsequent scanning emission wavelengths of 247.55 - 824.879 nm at 4.7 nm intervals by varying excitation wavelengths from 220 to 500 nm at 2 nm increments using excitation and emission slit widths of 5.0 nm bandpass. Before measurement, the filtered samples (syringe filters, CHROMAFIL Xtra RC, 25 mm, 0.45 µm) prepared for fluorescence analysis were diluted with Milli-Q water to adjust DOC concentration to 1 mg/L. The obtained EEM data were processed according to the method proposed by M. Park and Snyder (2018). Furthermore, several fluorescence parameters and indices were calculated based on EEM data to indicate humic content and source of DOM, including humic-like fluorescence parameter (Fn(355)), protein-like fluorescence parameter (Fn(280)),

fluorescence index (FI), humification index (HIX), and Biological index (BIX). For a detailed data processing procedure, see **Appendix C**.

2.4 Statistical analysis

Microsoft Excel 2022 was used to tabulate the data and perform simple statistics such as mean and standard deviation calculations. Standard deviations of the measurements were used as experimental errors. Furthermore, a one-way ANOVA (α = 0.05) followed by a post hoc Tukey HSD analysis (α = 0.05) was performed to determine which reaction temperatures or acidic pretreatments were statistically different from each other with respect to several important parameters using an online calculator (URL: https://astatsa.com/OneWay_Anova_with_TukeyHSD/). In addition, Kendall rank correlation was used to assess monotonic relationships (whether linear or not) between two parameters at a confidence level of 95 % using MATLAB R2021b. Similarly, principal component analysis (PCA) was performed on standardised data sets (data were centred to have mean = 0 and scaled to have standard deviation = 1) to better classify TH tests based on their different reaction temperatures and acidic pretreatments using MATLAB R2021b. The experimental parameters employed encompassed the variations in the concentrations of soluble carbohydrates, proteins, HS, DOC, SCOD, ammonium, orthophosphate, solid content, colour, etc. Furthermore, the evaluation also considered changes in fluorescence indices or parameters such as HIX, FI, BIX, URI, $SUVA_{254}$, etc. For each PCA assessment, the respective contribution to the total variance in the PCA analysis of each principal component (PC) was calculated, and only the PCs which satisfied the Kaiser's rule (Kaiser, 1960) were selected to manifest PCA assessment in biplots.

2.5 PHREEQC

Equilibrium simulation was performed to predict the pH change of WAS-2 after the acidic pretreatments, using PHREEQC version 3 (USGS) and databases of phreeqc.dat and minteq.v4.dat (Parkhurst & Appelo, 2013). The pH decrease in WAS-2 after HAc addition was calculated with an ion-association model included in PHREEQC based on the theory of specific ion interaction, using soluble phase characteristics of raw WAS-2 as model input (see Solution 1 WAS-2 in **Appendix E**). In addition, the pH was simulated for TH of WAS-1 with CO_2 pressurised based on the CO_2 solubility. The built-in Peng-Robinson equation was used to calculate the CO_2 solubility at different reaction temperatures and pressures (Peng & Robinson, 1976).

Chapter 3

Results and Discussion

3.1 Effect of reaction temperature and pre-digestion on TH

To understand the main effects of both the TH temperature and the anaerobic pre-digestion on TH performance, various methods were implemented to analyse the liquid fraction of WAS-1 and DWAS-1 before and after TH. Key parameters such as COD, DOC, ammonium, orthophosphate, and macromolecules (proteins, carbohydrates, and HS) were measured to evaluate the solubilisation and the hydrolytic efficiency of TH; the sludge disintegration effect was evaluated based on the molecular weight distribution of DOM measured by HPSEC; recalcitrant compounds were characterised using fluorescence spectroscopy.

Each measured key parameter of WAS-1 and DWAS-1 depended on the reaction temperature. Two different reaction temperature ranges were applied in multiclave tests: 180 - 200 °C for TH of WAS-1 and 180 - 210 °C for TH of DWAS-1. After TH, the produced hydrolysates were sent to dewatering tests using different separation techniques: centrifuge, hydraulic press, or glass fibre filtration (for a detailed procedure, see **Section 2.2.1**). Different techniques could result in different compositions of the separated hydrolysates. Therefore, the obtained liquid fraction of hydrolysates after dewatering tests was filtered again with a syringe membrane filter (0.45 μm) for the measurement of the key parameters mentioned above.

3.1.1 Results of SCOD, DOC and DCOS

SCOD and DOC

COD solubilisation, as a primary indicator for hydrolytic efficiency, was observed initially at 180 °C for both TH of WAS-1 and DWAS-1 (**Figure 3.1 (A)**). The soluble COD (SCOD) concentration in WAS-1 hydrolysates increased at 180 - 190 °C, but no significant difference in SCOD was found for WAS-1 TH-treated at 190 - 200 °C ($p > 0.05$). However, this does not indicate that a higher degree of COD solubilisation cannot be achieved at 200 °C and above. Jeong et al. (2019) and Wilson and Novak (2009) reported TH tests of WAS at 180 - 220 and 190 - 220 °C, showing that the SCOD concentration increased at higher temperatures. In contrast to the increase in SCOD concentration, the incremental increase in DOC concentration per increase in reaction temperature was lower than that of SCOD after the initial TH at 180 °C (**Figure 3.1 (B)**). Furthermore, a slight drop in DOC concentration was observed for DWAS-1 TH-treated at 205 °C. (Fang et al., 2020; Wang et al., 2011) reported the production of CO_2, CO and a small amount of CH_4 increased with higher temperatures due to mild torrefaction and decarboxylation (Fang et al., 2020; Wang et al., 2011). This could explain the drop in DOC concentration observed in our study, but a further study of off-gas is required to confirm this carbon loss.

Regarding the effect of anaerobic pre-digestion on TH performance, we found that TH appeared to be more effective on WAS-1 than on DWAS-1. DWAS-1 requires a higher reaction temperature to reach an equivalent COD solubilisation to WAS-1. To achieve a COD solubilisation of 40 %, a temperature of 180 °C was required by WAS-1, while 190 °C was required by DWAS-1. DWAS-1 was anaerobically digested before sampling. During anaerobic digestion, biodegradable substances were degraded and converted into biogas, usually resulting in lower concentrations of VFA (**Table 3.1**), SCOD, and DOC (**Figures 3.1 (A) and (B)**). Therefore, COD and DOC were partially degraded and solubilised during the pre-digestion, explaining why the following TH treatment on DWAS-1 was not as effective as that on WAS-1. TH of DWAS-1 targets the anaerobically non-biodegradable organic compounds formed or released during the pre-digestion (X. Liu et al., 2021).

Table 3.1: The concentrations of VFA in feedstocks.

VFA (mg COD/L)	WAS-1	DWAS-1
Acetic acid (C2)	1926 ± 50	12.1 ± 0.8
Propionic acid (C3)	1750 ± 20	11.9 ± 0.3
Isobutyric acid (IC4)	366 ± 2	Undetected
Butyric acid (C4)	1560 ± 20	Undetected
Isovaleric acid (IC5)	783 ± 8	Undetected
Valeric acid (C5)	770 ± 20	Undetected
Isocaproic acid (IC6)	59.9 ± 0.7	Undetected
Caproic acid (C6)	49.3 ± 0.9	Undetected

To justify the characteristics of WAS-1 measured in our study, we compared WAS-1 with other raw WAS used in previous studies and found that the concentrations of SCOD, ammonium, and orthophosphate in raw WAS-1 were exceptionally high (**Table 3.2**). This was due to a delayed feedstock characterisation. Freshly collected WAS-1 and DWAS-1 were used for TH tests at different reaction temperatures and then stored in a fridge at 4 °C. The characterisation of WAS-1 and DWAS-1 was conducted after long-term anaerobic storage. During the storage, hydrolysis of biodegradable substances was likely to occur, which increased the SCOD concentration in WAS-1. Therefore, the original WAS-1 used for TH tests is presumed to contain a lower concentration of SCOD than the measured result. The COD solubilisation after TH could be underestimated.

Table 3.2: Comparison in characteristics of raw WAS obtained in other studies with WAS-1.

Raw WAS reference	SCOD (mg O_2/L)	TCOD (mg O_2/L)	TS (%)	Ammonium (NH_4^+-N/L)	Orthophosphate (mg PO_4^{3-}-P/L)
WAS-1 (used in our study)	6130 ± 40	$54{,}200 \pm 300$	3.94 ± 0.02	680 ± 6	844 ± 4
Jeong et al. (2019)	1690	51,210	4.99	160.00	Not available
Wilson and Novak (2009)	820 ± 10	$65{,}700 \pm 4300$	6.0	100	Not available
Toutian et al. (2020)	1225 ± 601	$95{,}133 \pm 9265$	7.2 ± 0.1	112 ± 8	380 ± 150

DCOS

The dissolved carbon oxidation state (DCOS) reflects the mean oxidation state of DOC in the samples (**Figure 3.1 (C)**). Different biomass or organic waste corresponds to different carbon oxidation states (COS) (**Figure 3.1 (E)**). Generally, COS can predict the biogas composition, that is, the ratio between CH_4 and CO_2 (**Figure 3.1 (D)**). Theoretically, the lower the COS is, the more CH_4 will be produced relative to CO_2 (Angelidaki et al., 2011). Therefore, DCOS is used to evaluate the methane potential of hydrolysates in the soluble phase. Only the liquid fraction of hydrolysed sludge is sent to AD treatment in the design of TORWASH®.

As shown in **Figure 3.1 (C)**, WAS-1 had a positive DCOS of 0.48 $\pm$ 0.03, representing the oxidation state of organic carbon in the soluble fraction of raw WAS-1. The soluble fraction of WAS is mainly composed of soluble microbial products and loosely bound EPS. Urrea et al. (2016) found that the COS was 0.04 for soluble microbial products and 0.03 for loosely bound EPS, which are lower than the DCOS of WAS-1 (0.48 $\pm$ 0.03). This suggests that oxidised molecules, such as organic acids or amino acids, were formed during the storage of WAS-1 (**Figure 3.1 (D)**). In addition, we found that the DCOS decreased after anaerobic pre-digestion from 0.48 $\pm$ 0.03 (WAS-1) to -0.83 $\pm$ 0.03 (DWAS-1). This suggests that the organic carbon in the liquid fraction of WAS-1 was reduced during digestion. The reduction could result from the consumption of biodegradable substances with DCOS $\geq$ 0 (acetic acid, DCOS = 0) and the release of tightly-bound EPS (DCOS = -0.55, Urrea et al. (2018)). Moreover, the formation of aromatics, such as humic substances (HS, DCOS = -0.4 to -0.03, Kroll et al. (2011)), could also contribute to the decrease in DCOS during anaerobic digestion (**Figure 3.1 (D)** and **Figure 3.5 (A)**). Overall, the raw WAS-1 was hydrolysed to a limited extent during storage, and more reduced organic carbon was observed after anaerobic digestion.

Regarding the change in DCOS during TH, we found WAS-1 and DWAS-1 responded differently to the initial TH at 180 °C; DOC in WAS-1 was reduced after TH (i.e., increase in DCOS), whereas DWAS-1 was oxidised (i.e., decrease in DCOS), as shown in **Figure 3.1 (C)**. In addition, the DCOS of hydrolysates decreased with increasing reaction temperatures for TH of WAS-1 and DWAS-1 (omitting the hydrolysate of DWAS-1 at 200 °C as an outlier). The DCOS change during TH could result from a combined behaviours of carbohydrates (COS $\approx$ 0, **Figure 3.1 (D)**), proteins (1 < COS < 0, **Figure 3.1 (D)**), and HS (DCOS = -0.4 to -0.03, Kroll et al. (2011)). A negative correlation was found between the HS concentration and DCOS, Tau-b = -0.6, $p < 0.05$, as shown in **Figure 3.2**, Tau-b is Kendall's tau-b correlation coefficient. Increased production of HS at higher reaction temperatures could lower the overall DCOS and anaerobic biodegradability (**Figure 3.5 (A)**). Therefore, the reduction in DCOS does not necessarily result in an increased ratio of CH_4 in biogas generated from the liquid fraction of the hydrolysed (**Figure 3.1 (C)**).

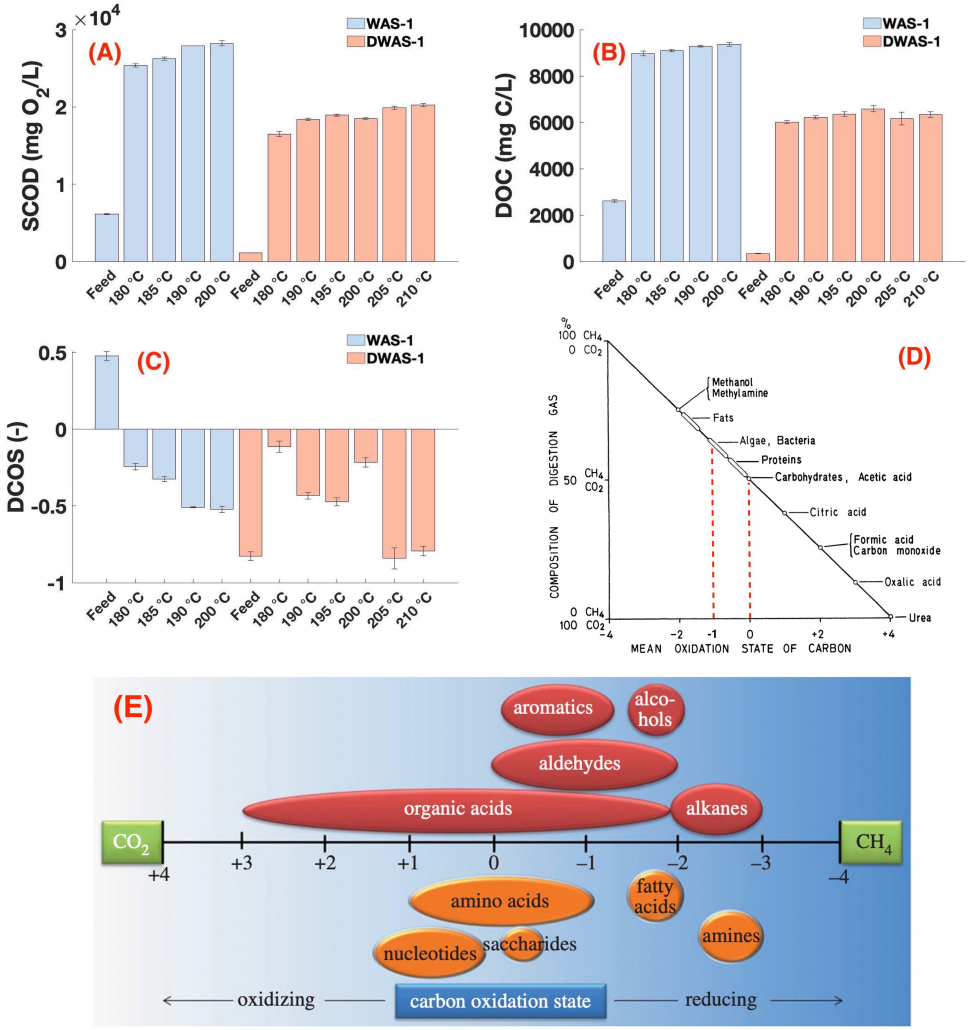

Figure 3.1: Effects of reaction temperatures on SCOD (A), DOC (B) and DCOS (C) of thermally-hydrolysed WAS-1 and DWAS-1 from multiclave. (D): Composition of the digestion gas vs. the mean oxidation state of the carbon in the substrate (Gujer & Zehnder, 1983). (E): Illustration of the range of oxidation states of carbon in common bio-molecules and other organic compounds (Amend et al., 2013).

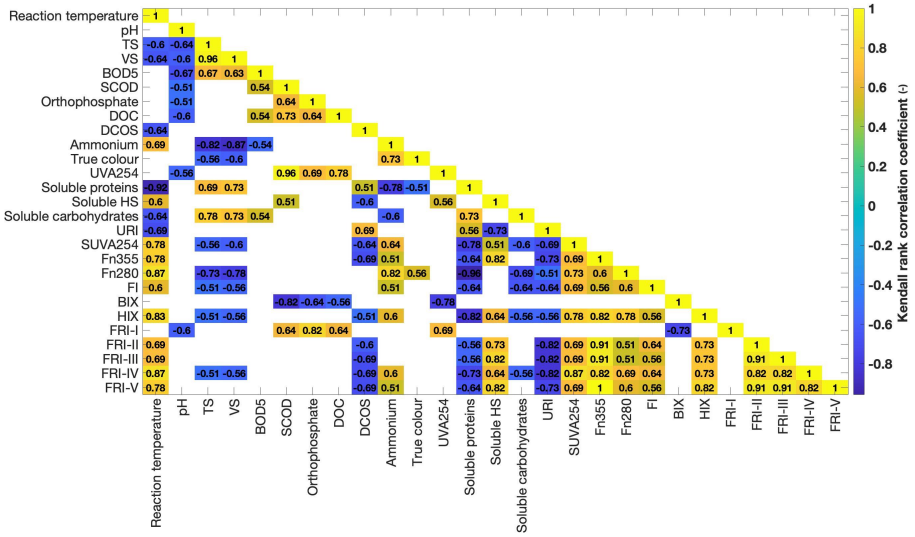

Figure 3.2: Heatmap of Kendall rank correlation coefficient for WAS-1 and DWAS-1 subjecting to TH at different reaction temperatures. Insignificant correlations ($p > 0.05$) are shown as blank cells.

3.1.2 Results of in ammonium and orthophosphate

Ammonium

The result of ammonium change is shown in **Figure 3.3 (A)**. We found that the ammonium concentration in raw WAS-1 was higher than that of WAS-1 hydrolysates produced at 180 - 200 °C, and a significant increase in ammonium concentration only occurred at 200 °C. This differs from what Wilson and Novak (2009) observed; the ammonium concentration increased during TH of WAS at 130 - 220 °C compared with raw WAS. During TH, ammonia could be produced from the cleavage of amine functional groups of amino acids and the destruction of the peptide bonds (Wilson & Novak, 2009). The produced ammonia can react with water, producing ammonium and hydroxide, but in the meantime, ammonium can dissociate and reproduce ammonia. This process depends on the dissociation constant (pKa) of ammonium and pH (**Figure 3.3 (C)**). The pKa of ammonium decreases with increasing temperature. Therefore, more ammonia will present at higher temperatures relative to ammonium. Also, the solubility of ammonia in water decreases with increasing temperature (Engineering ToolBox, 2008). Hence, some ammonia can be lost in the air phase when depressurising the reactor. The ammonia loss may explain the ammonium drop after TH of WAS-1. However, ammonia loss was not observed in TH of DWAS-1 at 180 - 220 °C. Instead, we found that ammonium concentration in DWAS-1 hydrolysates increased with elevated reaction temperature, especially at 195 °C and above, although the ammonium concentration in raw DWAS-1 was inherently higher than that of raw WAS-1. The increase in ammonium concentration indicates the hydrolysis of protein. As shown in **Figure 3.5 (B)**, the concentration of soluble proteins decreased with increasing reaction temperature, suggesting proteins could partially be hydrolysed during TH treatment. However, it is unclear why the ammonia release due to TH was more pronounced for WAS-1 than for DWAS-1. We can speculate that the protein hydrolysis is not the main contributor to the decrease in soluble proteins concentration for WAS-1 TH-treated at 180 - 200 °C.

Orthophosphate

The phosphorus transformation during TH is more complex than that of ammonium-nitrogen. As shown in **Figure 3.4**, soluble orthophosphate can derive from the hydrolysis of organophosphate and polyphosphate or the dissolution of amorphous phosphates. Meanwhile, soluble orthophosphate can be adsorbed or precipitated with minerals, forming Ca/Fe/Al-associated P species (Fang et al., 2020). The adsorption and precipitation of orthophosphate are pH-dependent Yu et al. (2021). As shown in **Figure 3.2**, a negative weak correlation was found between orthophosphate concentrations and pH, Tau-b = -0.51, $p < 0.05$. In addition, we found that orthophosphate concentration decreased after anaerobic pre-digestion, along with an increase in pH (**Figures 3.3 (B) and (D)**). More orthophosphate could precipitate at higher pH, resulting in a lower concentration of soluble orthophosphate. The pH increased after anaerobic pre-digestion from 6.1 (raw WAS-1) to 7.7 (raw DWAS-1) could result from the depletion of VFA (**Table 3.1**) and the production of ammonia from protein hydrolysis (**Figure 3.3 (A)**).

Regarding the effect of reaction temperature on phosphorus transformation, we found that the orthophosphate concentration in raw WAS-1 was higher than that of WAS-1 hydrolysates (**Figure 3.3 (B)**). The possible explanation is the delayed feedstock characterisation. During the long-term storage of WAS-1, orthophosphate could be released from polyphosphate stored in the polyphosphate-accumulating organism under anaerobic conditions (Seviour et al., 2003), which increased the orthophosphate concentration in raw WAS-1. Leaving the interference of the delayed characterisation aside, the orthophosphate concentration was generally insusceptible to the reaction temperature (**Figure 3.3(B)**): no significant differences ($p > 0.05$) were found for WAS-1 TH-treated at 180 - 190 °C, and only mild fluctuation (640 $\pm$ 10 mg PO_4^{3-}-P/L) was observed for DWAS-1 TH-treated at 180 - 210 °C. Overall, the phosphorus release was not well observed in TH of WAS-1 or DWAS-1 under TORWASH® conditions.

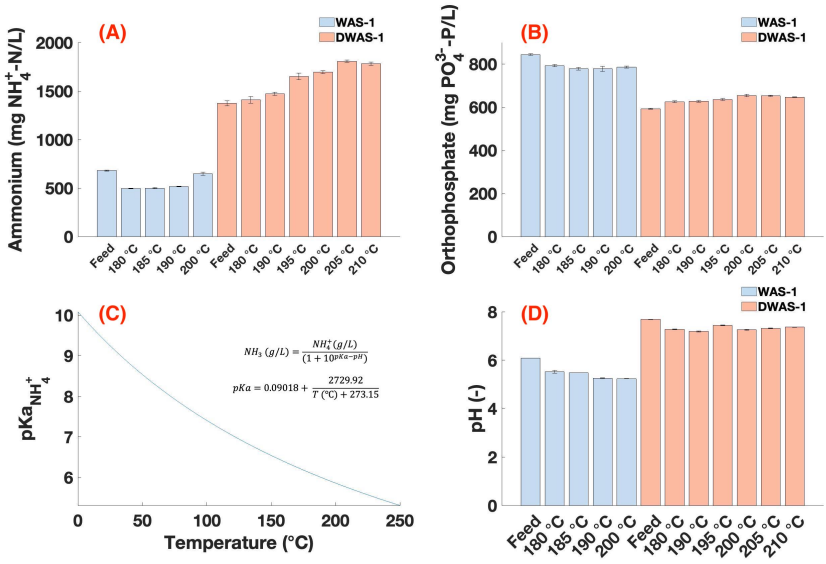

Figure 3.3: Effects of reaction temperatures on the concentrations of ammonium (A), orthophosphate (B), and pH (D) of thermally-hydrolysed WAS-1 and DWAS-1. (C): Temperature affecting the dissociation constant (pKa)for ammonium (Isaksson, 2018).

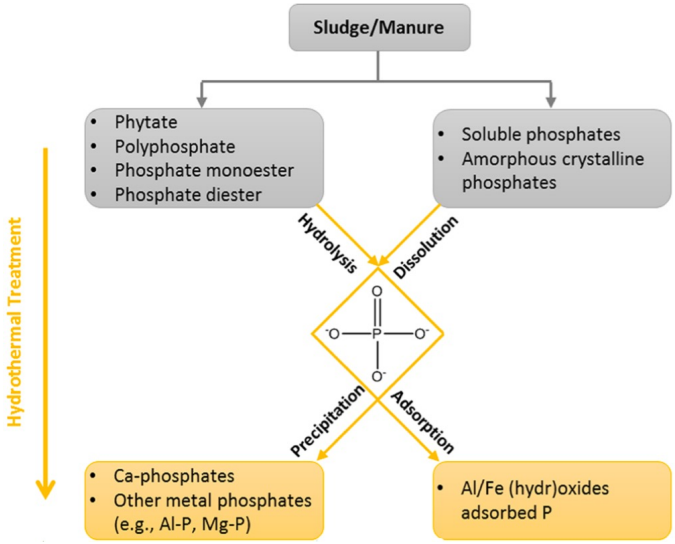

Figure 3.4: Schematic illustration of the mechanisms of phosphorus transformation during TH of sludge and manure proposed by Fang et al. (2020).

3.1.3 Results of soluble proteins, carbohydrates, and HS

Soluble proteins

Soluble proteins concentration were strongly affected by TH at 180 °C and above, as shown in **Figure 3.5 (B)**. Soluble proteins concentration decreased monotonically with increasing reaction temperature: a strong negative correlation was found between these two variables, Tau-b = -0.92, $p < 0.05$ (**Figure 3.2**). This suggests that protein degradation is the dominant process under TORWASH® conditions. During TH, both protein hydrolysis and denaturation take place. Wilson and Novak (2009) stated that the proteins (BSA) could be hydrolysed into smaller molecular weight peptides, individual amino acids, and VFA in a temperature range of 130 - 220 °C. In addition, ammonium was often produced during protein hydrolysis (Wilson & Novak, 2009). However, the ammonium concentration in WAS-1 hydrolysates, produced at 180 - 200 °C, remained relatively constant (**Figure 3.3 (B)**). Thus, the denaturation could be the primary process for protein degradation for TH of WAS-1. The denaturation of proteins often occurs at 75 °C and above (De Graaf, 2000). The denatured proteins could precipitate irreversibly, corresponding to a decrease in soluble proteins concentration (Neyens et al., 2004). In addition, considering the presence of carbohydrates in the WAS-1 and DWAS-1, part of the proteins could participate in the Maillard reaction (Gonzalez et al., 2018), further decreasing the soluble proteins concentration.

Soluble carbohydrates

Compared with the change in soluble proteins concentration, a different trend was found in soluble carbohydrates concentration (**Figure 3.5 (C)**), which initially increased but then decreased with a further increase in reaction temperature. This carbohydrates behaviour suggests that the predominant process in polysaccharides was initially solubilisation at lower reaction temperatures, until reaching maxima at 185 and 195 °C for TH of WAS-1 and DWAS-1, respectively. The subsequent decrease could result from the Maillard and caramelisation reactions. Wilson and Novak (2009) reported that the caramelisation occurred at 190 °C and above. Therefore, competition for carbohydrates between the

Maillard and caramelisation reactions could occur. The competition depends on reaction temperatures and available reactants such as mono- or dimeric reducing sugars. As reaction temperature increased, more non-reducing long-chain polysaccharides could be hydrolysed into mono- or dimeric reducing sugars, providing more ideal reactants for the Maillard and caramelisation reactions (Wilson & Novak, 2009).

Additionally, the phenol sulfuric acid method used in our present study could overestimate the concentration of soluble carbohydrates in WAS-1 and DWAS-1 hydrolysates. This method measured not only soluble carbohydrates but also the furfural derivatives produced from Maillard and caramelisation reactions. Therefore, the measured result included soluble carbohydrates and furfural. However, it is difficult to evaluate the conversion between carbohydrates and furfural based on current results. A further study is required to investigate how reaction temperature affects the furfural production during TH of WAS.

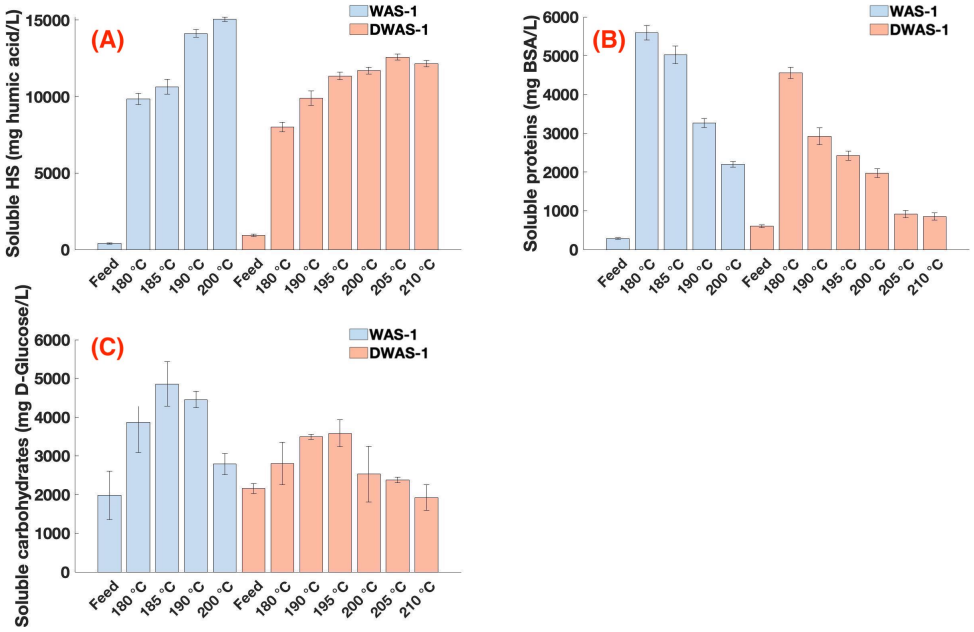

Figure 3.5: Effects of reaction temperatures on the concentrations of soluble HS (A), soluble proteins (B), and soluble carbohydrates (C) of thermally-hydrolysed WAS-1 and DWAS-1.

Soluble HS

As mentioned above, the Maillard reaction consumes proteins and carbohydrates during TH. The products from the Maillard reaction are considered HS-like or potential HS precursors. Specifically speaking, these products are primarily melanoidins, produced in the final stage of the Maillard reaction, known as synthetic humic acid (Blondeau, 1989; Cooper et al., 2019; Nakaya & Nakashima, 2016).

As shown in **Figure 3.5 (A)**, substantial production of HS was observed after the initial TH at 180 °C: the soluble HS concentration in WAS-1 and DWAS-1 increased from 400 ± 40 to 9800 ± 400 mg/L and from 930 ± 70 to 8000 ± 300 mg/L, respectively. When the reaction temperature was increased from 180 to 190 °C, the soluble HS concentration in WAS-1 hydrolysate further increased by 44 %. Correspondingly, a 50 % increase was

observed in colour content (**Figure 3.8 (A)**) and 25 % in UVA_{254} (**Figure 3.8 (B)**), suggesting a further production of melanoidins at 190 °C. In addition, a progressive increase in soluble HS concentration in DWAS-1 hydrolysates was observed at 180 - 205 °C and no further increase at 205 - 210 °C.

3.1.4 Results of HPSEC

The results of HPSEC are shown in **Figure 3.6**. UV-absorbing DOM in the liquid phase of thermally-hydrolysed WAS-1 or DWAS-1 were separated based on the hydrodynamic radius, then successively detected at 210 and 254 nm. The DOM in samples was divided into several fractions: > 30 kDa, 20 - 30 kDa, 10 - 20 kDa, 3.5 - 10 kDa, 1 - 3.5 kDa, and 0.1 - 1 KDa, and < 0.1 kDa. The molecular weight distribution results obtained at UV 210 and 254 nm were rather similar. The fraction of DOM < 0.1 kDa increased progressively at higher reaction temperatures, whereas the fractions of 10 - 20, 3.5 - 10, and 1 - 3.5 kDa decreased as temperature increased. Interestingly, the molecular weight fraction 0.1 - 1 kDa remained relatively stable when subjected to different reaction temperatures: no significant difference ($p > 0.05$) was found in this fraction at UV 210 nm for WAS-1 TH-treated at 180 - 200 °C. Overall, high molecular weight DOM was disintegrated into small molecular weight DOM under TORWASH® conditions. In addition, Dwyer et al. (2008) and Y. Liu et al. (2015) reported that high molecular weight recalcitrant compounds, such as melanoidins > 10 kDa, could be formed at 140 °C and above. However, in our study, no significant differences were found in DOM fraction > 10 kDa for WAS-1 TH-treated at 180 - 200 °C at UV 210 and 254 nm, and only a decrease was found in fraction > 10 kDa for DWAS-1 TH-treated at 180 - 210 °C at UV 210 and 254 nm. This does not indicate the absence of polymerisation under TORWASH®. The molecular weight distributions obtained from HPSEC only qualitatively determine the proportion of each molecular weight fraction. Therefore, the polymerisation is likely to occur during TH, but compared to the disintegration effect of TH, the polymerisation can not be well observed. Moreover, Mohsin et al. (2018) reported that insoluble melanoidins were produced at 150 °C for TH of D-glucose and L-alanine. Therefore, it is possible that high molecular weight recalcitrant compounds could precipitate out of the soluble phase. Overall, the stronger sludge disintegration occurred at higher reaction temperatures. Once the sludge aggregates are disintegrated, organic compounds are concomitantly solubilised. This facilitates the hydrolysis of particulate organics and macromolecules in the following AD treatment (Nazari et al., 2017; Zhen et al., 2017).

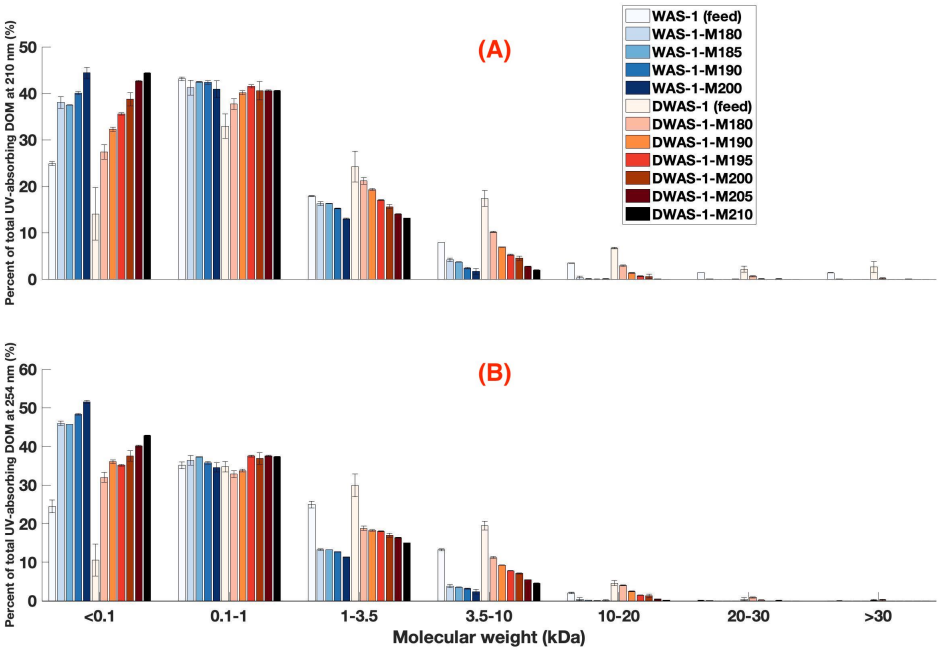

Figure 3.6: Effect of reaction temperature on the size fractionation of UV-absorbing DOM at 210 (A) and 254 nm (B) for TH of WAS-1 and DWAS-1.

3.1.5 Results of BMP and BOD tests

BMP

BMP tests were conducted on filtrated hydrolysates, WAS-1-A190 and DWAS-1-A205, and feedstocks, WAS-1 and DWAS-1, for assessment of anaerobic biodegradability. Due to the large amount of sample required by AMPTS-II, the volumes of hydrolysates produced from multiclave were insufficient for BMP tests. Therefore, the following results focus on the effect of anaerobic pre-digestion on TH performance.

As shown in **Figure 3.7(A)**, no significant difference in BMP was found between WAS-1 (raw) and WAS-1-M190, indicating the BMP was not improved after TH at 190 °C. This conflicts with the previous study by Jeong et al. (2019) that the BMP in WAS hydrolysates increased after TH at 180 - 220 °C compared with raw WAS. However, the total methane production reported by Jeong et al. (2019) included both liquid and solid fractions of WAS hydrolysates. In contrast, our study only considers the liquid fraction to simulate the TORWASH® process, in which only the liquid fraction is used for AD treatment. Therefore, The hydrolysates, WAS-1-A190 and DWAS-1-A205 produced from 20 L autoclave, were filtered with a glass fibre filter (pore size 2.7 μm) before BMP tests. As shown in **Table 3.3**, solids were lost after filtration. The methane potential in the solid fraction of WAS-1 would also increase after TH at 190 °C. D. Yang et al. (2019) reported that the BMP in the liquid fraction of WAS hydrolysates, produced at 160 °C, could account for 62 - 94 % of the BMP of raw sludge and 51 - 73 % of the sum of BMP in both liquid and solids fractions. Therefore, the dry AD process is suggested as the post-treatment for the solid fraction of WAS hydrolysates to increase methane production further.

By comparing WAS-1 with DWAS-1, anaerobic pre-digestion resulted in reduced methane production. During pre-digestion, VFA and SCOD were consumed (**Table 3.1** and **Figure**

Table 3.3: Solid content of the substrates for BMP tests.

Sample	TS (%)	VS (%)	VS/TS (%)
WAS-1	3.94	3.04	77.15
WAS-1-A190 (filtrate)	2.25	1.81	80.46
DWAS-1	3.94	2.86	72.59
DWAS-1-A205 (filtrate)	1.37	1.06	76.79

3.1 (A)), resulting in lower ultimate methane production of raw DWAS-1 than that of raw WAS-1. In addition, for TH at 205 °C, higher BMP was achieved in DWAS-1-A205 compared with raw DWAS-1, suggesting TH of anaerobically pre-digested WAS increased the anaerobic biodegradability of the digestate.

Interestingly, no significant difference ($p > 0.05$) was found between WAS-1-A190 and DWAS-1-A205 (**Figure 3.7(A)**), suggesting that the liquid fraction of DWAS-1 could reach an equivalent degree of anaerobic biodegradability as that of WAS-1 by applying a higher reaction temperature. Nielsen et al. (2011) found that the final methane yield increased by 18 % when WAS anaerobically pre-digested at 37 °C for 19 days before TH at 170 °C for 15 min. Therefore, the application of inter-staged TH (AD-TH-AD) may further increase biogas production. However, evaluating the final methane potential for TH with anaerobic pre-digestion is difficult. We do not have the information on how much methane was produced during the anaerobic pre-digestion of WAS-1. The exact anaerobic pre-digestion conditions (e.g., time and temperatures) were also unknown. In addition, the BMP results above should be rejected for any quantitative analysis. The relative standard deviation of the BMP in the blank samples was above 5 %, which did fulfil the criteria for the BMP results assessment proposed by Holliger et al. (2016).

BOD

Additionally, BOD_5 was measured to assess the effect of TH on aerobic biodegradability. As shown in **Figure 3.7(B)**, BOD_5 increased after the initial TH of WAS-1 at 180 °C, and no significant differences were found in BOD_5 for WAS-1 TH-treated at 180 - 200 °C. Therefore, the aerobic biodegradability in the soluble phase of thermally hydrolysed WAS-1 stayed relatively constant under TORWASH®. In contrast, a different result was observed for DWAS-1 samples. BOD_5 in DWAS-1 hydrolysates increased with increasing reaction temperature, reaching a maximum value at 190 °C, decreased at 195 - 200 °C, and then mildly increased again at 205 °C. The decrease in BOD_5 could be interpreted as the potential production of recalcitrant compounds that were aerobically non-biodegradable, e.g., melanoidins. Additionally, for TH of DWAS-1, the drastic decrease in BOD_5 at 200 °C coincides with the reduction in soluble carbohydrates concentration at 200 °C. The products of caramelisation could be the source of aerobically non-biodegradable compounds. Moreover, the increase in BOD_5 at 205 °C suggests a potential degradation of recalcitrant compounds.

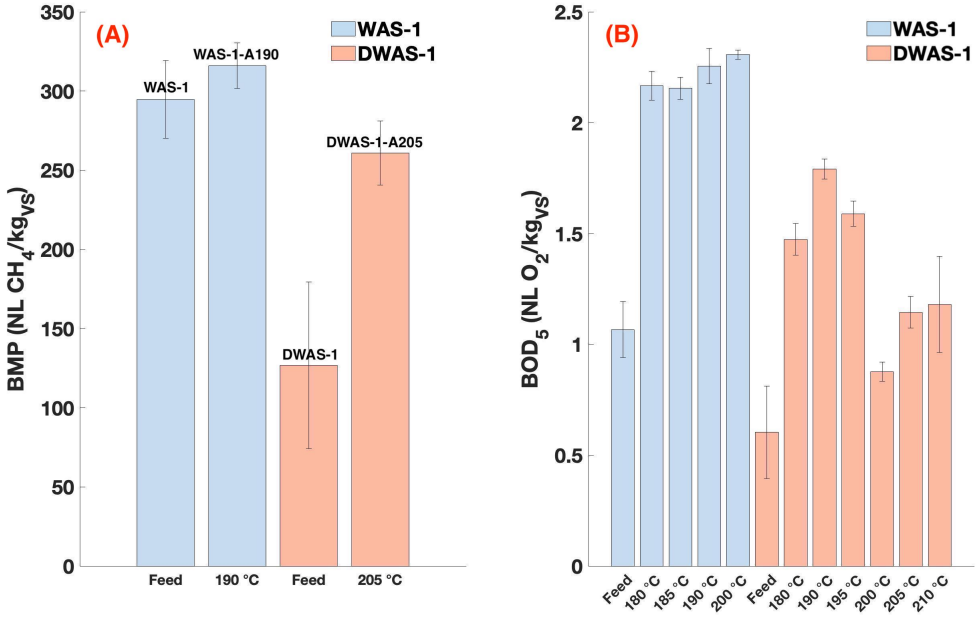

Figure 3.7: Effects of reaction temperatures on the concentration of BOD_5 (A) and BMP (B) of thermally-hydrolysed WAS-1 and DWAS-1. Note: the filtered hydrolysates, used for BMP tests, were produced from 20 L autoclave TH tests; the hydrolysates produced from multiclave were used for BOD tests. BMP and BOD are expressed as the volume of dry methane gas and oxygen gas under standard conditions (273.15 K and 101.33 kPa) per mass of volatile solids (VS) added, respectively.

3.1.6 Results of colour, UVA_{254}, URI and $SUVA_{254}$

Surrogate parameters, such as colour, UVA_{254}, URI and $SUVA_{254}$, were chosen to indirectly analyse the hydrophobicity, aromaticity, and certain chemical functions of the recalcitrant compounds (Faixo et al., 2021).

Colour
The liquid fraction of the WAS-1 and DWAS-1 appeared to be brownish after TH at 180 °C and above. Bougrier et al. (2008) suggested that colour formation was associated with the production of coloured matter such as Amadori products and melanoidins from the Maillard reaction. Melanoidins are produced by polymerising low molecular weight intermediates from Maillard reactions (Zhang et al., 2020). Dwyer et al. (2008) reported that the melanoidins formation was reliant on the reaction temperature, and they found that the colour increased for WAS TH-treated at 140 - 165 °C. As shown in **Figure 3.8 (A)**, a drastic increase in colour (by approximately 40 %) was observed for TH of WAS-1 at 185 - 190 °C. However, with a further increase in reaction temperature (> 190 °C), the content of coloured matter stayed relatively constant: colour = 13,600 $\pm$ 200 mg Pt-Co/L for WAS-1 TH-treated at 190 - 200 °C, 19,100 $\pm$ 600 for DWAS-1 TH-treated at 190 - 210 °C. Theoretically, more melanoidins are produced at higher temperatures, increasing the colour content. Mohsin et al. (2018) suggested that melanoidins produced at higher reaction temperatures could be insoluble, which no longer contribute to the browning in the liquid phase.

UVA_{254}
An increase in UVA_{254} occurred at above 180 °C, as shown in **Figure 3.8 (B)**, suggesting increased production of UV-absorbing DOM with conjugated double bonds (C=O and C=C) and aromatic structures, e.g., furfural, hydroxymethylfurfural and melanoidins (Ignatev & Tuhkanen, 2019). In addition, a drastic increase in UVA_{254} was observed for TH of WAS-1 at 185 - 190 °C, and a progressive increase in UVA_{254} was found for DWAS-1 TH-treated at 180 - 195 °C. This somehow fits the postulation of Gonzalez et al. (2018) that further production of recalcitrant compounds could occur at around 190 °C for TH of WAS

URI
Mean URI values (UVA_{210}/UVA_{254}) were obtained from chromatograms of HPSEC at UV 210 and 254 nm, indicating the relative density between aliphatic functional groups and conjugated double bonds. Generally, proteinaceous compounds (more aliphatic but less aromatic) correspond to higher URI values than humic substances (more conjugated double bonds and more aromatic) (Ignatev & Tuhkanen, 2019; Trubetskaya et al., 2020). As shown in **Table 3.4**, a negative correlation between reaction temperature and URI value was found, Tau-b = -0.69, $p < 0.05$, indicating that more HS-like or aromatic compounds were generated in the soluble fraction of hydrolysates at higher reaction temperatures for TH of WAS-1 and DWAS-1 (**Figure 3.8 (C)**). Furthermore, URI values were found positively correlated with soluble proteins concentration (Tau-b = 0.56, $p < 0.05$), but negatively correlated soluble HS concentration (Tau-b = -0.73, $p < 0.05$), which was in line with the study of Her et al. (2008). In addition, The URI value of WAS-1 was three times higher than that of DWAS-1, suggesting that DOM was converted from non-aromatic to aromatic groups during anaerobic pre-digestion.

Table 3.4: URI values of standard/reference materials (Her et al., 2008).

Compounds	URI	Aromaticity
Suwannee River humic acid (SRHA) reference material (1R101H)	1.59	Highest
Suwannee River fulvic acid (SRFA) standard material (1S101F)	1.88	Intermediate
BSA (molecular weight ~ 70,000 Da)	13.5	Lowest

$SUVA_{254}$

Specific ultraviolet absorbance at 254 nm ($SUVA_{254}$) is another specific indicator of aromaticity of DOM, a property of recalcitrance (Ignatev & Tuhkanen, 2019). SUVA > 4 indicates mainly hydrophobic and especially aromatic DOM; SUVA < 3 indicates mainly hydrophilic DOM (Nguyen et al., 2020). As shown in **Figure 3.8 (D)**, the hydrolysates of WAS-1 and DWAS-1 had SUVA values below 2, suggesting they contained mainly hydrophilic DOM. Furthermore, a positive correlation was found between reaction temperature and SUVA value, Tau-b = 0.54, $p < 0.05$. More DOM was transformed from hydrophilic to hydrophobic and aromatic (humic/fulvic-like) at higher reaction temperatures. Additionally, $SUVA_{254}$ values exhibited a negative correlation with URI values, Tau-b = -0.69, $p < 0.05$ (**Figure 3.2**), which was in line with the finding of Her et al. (2008), however, they suggested a further verification of this relationship. Moreover, the $SUVA_{254}$ (UVA_{254}/DOC) of raw WAS-1 was the lowest compared with other samples due to its relatively low UVA_{254}. In addition, the $SUVA_{254}$ decreased after anaerobic pre-digestion. In line with the results of URI, hydrophobicity and aromaticity of DOM increased during anaerobic pre-digestion.

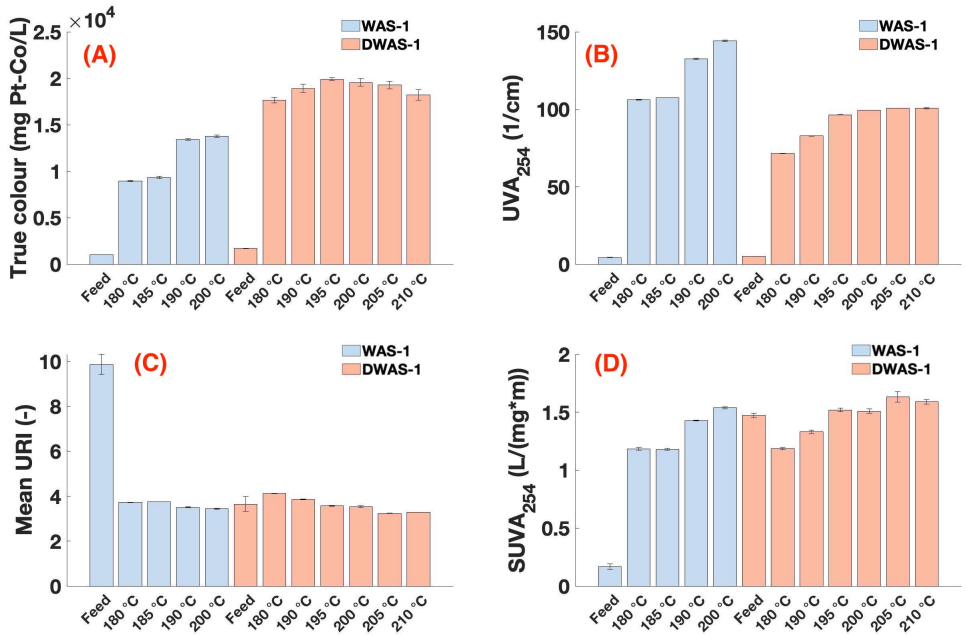

Figure 3.8: Effects of reaction temperatures on the concentration of true colour (A), UVA_{254} (B), URI (C) and $SUVA_{254}$ (D) of thermally-hydrolysed WAS-1 and DWAS-1.

.

3.1.7 Fluorescence EEM

Fluorescence regional integration
The obtained fluorescence Excitation emission matrices (EEMs) were delineated into five fluorescent regions (I-V) according to **Table C.1**. Fluorescence regional integration (FRI) was then calculated within each region to pseudo-quantify the relative DOM content in the defined region. Among the five regions, tyrosine-like protein (I) and soluble microbial byproduct-like matter (IV) were considered biodegradable, whereas tryptophan-like protein (II), fulvic acid-like matter (III), and humic acid-like matter (V) were regarded as non-biodegradable (Jia et al., 2013).

As shown in **Figure 3.9 (A)**, the total FRI of WAS-1 was around 50 % lower than that of DWAS-1, suggesting that the overall DOM content decreased during anaerobic pre-digestion. Specifically, we found that the FRI of tyrosine-like protein (I), tryptophan-like protein (II), and soluble microbial byproduct-like matter (IV) decreased by 74 %, 32 %, and 67 %, respectively. The reduction of tyrosine-like protein was more pronounced than that of tryptophan-like protein. This was in line with the study of (Jia et al., 2013) that the biodegradability of tyrosine-like protein was higher than that of tryptophan-like protein. In addition, we found that the FRI of fulvic-acid like matter (III) and humic-acid like matter (V) increased by 58 % and 50 % after anaerobic pre-digestion, respectively. This was consistent with the results of soluble HS concentration (**Figure 3.5 (A)**), indicating a humification of DOM during the anaerobic pre-digestion.

For the initial TH at 180 °C, the total FRI in hydrolyses of WAS-1 and DWAS-1 increased by 9 and 10 times concerning raw WAS-1 and DWAS-1. We observed that the total FRI of WAS-1 and DWAS-1 hydrolysates progressively increased with increasing reaction temperatures, except for WAS-1 TH-treated at 185 °C and DWAS-1 at TH-treated 210 °C. The increase in total FRI was mainly attributed to the increase in FRI of tryptophan-like protein (II), fulvic acid-like matter (III) and humic acid-like matter (V). A two-fold increase was found in FRI of fulvic acid-like matter (III) and humic acid-like matter (V) for WAS-1 TH-treated at 185 - 190 °C, suggesting that a temperature of 190 °C was critical for the production of humic acid-like matter and fulvic acid-like matter for TH of WAS-1. In addition, the percent fluorescence response was calculated, as shown in **Figure 3.9 (B)**, representing the fraction of FRI in the individual region with respect to total FRI. We found that the fulvic acid-like matter was the major component of HS, accounting for around 70 % of the sum of fulvic acid-like matter and humic acid-like matter. Moreover, the fraction of soluble microbial byproduct-like (IV) was relatively insusceptible to the reaction temperature applied.

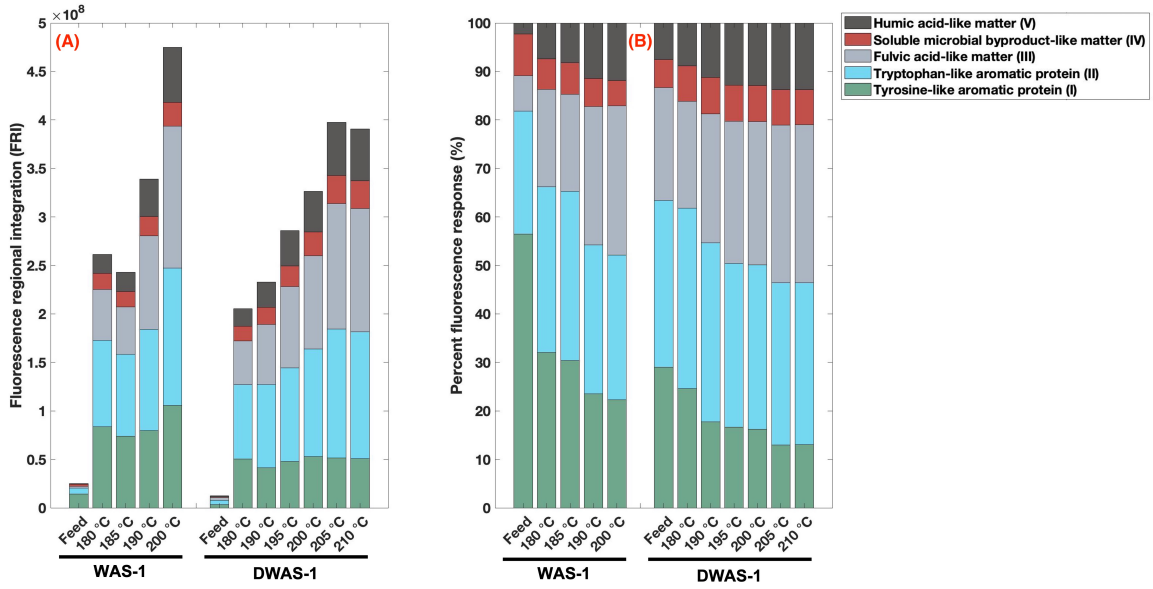

Figure 3.9: FRI (A) and distribution of FRI (B) in nonfractionated DOM from thermally-hydrolysed WAS-1 and DWAS-1 at different reaction temperatures. (B): the percent fluorescence response is the ratio of FRI of specific region to the total FRI (FRI_{I-V}/FRI_{total}.

Distribution of HIX, BIX and FI

Fluorescence indices, humidification index (HIX), biological index (BIX), and fluorescence index (FI) provided additional information for understanding the effect of reaction temperature on the properties and sources of the DOM.

HIX qualitatively assesses the degree of humification of humic acid. HIX < 4 suggests that the DOM in aqueous samples are mainly produced by microorganisms with low humification extent (Huguet et al., 2009). **Figure 3.10 (A)** shows the distribution between HIX and BIX. The HIX values were maintained in a range of 1.0 - 2.4 for WAS-1 and DWAS-1 hydrolysates, exhibiting a low degree of DOM humification characteristics. Furthermore, a positive correlation was found between HIX value and reaction temperature, Tau-b = 0.83, $p < 0.05$ (**Figure 3.2**), suggesting that the elevation in reaction temperature could facilitate the humification process during TH.

In comparison with HIX, biological index (BIX) values (**Figure 3.10 (A)**) stayed relatively constant: BIX = 0.91 $\pm$ 0.04 for WAS-1 TH-treated at 180 - 200 °C; BIX = 1.24 $\pm$ 0.02 for DWAS-1 TH-treated at 180 - 210 °C. BIX reflects the microorganism's contribution to DOM (Huguet et al., 2009). The BIX values of hydrolysates WAS-1 and DWAS-1 were both greater than 0.8, indicating that DOM was mainly endogenous DOM produced by microorganisms (Jin et al., 2020). Moreover, DWAS-1 hydrolysates had higher BIX values than those of WAS-1 hydrolysates, displaying stronger autogenetic characteristics in DOM (Zhou et al., 2019).

Figure 3.10 (B) shows the distribution between HIX and fluorescence index (FI) to further evaluate the source of DOM, whether it was from a terrestrial origin (FI $\leq$ 1.4), a microbial origin (F $\geq$ 1.9) or a mixed origin in-between (1.4 < FI < 1.9) (Birdwell & Engel, 2010). The FI values of hydrolysates of WAS-1 and DWAS-1 were both higher than 1.8

except for WAS-1-M185, FI = 1.74, implying that the DOM mainly came from the metabolic process of microorganisms (e.g. extracellular release substances of microbes) (Mcknight et al., 2001). In addition, FI exhibited an increasing trend at higher reaction temperatures; this was associated with increased solubilisation of microbially-derived material.

Based on the two distributions of HIX, FI and BIX (**Figure 3.10**), potential clustering of the hydrolysates was achieved according to the reaction temperature applied. Both distributions demonstrated two clear clusters in blue circles for the hydrolysates of WAS-1, suggesting a critical change in the properties in DOM at 190 °C. Furthermore, **Figure 3.10 (B)** exhibited two more clusters in red circles for separating the hydrolysates of DWAS-1, suggesting a critical change in the properties of DOM at above 200 °C.

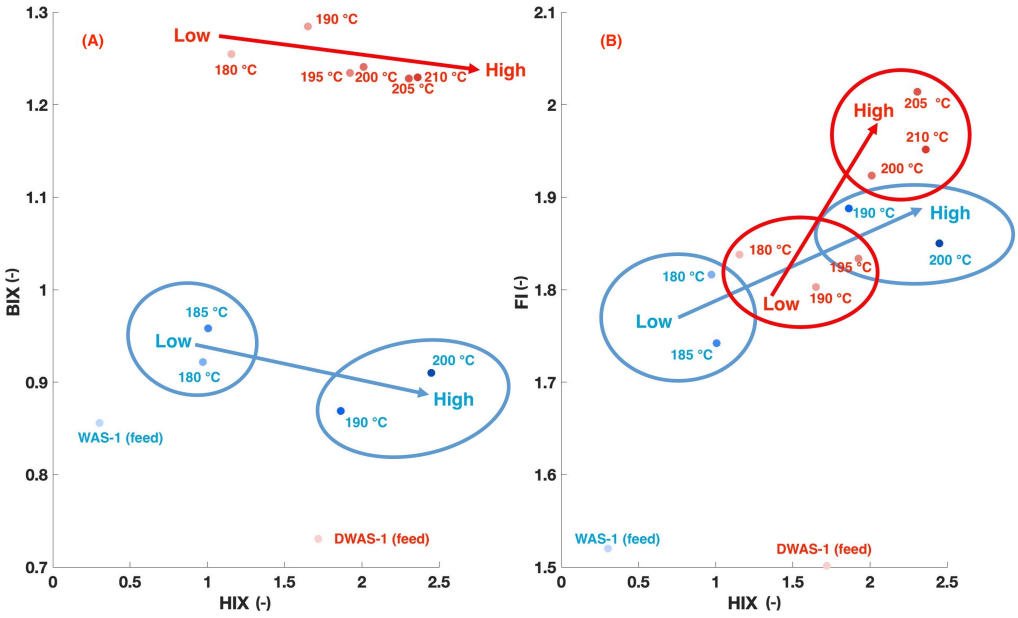

Figure 3.10: Distributions of HIX vs. BIX (A), and HIX vs. FI (B) for thermally-hydrolysed WAS-1 and DWAS-1 subjecting to different reaction temperatures. Arrows indicate an increase of reaction temperature. Circles indicate clusters with similarity.

3.1.8 PCA

PCA was performed to pinpoint the effects of reaction temperature and anaerobic predigestion on the variations of macromolecular compounds, solubilisation metrics and fluorescence indices. As shown in **Figure 3.11**, the scores of samples are shown as observation points in a plane formed by two principal components (PCs). In addition to the observations, variables are plotted as loading vectors to indicate how they correlate with one another or PCs. The PCA assessment is based on the biplot, which can be interpreted as follows (Kirkwood et al., 2013; Rossiter, 2014):

- The more a loading vector is parallel to a PC axis, the more it contributes to that PC and vice versa.

- The longer of a loading vector is in a PC plane, the more variability it presents in that plane; short vectors are thus better represented in other dimensions.
- The relative angle between any two loading vectors of variables represents their pairwise correlation: small angles represent high positive correlation, right angles represent lack of correlation, and opposite angles represent high negative correlations.

The variance explained in the PC1 direction contributed to 59.90 % of the total variance, and 36.12 % of the total variance was explained in the PC2 direction, in total 96.02 % was explained. Two PCs contributed to the separation of the hydrolysates produced at different reaction temperatures from different sources.

The hydrolysates of WAS-1 were clustered together in the upper-left quadrants (negative PC1 but positive PC2 scores), whereas most of the hydrolysates of DWAS-1 were mainly grouped in the right quadrants (positive PC1 scores), except for DWAS-1 hydrolysate produced at 180 °C. The distribution of WAS-1 and DWAS-1 hydrolysates in the PC plane shows that WAS-1 and DWAS-1 responded differently to TORWASH® temperature conditions. Specifically, we found that hydrolysates of WAS-1 and DWAS-1 can be distinguished based on parameters including pH, SCOD, DOC, BOD_5, FRI-I (tyrosine-like protein), BIX, ammonium, and orthophosphate. As discussed previously, pH increased after anaerobic pre-digestion, resulting in a lower orthophosphate concentration. Also, during pre-digestion, biodegradable substances were consumed. Therefore, DWAS-1 hydrolysates had lower concentrations of SCOD, DOC, and tyrosine-like protein than those in WAS-1 hydrolysates, and the DOM in DWAS-1 hydrolysates displayed stronger autogenetic characteristics than that of WAS-1 hydrolysates. In addition, the release of ammonium from protein hydrolysis was found more pronounced for TH of DWAS-1 than for WAS-1.

Regarding the spatial proximity between individual observation points, there was a strong similarity between WAS-1 hydrolysates produced at 180 °C and 185 °C, suggesting that the DOM composition stayed relatively constant at 180 - 185 °C. Instead, the WAS-1 hydrolysate produced at 190 °C is distant from those produced at 180 °C and 185 °C. At a temperature of 190 °C, we observed stronger protein hydrolysis and soluble HS production, resulting in a further increase in FRI-III (fulvic acid-like matter), FRI-V (humic acid-like matter), Fn(355), and $SUVA_{254}$ but a further decrease in DCOS and URI. In addition, another cluster was found between DWAS-1 hydrolysates produced at 205 °C and 210 °C. The increase in reaction temperature from 205 to 210 °C might no longer influence the properties of DOM in DWAS-1 hydrolysates.

Furthermore, PCA also displays the correlation between variables. We found that the reaction temperature was positively correlated (linear) with $SUVA_{254}$, HIX, FRI-V (humic acid-like matter), Fn(355) (humic-like fluorescence parameter), and FRI-III(fulvic acid-like matter) but negatively correlated with URI, DCOS. This confirms that the degree of humification increased with increasing reaction temperature. In addition, the reaction temperature was positively correlated with FRI-II (tryptophan-like protein) and Fn(280) (protein-like fluorescence parameter) but negatively correlated with soluble proteins concentration. More aromatic proteins were found in the hydrolysates of WAS-1 and DWAS-1 despite more soluble proteins being hydrolysed at higher reaction temperatures.

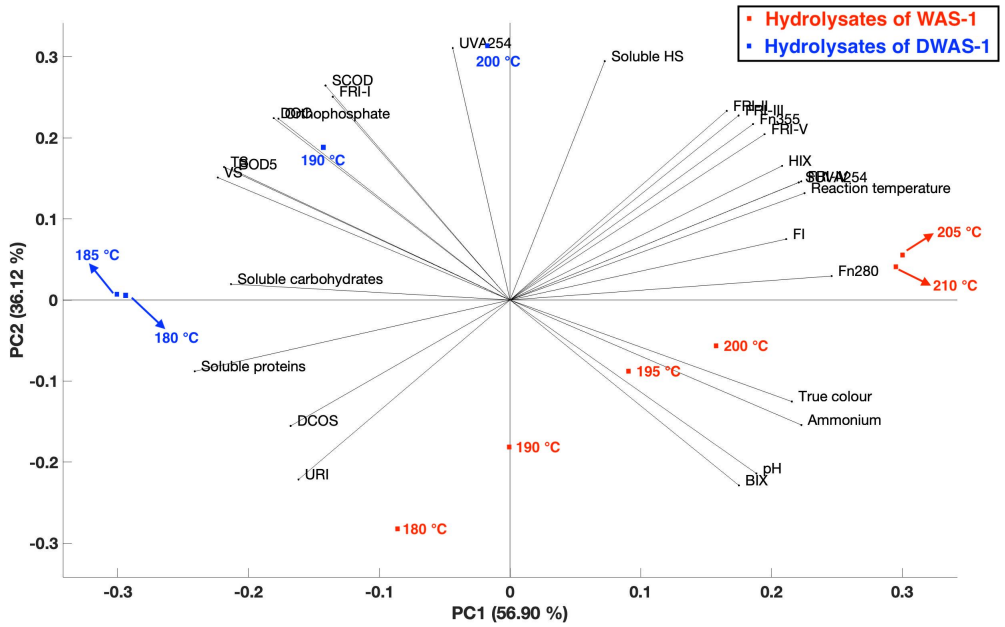

Figure 3.11: Biplot of PC1 and PC2, showing both scores of samples and loading vectors of variables. The scores of WAS-1 hydrolysates are shown as blue dots. The scores of DWAS-1 hydrolysates are shown as red dots. Loading vectors of variables are demonstrated as black lines radiating from the origin. Solid arrows distinguish the hydrolysates close to each other.

3.2 Effect of acidic pretreatments on TH

Three acidic pretreatments were applied before TH of WAS-2 at 190 °C: acetic acid (HAc) addition (WAS-2-HAc), CO_2 pressurisation at 10 and 20 bar (WAS-2-10CO_2 and WAS-2-20CO_2), the combination of both (WAS-2-HAc+10CO_2 and WAS-2-HAc+20CO_2), and WAS-2-control as blank control.

3.2.1 Results of pH and VFA

As shown in **Table 3.5**, the pH in WAS-2-control decreased from 6.3 to 5.3 after TH. Similarly, the pH in WAS-2-10CO_2 and WAS-2-20CO_2 decreased from 6.3 to 5.5 after TH. However, the pH values in the hydrolysates, WAS-2-HAc, WAS-2-HAc+10CO_2, and WAS-2-HAc+20CO_2, were maintained at 4.2 - 4.3 before or after TH. According to Jeong et al. (2019) and Wilson and Novak (2009), the decrease in pH during TH can be attributed to the production of VFA. As shown in **Table 3.6**, the total VFA concentration in WAS-2-control increased by six times after TH compared with raw WAS-2, resulting in a decrease in pH after TH. In addition, the CO_2 pressurisation seemingly promoted the production of VFA, particularly in propionic acid, butyric acid, and isovaleric acid. We found that the total VFA concentration of WAS-2-10CO_2 was 15 % higher than that of WAS-2-control. Moreover, the VFA production also increased with CO_2 pressure; the total VFA concentration of WAS-2-20CO_2 was approximately 20 % higher than that of WAS-2-10CO_2. However, this phenomenon was not well observed in WAS-2-HAc+10CO_2 and WAS-2-HAc+20CO_2 compared with WAS-2-HAc. The intrinsic mechanism of the effect of CO2 on VFA production requires further study.

pH simulation

To investigate the pH variation during TH, pH during TH tests was simulated with PHREEQC based on the Peng-Robinson equation. It should be noted that this simulation results could deviate from the measurement. PHREEQC is inadequate to model the current experimental conditions (high temperature, high pressure, composition of WAS-2). Current results could roughly demonstrate the general trends of pH and pressure during TH with acidic pretreatments. As shown in **Table 3.5**, the pH in WAS-2-10CO_2 and WAS-2-20CO_2 could drop from 6.2 (raw WAS-2), respectively. Therefore, CO_2 pressurisation could lower the pH of WAS-2 to a limited extent. The following TH tests were simulated by increasing the reaction temperature from 20 to 190 °C, and the pH in WAS-2-10CO_2 and WAS-2-20CO_2 rose back to 6.4 and 6.1 from 5.5 and 5.2, respectively (**Figure 3.12**). The simulated increase in pH was due to the decrease in CO_2 solubility in water with increasing temperatures (Lucile et al., 2012). Therefore, CO_2 pressurisation may only temporarily lower the pH of WAS-2 during TH; based on the pH measurement, the actual pH values in WAS-2-10CO_2 and WAS-2-20CO_2 after TH were close to blank control (WAS-2-control). However, it is difficult to validate the simulation results; for the CO_2 + thickened WAS system under high temperature and pressure conditions, data are scarce. Regarding the simulation of combined pretreatments, WAS-2-HAc+10CO_2 and WAS-2-HAc+20CO_2, the pH values after HAc addition stayed relatively constant at 3.8 - 3.9 during CO_2 pressurisation and TH. However, the actual pH measured after HAc addition was 4.2 - 4.3, which was higher than the simulated results of 3.9. Therefore, the model underestimated the buffer capacity of WAS-2 when only using the results of VFA, ammonium, orthophosphate, and alkalinity (HCO_3^-) as model input (**Appendix E**).

Pressure simulation

In addition, the PHREEQC code also simulated the pressure change during TH. As shown in **Table 3.5**, the total pressure increased due to thermal expansion and water evaporation. However, the simulated total pressure was higher than the actual records (**Appendix A**). The overestimation of total pressure could be due to an inaccurate estimation of the volume of reactor headspace.

Table 3.5: PHREEQC results of TH with acidic pretreatments compared with measured pH and pressure [1].

Parameter	WAS-2-control	WAS-2-HAc	WAS-2-10CO_2	WAS-2-20CO_2	WAS-2-HAc+10CO_2	WAS-2- HAc+20CO_2
pH measured						
Initial pH [2] (-)	6.3	6.3	6.3	6.3	6.3	6.3
pH after HAc addition (-)	-	4.3	-	-	4.2	4.2
pH after TH [3] (-)	5.3	4.3	5.5	5.5	4.2	4.3
pH simulated						
pH after HAc addition (-)	-	3.9	-	-	3.9	3.9
pH after CO_2 pressurisation [4] (-)	-	-	5.5	5.2	3.9	3.9
pH during TH [5] (-)	7.2	3.8	6.4	6.1	3.9	3.9
pH after TH [6] (-)	6.8	3.7	6.4	6.4	3.8	3.8
Pressure measured						
Total pressure (bar)	11.8	12.1	28.0	49.9	28.6	45.9
Pressure simulated [7]						
CO_2 partial pressure (atm)	2.08	2.63	21.70	43.20	21.42	43.01
H_2O partial pressure (atm)	12.59	12.59	13.64	14.81	13.55	14.71
Total pressure (atm)	16.06	16.55	35.34	58.01	34.97	57.73

[1] The PHREEQC code can be found in **Appendix E**.
[2] The pH of raw WAS-2 was used as the input of the model.
[3] The pH measured after depressurising and cooling the TH-treated sample to 20 °C.
[4] The pH simulated assuming the
[4] The pH simulated during TH at 190 °C.
[5] The pH simulated after depressurising and cooling the thermally hydrolysed sample to 20 °C.
[6] The pressure simulated during TH of WAS-2 at 190 °C, assuming the volume of reaction headspace was 1.1 L.

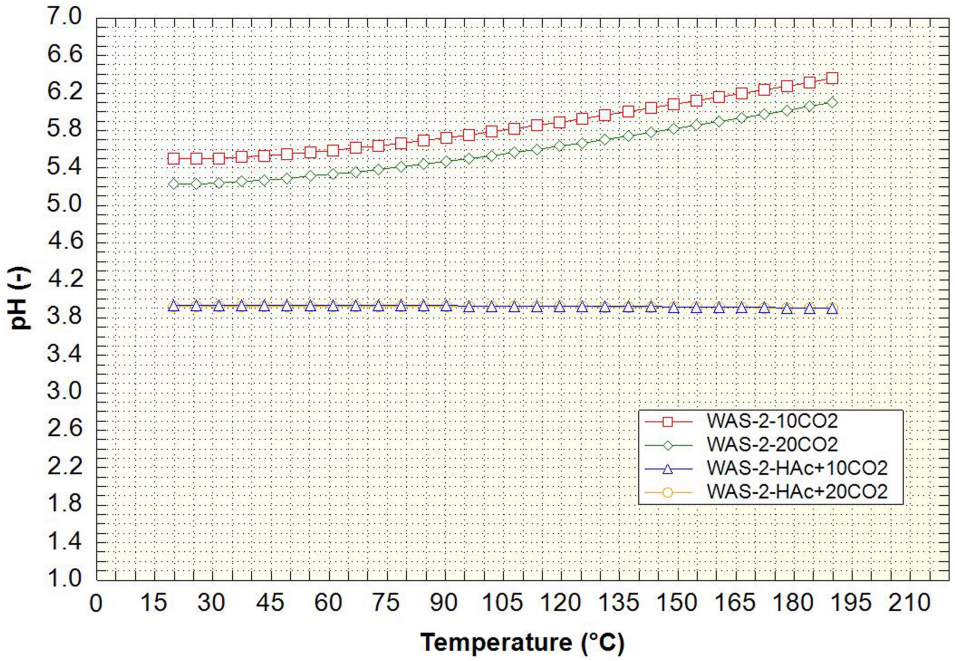

Figure 3.12: PHREEQC simulation of pH vs. temperature at 20 - 190 °C for TH tests pressurised with 10 and 20 bar. Note: the curve of WAS-2-HAc+10CO_2 overlaps with the curve of WAS-2-HAc+20CO_2.

Table 3.6: Soluble phase characteristics of raw WAS-2 before and after TH with acidic pretreatments

Parameter	WAS-2	WAS-2-control	WAS-2-HAc [1]	WAS-2-10CO_2	WAS-2-20CO_2	WAS-2-HAc+10CO_2 [1]	WAS-2-HAc+20CO_2 [1]
SCOD (mg O_2/L)	1147.7 ± 0.6	30200 ± 200	41400 ± 200	30100 ± 90	30100 ± 200	42000 ± 100	41300 ± 300
DOC (mg C/L)	481 ± 6	11800 ± 100	16300 ± 100	11700 ± 100	11840 ± 90	16500 ± 200	16300 ± 400
Ammonium (mg NH_4^+-N/L)	179 ± 4	860 ± 10	905 ± 9	784 ± 5	900 ± 40	852 ± 5	905 ± 8
Orthophosphate (mg PO_4^{3-}-P/L)	480 ± 2	1034 ± 5	1310 ± 10	1009	1065 ± 5	1270 ± 10	1390 ± 10
VFA (mg COD/L)							
Acetic acid (C2)	66 ± 6	1200 ± 40	19600 ± 200	1220 ± 40	1300 ± 30	19000 ± 400	18920 ± 70
Propionic acid (C3)	104 ± 1	420 ± 10	422 ± 4	600 ± 10	760 ± 10	422 ± 7	578 ± 6
Isobutyric acid (IC4)	27.0 ± 0.4	78.4 ± 3	67.5 ± 0.5	103 ± 2	141 ± 2	77 ± 1	112.8 ± 0.4
Butyric acid (C4)	8.63 ± 0.04	105 ± 2	102.8 ± 0.5	162 ± 4	198 ± 4	111 ± 2	145 ± 1
Isovaleric acid (IC5)	85 ± 1	201 ± 2	155 ± 3	293 ± 5	383 ± 9	188 ± 7	262 ± 4
Valeric acid (C5)	11.1 ± 0.2	60 ± 2	52 ± 1	92 ± 3	128 ± 5	60 ± 1	100 ± 8
Isocaproic acid (IC6)	Undetected	41 ± 3	40 ± 3	48 ± 8	64.5 ± 0.5	46 ± 6	49.2 ± 0.8
Caproic acid (C6)	Undetected	86 ± 5	83 ± 3	Undetected	36 ± 2	78 ± 2	83 ± 2
Total	302 ± 6	2190 ± 50	20500 ± 200	2520 ± 40	3020 ± 40	19900 ± 400	20250 ± 80

[1] The concentration of added HAc was around 16,985 mg/L = 18,173.95 mg COD/L.

3.2.2 Results of SCOD and COD

The results of SCOD and COD are shown in **Table 3.6**. We found that CO_2 pressurisation at 10 and 20 bar did not influence the solubilisation of COD and organic carbon whether or not the WAS-2 was pre-added with HAc: no significant differences ($p > 0.05$) were found in SCOD or DOC concentrations between WAS-2-control, WAS-2-10CO_2 and WAS-2-20CO_2; also, no significant differences ($p > 0.05$) were found in SCOD and DOC concentrations between WAS-2-HAc, WAS-2-HAc+10CO_2, and WAS-2-HAc+20CO_2.

3.2.3 Results of ammonium and orthophosphate

As shown in **Table 3.6**, no significant differences ($p>0.05$) were found in ammonium concentration in hydrolysates of WAS-2, except for WAS-2-10CO_2, in which the ammonium was below the average. Correspondingly, the soluble proteins concentration in WAS-2-10CO_2 was significantly higher ($p < 0.05$) than in the other hydrolysates, including the blank control (**Figure 3.13 (A)**). This suggests that less ammonium was released from protein hydrolysis, resulting in a relatively higher ammonium concentration in WAS-2-10CO_2. Regarding the effect of acidic pretreatments on the solubilisation of orthophosphate, we found that the orthophosphate concentrations in WAS-2-HAc, WAS-2-HAc+10CO_2, and WAS-2-HAc+20CO_2 were 30 % higher than that of blank control (**Table 3.6**). The addition of HAc decreased the pH in WAS-2 to 4.2; therefore, more orthophosphate would solubilise at that pH. However, the solubilisation of orthophosphate was not well observed in sampled pre-added with only CO_2 with respect to the control.

3.2.4 Results of soluble HS, proteins and carbohydrates

Soluble HS

As shown in **Figure 3.13 (A)**, the soluble HS concentration in hydrolysates with acidic pretreatments decreased by 10 % on average compared with the blank control. However, no significant differences ($p > 0.05$) were found in soluble HS concentration between the acidic pretreatments. The decrease in soluble HS concentration suggests a reduced production of melanoidins, and the acidic pretreatments could mitigate the production of melanoidins to a limited extent. Two mechanisms are proposed to interpret the decrease in soluble HS concentration: (1) the mitigation of the Maillard reaction; (2) the reduction in humic acid solubility at lower pH (Wu et al., 2002):

(1) The mitigation of the Maillard reaction

The Maillard reaction begins with aldose and amine condensation. Acyclic aldoses and unprotonated amine are considered reactive species. The relative content of acyclic aldoses to cyclic aldoses decreases with decreasing pH. Also, less unprotonated amine would present at lower pH. Therefore the condensation of aldose and amine could be limited to a certain degree. Moreover, the increased CO_2 partial pressure could influence the progression of Strecker degradation that occurs in the intermediate stage of the Maillard reaction. Ideally, fewer aldehydes are produced from Strecker degradation at high pressure of CO_2. To summarise, the mitigation of the Maillard reaction could be achieved by influencing the aldose-amine condensation and Strecker degradation. If the proposed mechanism is true, theoretically, fewer reactants will be available for producing melanoidins in the final stage of the Maillard reaction.

(2) The reduction in humic acid solubility at lower pH

Given that the pH values in WAS-2 hydrolysates were below 5.5, HS in our samples were mainly composed of humic acids and fulvic acids. Therefore, the reduction in humic acid

solubility at lower pH could result in a decrease in soluble HS concentration. The addition of HAc directly lowered the pH of WAS-2 hydrolysates from 6.3 to 4.3. A proportion of humic acid would precipitate out of the soluble phase.

Soluble proteins and carbohydrates

As shown in **Figures 3.13 (B) and (C)**, WAS-2-10CO_2 and WAS-2-20CO_2 had higher concentrations of soluble proteins and carbohydrates than those of WAS-2-control. The addition of CO_2, especially at 10 bar, seemingly increased the concentrations of soluble proteins and carbohydrates. However, this phenomenon was not observed in the acid pretreatments of HAc+CO_2: no significant differences ($p > 0.05$) were found in concentrations of soluble proteins and carbohydrates between WAS-2-HAc+10CO_2, WAS-2-HAc+20CO_2, and WAS-2-control.

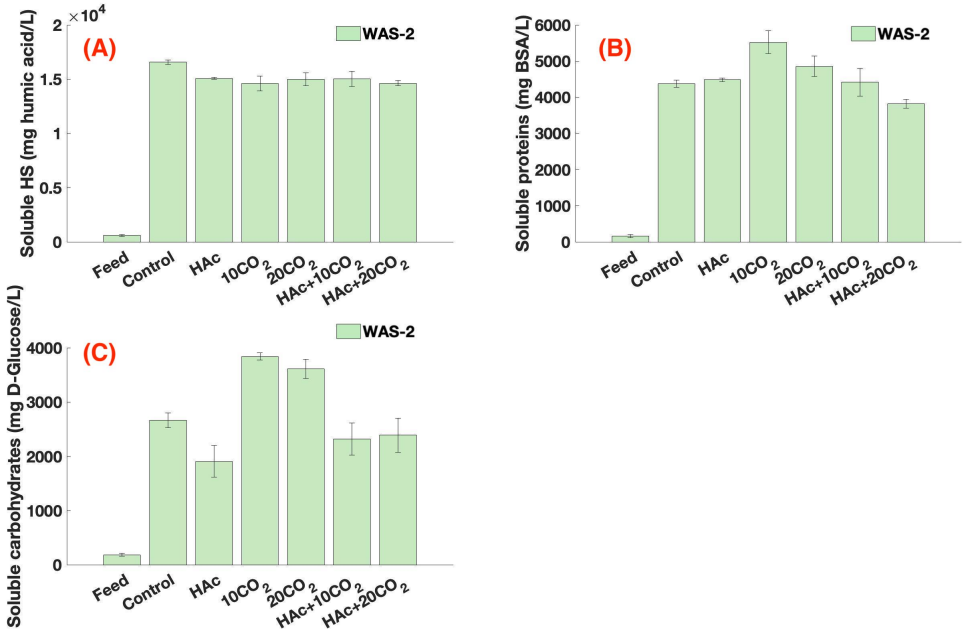

Figure 3.13: Effects of acidic pretreatments on the concentrations of soluble HS (A), soluble proteins (B), and soluble carbohydrates (C) in thermally-hydrolysed WAS-2.

3.2.5 Results of colour, UVA_{254} and $SUVA_{254}$

As shown in **Figure 3.14 (A)**, acidic pretreatments reduced the production of coloured matter after TH. The effect of acidic pretreatments on colour reduction followed a descending order: HAc+20CO_2 > HAc+10CO_2 > 20CO_2 > 10CO_2 > HAc. The combined addition of HAc and CO_2 was more effective on colour reduction than the other acidic pretreatments. The decreased colour content indicates a reduced production of Amadori products and melanoidins. In addition, UVA_{254} in hydrolysates with acidic pretreatment was reduced by 13 % on average relative to the control (**Figure 3.14 (B)**). Corresponding, it could be associated with an average 10 % decrease in soluble HS concentration after acidic pretreatments. Furthermore, $SUVA_{254}$ was calculated to provide additional information (**Figure 3.14 (C)**). The $SUVA_{254}$ values of WAS-2-HAc, WAS-2-HAc+10CO_2 and WAS-2-HAc+20CO_2 were lower than the other hydrolysate due to the addition of

HAc (16985 mg HAc added/L ≈ 6794 mg DOC /L). As for hydrolysates pretreated with only CO_2, $SUVA_{254}$ values of WAS-2-10CO_2 and WAS-2-20CO_2 were lower than that of the control, suggesting a reduction in the content of heterocyclic and aromatic DOM (Nguyen et al., 2020).

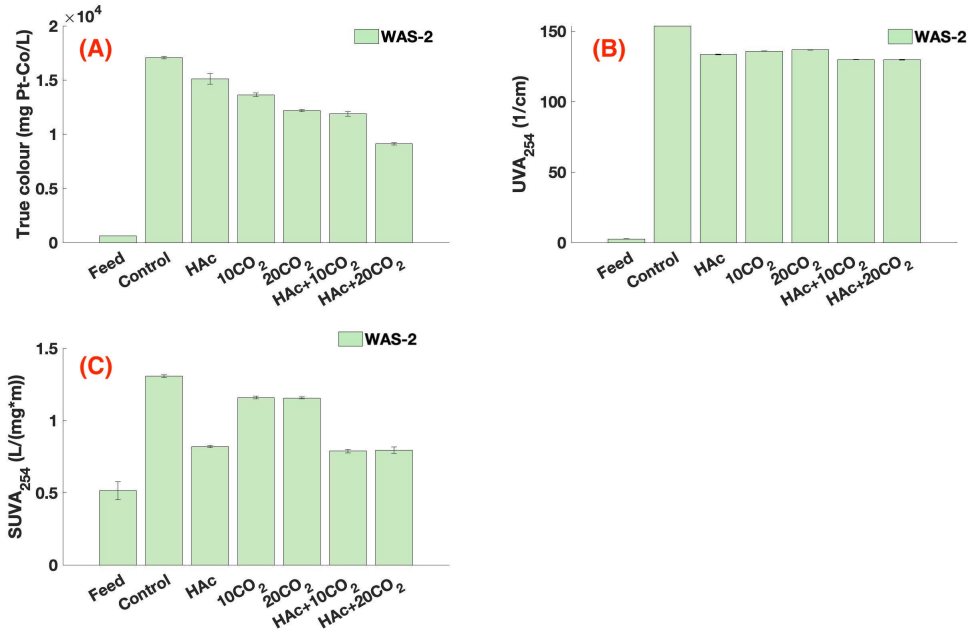

Figure 3.14: Effects of acidic pretreatments on the concentration of true colour (A), UVA_{254} (B), and $SUVA_{254}$ (C) in thermally-hydrolysed WAS-2.

3.2.6 Fluorescence EEM

Fluorescence regional integration

As shown in **Figure 3.15 (A)**, the total FRI values of WAS-1 hydrolysates with acidic pretreatments were lower than that of blank control. Specifically, the total FRI of WAS-2-HAc, WAS-2-10CO_2, WAS-2-20CO_2, WAS-2-HAc+10CO_2, and WAS-2-HAc+20CO_2 decreased by 17 %, 18 %, 13 %, 22 %, 13 % relative to WAS-2-control. Among these acidic pretreatments, the effect of HAc + 10 bar CO_2 on total FRI reduction was more pronounced than that of HAc and 10 bar CO_2, followed by 20 bar CO_2 and HAc + 20 bar CO2. Unexpectedly, 20 bar CO_2 was less effective than 10 bar CO_2.

Regarding the changes in the specific fluorescent regions, the FRI of tyrosine-like protein (I) and soluble microbial byproduct-like matter (IV) in pretreated samples stayed relatively constant in respect of the control. The decrease in total FRI can be primarily attributed to the decrease in FRI of fulvic acid-like matter (III). Fulvic acid-like matter (III) was the major fraction in WAS-2-control, accounting for 32 % of total FRI (**Figure 3.15 (B)**). We found that the FRI of fulvic acid-like matter (III) in WAS-2-10CO_2 was 28 % lower than that of control. The acidic pretreatments of 20 CO_2 and HAc+10CO_2 had similar effects that the FRI of fulvic acid-like matter (III) of WAS-2-20CO_2 and WAS-2-HAc+10CO_2 decreased by 22 % and 26 % compared with WAS-2-control. The pretreatments of HAc and HAc+20CO_2 were less effective on fulvic acid-like matter reduction, corresponding to 19 % and 15 % decreases relative to WAS-2-control. The effects of acidic pretreatments

on reducing fulvic acid-like matter were akin to that of humic acid-like matter. Still, 10 bar CO_2 was the more effective regarding the other pretreatments: the FRI of humic acid-like matter (V) of WAS-2-10CO_2 and WAS-2-HAc+10CO_2 decreased by 30 % and 29 % compared with WAS-2-control. As shown in **Table 3.7**, Fn(355) (humic-like fluorescence parameter) represents the relative contents of the humic-like substances. The Fn(355) values of WAS-2-10CO_2 and WAS-2-HAc were lower than that of other hydrolysates, which is consistent with the results of FRI of humic acid-like matter (V). In addition to Fn(355), humidification indices (HIX), in **Table 3.7**, indicates the degree of humification in the humic acid-like matter. We found that the addition of 10 and 20 bar CO_2 can effectively decrease the HIX values from 2.5 (WAS-2-control) to 1.8 (WAS-2-10CO_2 and WAS-2-20CO_2), whereas the fluorescence index (FI) and biological index (BIX) did not change. This suggests that the source of DOM did not change after acidic pretreatments, but the complexity of humic acid-like matter was reduced to a limited extent.

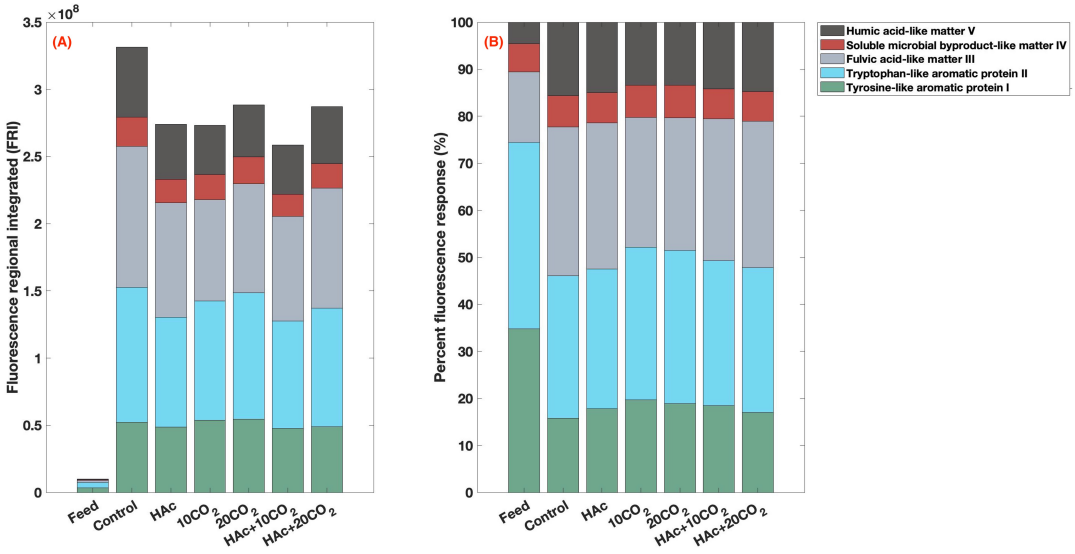

Figure 3.15: FRI (A) and distribution of FRI (B) in non-fractionated DOM from samples of thermally-hydrolysed WAS-2 with different acidic pretreatments.

Table 3.7: Effect of acidic pretreatments on fluorescence indices and parameters.

Parameter	WAS-2	WAS-2-1-control	WAS-2-HAc	WAS-2-10CO_2	WAS-2-20CO_2	WAS-2-HAc+10CO_2	WAS-2-HAc+20CO_2
HIX (-)	0.9	2.5	2.4	1.8	1.8	2.2	2.3
BIX (-)	0.7	1.0	0.9	1.0	1.0	1.0	0.9
FI (-)	1.6	1.8	1.8	1.8	1.8	1.8	1.8
Fn(355) (R.U.)	9.9	1653.1	1267.1	1104.7	1203.9	1111.8	1345.8
Fn(280) (R.U.)	65.1	1811.4	1424.5	1632.6	1757.3	1372.1	1554.8

R.U. is Raman units.

3.2.7 PCA

Figure 3.14 (A) shows the results of PCA on TH of WAS-2 with acidic pretreatments. The first two PCs explained 78.52 % of the total variance. The hydrolysates with treatments of 10CO_2 and 20CO_2 were clustered together in the lower-right quadrant (positive PC1 scores but negative PC2 scores), whereas the HAc, HAc+10CO_2, HAc+20CO_2 were

clustered in the left quadrants (negative PC1 scores). Both clusters were distant from the control located in the upper-right quadrant (positive PC1 and PC2 scores), suggesting low spatial proximity between control and pretreated samples. We found that control and pretreated samples can be distinguished by the following parameters: FRI-III (fulvic acid-like matter), FRI-V (humic acid-like matter), Fn(355), colour content, and soluble HS concentration. In addition, The cluster of $10CO_2$ and $20CO_2$ was furthest apart from the cluster of HAc, HAc+$10CO_2$, and HAc+$20CO_2$. This suggests that the effect of acidic pretreatments with only CO_2 pressurisation differs from that of the HAc addition. We found that the concentrations of orthophosphate, SCOD, and DOC in WAS-2-HAc, WAS-2-HAc+$10CO_2$, and WAS-2-HAc+$20CO_2$ were higher than those in WAS-2-$10CO_2$ and WAS-2-$20CO_2$. Unlike CO_2 pressurisation, HAc addition can effectively lower the pH in samples. Therefore, orthophosphate solubilisation was observed in the hydrolysates pre-added with HAc. Moreover, the concentrations of soluble carbohydrates and protein (including tyrosine-like protein) in WAS-2-$10CO_2$ and WAS-2-$20CO_2$ were higher than those in hydrolysed pretreated with HAc.

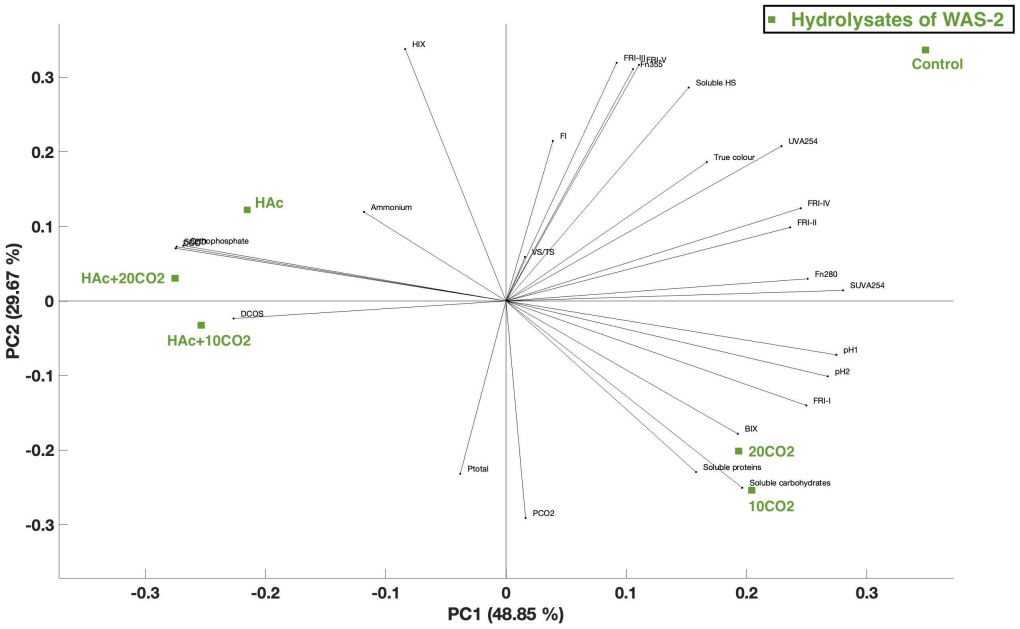

Figure 3.16: Biplot of PC1 and PC2, presenting both scores of hydrolysates of WAS-2 (green dots) and loading vectors of variables (black lines radiating from the origin). Solid arrows distinguish the samples close to each other. Ptotal is the average total pressure in the reactor headspace during TH. PCO2 is the CO_2 pressure in the reactor headspace before TH. pH1 is the pH value of sample before TH. pH2 is the pH value of sample after TH.

3.2.8 General discussion for TH with acidic pretreatments

Overall, we observed that acidic pretreatments reduced the production of soluble HS by 10 % on average, corresponding to a 13 % decrease in UVA_{254}. Also, a substantial colour decrease of 12 - 46 % was found in the pretreated samples compared with the control. This could benefit the UV-disinfection during post-treatment of the hydrolysates. A reduction in UV absorbing compounds indicates a decreased UV-quenching ability of DOM; thereby, the energy demand for UV-disinfection could be reduced (Dwyer et al., 2008).

The acidic pretreatments, particularly the CO_2 pressurisation at 10 bar, could be advantageous to the downstream AD treatment. Compared with the WAS-2-control, the content of fulvic acid-like matter and humic acid-like matter in the soluble fraction of WAS-2-10CO_2 decreased by 28 % and 30 %, respectively. The DOM in hydrolysates behaved less recalcitrant after CO_2 addition, reducing the potential inhibition to the post-AD process. In addition, for the potential application of CO_2 pressurisation to the TORWASH® process, the CO_2 gas and hot steam after TH could be recovered by depressurising the off-gas in the thermal reactor to a flash tank. In contrast, acidic pretreatment using HAc could be more costly; however, the added HAc could be converted into biogas during post-AD treatment. In our study, the pH in hydrolysates with HAc addition was around 4.2. At this pH level, the solubilisation of orthophosphate occurred. The soluble phosphorus in the hydrolysate could be recovered from the post-treatment of struvite precipitation. According to the design of TORWASH® (Grootjes et al., 2019), the solid fraction of the hydrolysate is sent to an incinerator. Therefore, the more phosphorus recovered in the soluble phase after HAc addition, the less phosphorus would be released into the atmosphere.

Chapter 4

Conclusion

This study aimed to understand the effects of reaction temperatures on recalcitrant compounds formation and the effects of acidic pretreatments as potential mitigation on recalcitrant compounds production. To achieve the research objective, three questions were formulated. Corresponding to the results, the defined sub-research questions can be answered as follows:

1. **What are the differences between WAS and anaerobically pre-digested WAS before and after TH?**
    - SCOD and DOC were partially degraded and solubilised during the anaerobic pre-digestion of WAS; therefore, TH appeared to be more effective on WAS than on anaerobically pre-digested WAS in terms of COD solubilisation.
    - pH increased after anaerobic pre-digestion, resulting in the precipitation of orthophosphate. Overall, soluble orthophosphate concentration in the hydrolysates of pre-digested WAS was lower than that in the hydrolysates of WAS.
    - The change in ammonium concentration during TH of WAS differed from that during TH of pre-digested WAS. The ammonium concentration decreased after TH of WAS, whereas the ammonium concentration in hydrolysates of pre-digested WAS increased with elevated reaction temperature, although the ammonium concentration in pre-digested WAS was inherently higher than that of raw WAS.
    - BMP decreased after anaerobic pre-digestion but increased after TH treatment. No significant difference ($p > 0.05$) was found in BMP between WAS TH-treated at 190 °C and pre-digested WAS TH-treated at 205 °C, suggesting that the liquid fraction of pre-digested WAS could reach an equivalent degree of anaerobic biodegradability as that of WAS by applying a higher reaction temperature.
    - The BOD_5 in WAS increased after the initial TH at 180 °C, but the BOD_5 stayed relatively constant when further increasing the reaction temperature from 180 to 200 °C. In contrast, we found that the BOD_5 in hydrolysates of pre-digested WAS drastically decreased at 200 °C, suggesting a substantial production of aerobically non-biodegradable compounds.
2. **How can reaction temperature affect the formation of recalcitrant compounds?**
    - The concentration of soluble proteins monotonically decreased with increasing reaction temperature, indicating proteins were primarily hydrolysed or denatured under TORWASH® conditions. However, a different trend was found in soluble carbohydrates concentration. Solubilisation of carbohydrates was the dominant process at lower reaction temperatures, but with a further increase in

reaction temperature, competition for carbohydrates between the Maillard and caramelisation reactions could occur.

- TH disintegrated high molecular weight DOM > 1 kDa into low molecular weight DOM < 0.1 kDa, and stronger sludge disintegration occurred at higher reaction temperatures. Moreover, the production of high molecular weight melanoidin > 10 kDa from polymerisation was not well observed based on results of molecular weight distribution.
- The production of recalcitrant compounds (soluble humic substances) increased with increasing reaction temperature, corresponding to increases in UVA_{254}, colour content, and $SUVA_{254}$ but decreases in URI and DCOS. In line with the results of EEM-FRI, the contents of fulvic-acid like and humic-acid matter increased at higher reaction temperatures.

3. **What are the differences between acidifying TH systems through HAc addition and CO_2 pressurisation?**

   - CO_2 pressurisation did not change the pH of hydrolysates after TH; thereby, the orthophosphate concentrations in hydrolysates pretreated with CO_2 were found equivalent to that of control (no pretreatments). Contrarily, the addition of HAc effectively decreased the pH in hydrolysates from 6.3 to 4.2, resulting in the solubilisation of orthophosphate.
   - Only CO_2 pressurisation could enhance the production of VFA, particularly in propionic acid, butyric acid, and isovaleric acid. The effect of 10 bar CO_2 on VFA production was more pronounced than that of 20 bar CO_2.
   - Humic substances are considered recalcitrant. All acidic pretreatments applied decreased the production of soluble humic substances by 10 %, corresponding to a 13 % decrease in UVA_{254} on average. Also, less coloured matter was produced after acidic pretreatments; the effect of combined pretreatment (HAc+CO_2) on colour reduction was more pronounced than that of CO_2 addition, followed by HAc addition.
   - CO_2 pressurisation at 10 bar is the most effective acidic pretreatment in our study in terms of reducing the formation of fulvic-acid like and humic-acid like matter, followed by HAc + 10 bar CO_2. The effect of 20 bar CO_2 was less pronounced than that of 10 bar CO_2, whether or not the samples were pre-added with HAc.
   - Only CO_2 pressurisation could increase the concentrations of soluble proteins and soluble carbohydrates compared with control (no acid pretreatments).

Chapter 5

Limitations and Suggestions

Delayed feedstock characterisation
The feedstocks, WAS-1 and DWAS-1, were characterised after long-term anaerobic storage at 4 °C. Therefore, their chemical compositions may differ from the original ones used for TH tests, which influenced the evaluation of TH performance.

Experiment procedure improvement
In this study, the depressurisation of the thermal reactor was conducted at 100 °C, resulting in a substantial loss in water and other volatile substances due to evaporation. This could be minimised by depressurising the reactor vessel until it is cooled down to room temperature. In addition, the reactor may not be thoroughly cleaned after each test only by flushing with demi-water. Toutian et al. (2020) suggested that the reactor should be cleaned with water for 30 min at 170 °C to wash out the remainders. Moreover, the TH experiment in this study could not simulate the steam explosion which occurs during TORWASH® and other commercialised TH installations. A modification of the current thermal reactor is recommended to better simulate the TH process.

Inaccurate proteins and carbohydrates measurements
The concentrations of soluble proteins were measured with the modified Lowry method. However, this method only provides qualitative identification. According to Wilson and Novak (2009), it was possible that individual amino acids did not react positively in the Lowry method, resulting in an underestimation of soluble proteins concentration. Instead, Le et al. (2016) reported that the presence of amide bonds formed during TH could interfere with the reduced copper-amide bond complex in the Lowry method, resulting in an overestimated soluble proteins concentration. Despite EEM fluorescence spectroscopy being used in our study to analyse aromatic proteinaceous compounds, there was a limited study of non-aromatic proteinaceous compounds. Fourier-transform infrared spectroscopy is suggested to analyse the structural characterisation of non-aromatic proteins and polypeptides (H. Yang et al., 2015).

The concentration of soluble carbohydrates was determined with phenol sulfuric acid assay, which utilised the heat released from concentrated sulfuric acid to dehydrate the saccharides containing potential (or free) aldehydic or keto groups into furfural derivatives. Subsequently, these derivatives were condensed with phenols to form coloured complexes for colourimetric analysis (Rao & Pattabiraman, 1989). Therefore, this assay could overestimate the concentration of soluble carbohydrates in the thermally hydrolysed samples by including the furfurals produced from the Maillard and caramelisation reactions. To better understand the change in soluble carbohydrates and the mechanism of the Maillard reaction, intermediate Maillard reaction products (e.g., furfurals, aldehydes, etc.) should be analysed using high-performance liquid chromatography combined with mass spectrometry.

TH with CO_2 pressurisation
CO_2 was added to the thermal reactor as one of the acidic pretreatments. Based on the PHREEQC model, CO_2 may only temporarily change the pH of WAS during TH since its solubility decreases at higher temperatures. However, the model could not provide a rough estimation of pH and pressure since PHREEQC was based on aqueous calculation, which was inadequate to simulate the rheological change of sludge during TH. Therefore, a more practical model is needed. In addition, continuous pH monitoring is necessary for model validation and for understanding pH variation at different reaction temperatures and CO_2 partial pressures. The sensitivity analysis of CO_2 should be conducted with a progressive increase in CO_2 pressure since it was unexpected that the effect of 10 bar of CO_2 on fluorescence DOM reduction was more pronounced than that of 20 bar of CO_2. Furthermore, N_2 or other inert gases should be tested in comparison with CO_2.

Methane potential evaluation The BMP tests conducted in our study provided limited information. It is unknown to us how BMP changed in the hydrolysates of WAS-1 and DWAS-1 at different reaction temperatures. In addition, we only measured the BMP in soluble fractions of the hydrolysates, and the methane produced from anaerobic pre-digestion of WAS-1 was unknown. Therefore, evaluating the final methane production in both solid and liquid fractions of our samples is difficult. It is suggested to apply dry AD treatment to the solid fraction of the hydrolysate to increase methane production further. Moreover, specific methanogenic activity (SMA) tests are recommended to investigate the inhibition/toxicity of the hydrolysates produced under TORWASH® conditions. Regarding the hydrolysates produced from TH with acidic pretreatments, BMP and SMA tests are also suggested to study the effects of acidic pretreatments on the following AD process.

References

Abelleira-Pereira, J., Pérez-Elvira, S., Sánchez-Oneto, J., de la Cruz, R., Portela, J. R., & Nebot, E. (2015). Enhancement of methane production in mesophilic anaerobic digestion of secondary sewage sludge by advanced thermal hydrolysis pretreatment. *Water research*, *71*, 330–340. https://www.sciencedirect.com/science/article/pii/S0043135414008598

Aboulfoth, A. M., El Gohary, E. H., & El Monayeri, O. D. (2015). Effect of thermal pretreatment on the solubilization of organic matters in a mixture of primary and waste activated sludge. *Journal of Urban and Environmental Engineering*, *9*(1), 82–88. https://doi.org/10.4090/juee.2015.v9n1.082088

Aggrey, A., Dare, P., Lei, R., & Gapes, D. (2012). Evaluation of a two-stage hydrothermal process for enhancing acetic acid production using municipal biosolids. *Water Science and Technology*, *65*(1), 149–155. https://iwaponline.com/wst/article-abstract/65/1/149/15729

Ajandouz, E. H., Tchiakpe, L. S., Dalle Ore, F., Benajiba, A., & Puigserver, A. (2001). Effects of pH on caramelization and Maillard reaction kinetics in fructose-lysine model systems. *Journal of Food Science*, *66*(7), 926–931. https://doi.org/10.1111/j.1365-2621.2001.tb08213.x

Amend, J. P., LaRowe, D. E., McCollom, T. M., & Shock, E. L. (2013). The energetics of organic synthesis inside and outside the cell. https://doi.org/10.1098/rstb.2012.0255

Angelidaki, I., Karakashev, D., Batstone, D. J., Plugge, C. M., & Stams, A. J. (2011). Biomethanation and Its Potential. *Methods in Enzymology*, *494*, 327–351. https://doi.org/10.1016/B978-0-12-385112-3.00016-0

APHA, AWWA, & WEF. (1998). *Standard methods for the examination of water and wastewater*. APHA-AWWA-WEF.

Atienza-Martínez, M., Mastral, J. F., Ábrego, J., Ceamanos, J., & Gea, G. (2015). Sewage sludge torrefaction in an auger reactor. *Energy and Fuels*, *29*(1), 160–170. https://doi.org/10.1021/ef501425h

Bachir, S., Barbati, S., Ambrosio, M., & Tordo, P. (2001). Kinetics and mechanism of wet-air oxidation of nuclear-fuel-chelating compounds. *Industrial and Engineering Chemistry Research*, *40*(8), 1798–1804. https://doi.org/10.1021/IE000818T

Barber, W. P. (2016). Thermal hydrolysis for sewage treatment: A critical review. *Water Research*, *104*, 53–71. https://doi.org/10.1016/j.watres.2016.07.069

Bemiller, J. N. (2018). *Carbohydrate chemistry for food scientists*. Elsevier. https://books.google.com/books?hl=en&lr=&id=MRlxDwAAQBAJ&oi=fnd&pg=PP1&dq=BeMiller+J.N.+Carbohydrate+chemistry+for+food+scientists+(3ed.,+Elsevier,+2019)(ISBN+9780128120699)(O)(420s)+Ch+&ots=BH-ESqYLdj&sig=AOHBdBjIdt21MBtkPBSefoAVsp8

Birdwell, J. E., & Engel, A. S. (2010). Characterization of dissolved organic matter in cave and spring waters using UV-Vis absorbance and fluorescence spectroscopy. *Organic Geochemistry*, *41*(3), 270–280. https://doi.org/10.1016/j.orggeochem.2009.11.002

Blondeau, R. (1989). *Biodegradation of Natural and Synthetic Humic Acids by the White Rot Fungus Phanerochaete chrysosporium* (tech. rep. No. 5). https://journals.asm.org/journal/aem

Bolado-Rodríguez, S., Toquero, C., Martín-Juárez, J., Travaini, R., & García-Encina, P. A. (2016). Effect of thermal, acid, alkaline and alkaline-peroxide pretreatments on the biochemical methane potential and kinetics of the anaerobic digestion of wheat straw and sugarcane bagasse. *Bioresource Technology*, *201*, 182–190. https://doi.org/10.1016/j.biortech.2015.11.047

Bougrier, C., Delgenès, J. P., & Carrère, H. (2008). Effects of thermal treatments on five different waste activated sludge samples solubilisation, physical properties and anaerobic digestion. *Chemical Engineering Journal*, *139*(2), 236–244. https://doi.org/10.1016/j.cej.2007.07.099

Brunner, G. (2009). Near critical and supercritical water. Part I. Hydrolytic and hydrothermal processes. *The Journal of Supercritical Fluids*, *47*(3), 373–381. https://www.sciencedirect.com/science/article/pii/S0896844608002970

Byrappa, K., & Yoshimura, M. (2012). *Handbook of hydrothermal technology*. William Andrew.

Cantor, S. M., & Peniston, Q. P. (1940). The Reduction of Aldoses at the Dropping Mercury Cathode: Estimation of the aldehydo Structure in Aqueous Solutions. *Journal of the American Chemical Society*, *62*(8), 2113–2121. https://doi.org/10.1021/JA01865A056

Carlsson, M., Lagerkvist, A., & Morgan-Sagastume, F. (2012). The effects of substrate pre-treatment on anaerobic digestion systems: A review. *Waste Management*, *32*(9), 1634–1650. https://doi.org/10.1016/j.wasman.2012.04.016

Carrere, H., Antonopoulou, G., Affes, R., Passos, F., Battimelli, A., Lyberatos, G., & Ferrer, I. (2016). Review of feedstock pretreatment strategies for improved anaerobic digestion: From lab-scale research to full-scale application. https://doi.org/10.1016/j.biortech.2015.09.007

Chandra, R., Bharagava, R., & Rai, V. (2008). Melanoidins as major colourant in sugarcane molasses based distillery effluent and its degradation. *Bioresource technology*, *99*(11), 4648–4660. https://www.sciencedirect.com/science/article/pii/S0960852407008024?casa_token=gWd5b8QMMWwAAAAA:kxrG9ARB2Fov6T5gU_0g3niU7arU3fa5AZSl9XxjO6mWCEN2qpwZ_R_yEH5bnR1jZPEZeZWe

Chen, W., Westerhoff, P., Leenheer, J. A., & Booksh, K. (2003). Fluorescence Excitation-Emission Matrix Regional Integration to Quantify Spectra for Dissolved Organic Matter. *Environmental Science and Technology*, *37*(24), 5701–5710. https://doi.org/10.1021/es034354c

COLE, S. J. (1967). The Maillard Reaction in Food Products Carbon Dioxide Production. *Journal of Food Science*, *32*(3), 245–250. https://doi.org/10.1111/J.1365-2621.1967.TB01305.X

Cooper, J., Antony, A., Luiz, A., Kavanagh, J., Razmjou, A., Chen, V., & Leslie, G. (2019). Characterisation of dissolved organic matter in fermentation industry effluents and comparison with model compounds. *Chemosphere*, *234*, 630–639. https://doi.org/10.1016/j.chemosphere.2019.05.272

De Graaf, L. A. (2000). Denaturation of proteins from a non-food perspective. *Journal of Biotechnology*, *79*(3), 299–306. https://doi.org/10.1016/S0168-1656(00)00245-5

Dubois, M., Gilles, K. A., Hamilton, J. K., Rebers, P. A., & Smith, F. (1956). Colorimetric Method for Determination of Sugars and Related Substances. *Analytical Chemistry*, *28*(3), 350–356. https://doi.org/10.1021/ac60111a017

Dwyer, J., Starrenburg, D., Tait, S., Barr, K., Batstone, D. J., & Lant, P. (2008). Decreasing activated sludge thermal hydrolysis temperature reduces product colour, without

decreasing degradability. *Water Research*, *42*(18), 4699–4709. https://doi.org/10.1016/j.watres.2008.08.019

Engineering ToolBox. (2008). Solubility of Gases in Water vs. Temperature. https://www.engineeringtoolbox.com/gases-solubility-water-d_1148.html

Faixo, S., Gehin, N., Balayssac, S., Gilard, V., Mazeghrane, S., Haddad, M., Gaval, G., Paul, E., & Garrigues, J. C. (2021). Current trends and advances in analytical techniques for the characterization and quantification of biologically recalcitrant organic species in sludge and wastewater: A review. https://doi.org/10.1016/j.aca.2021.338284

Fang, C., Huang, R., Dykstra, C. M., Jiang, R., Pavlostathis, S. G., & Tang, Y. (2020). Energy and Nutrient Recovery from Sewage Sludge and Manure via Anaerobic Digestion with Hydrothermal Pretreatment. *Environmental Science and Technology*, *54*(2), 1147–1156. https://doi.org/10.1021/acs.est.9b03269

Frȼlund, B., Griebe, •. T., & Nielsen, P. H. (1995). *Enzymatic activity in the activated-sludge floc matrix* (tech. rep.).

Frȼlund, B. O., Palmgren, R., Keiding, K., & Nielsen, E. R. (1996). *EXTRACTION OF EXTRACELLULAR POLYMERS FROM ACTIVATED SLUDGE USING A CATION EXCHANGE RESIN* (tech. rep. No. 95).

Ge, S. J., & Lee, T. C. (1997). Kinetic Significance of the Schiff Base Reversion in the Early-Stage Maillard Reaction of a Phenylalanine-Glucose Aqueous Model System. *Journal of Agricultural and Food Chemistry*, *45*(5), 1619–1623. https://doi.org/10.1021/JF960458D

Ghasimi, D. S., Aboudi, K., de Kreuk, M., Zandvoort, M. H., & van Lier, J. B. (2016). Impact of lignocellulosic-waste intermediates on hydrolysis and methanogenesis under thermophilic and mesophilic conditions. *Chemical Engineering Journal*, *295*, 181–191. https://doi.org/10.1016/j.cej.2016.03.045

Göncüoğlu Taş, N., & Gökmen, V. (2017). Maillard reaction and caramelization during hazelnut roasting: A multiresponse kinetic study. *Food Chemistry*, *221*, 1911–1922. https://doi.org/10.1016/j.foodchem.2016.11.159

Gonzalez, A., Hendriks, A. T., van Lier, J. B., & de Kreuk, M. (2018). Pre-treatments to enhance the biodegradability of waste activated sludge: Elucidating the rate limiting step. *Biotechnology Advances*, *36*(5), 1434–1469. https://doi.org/10.1016/j.biotechadv.2018.06.001

González, J., Sánchez, M., & Gómez, X. (2018). Enhancing Anaerobic Digestion: The Effect of Carbon Conductive Materials. *C*, *4*(4), 59. https://doi.org/10.3390/c4040059

Grootjes, A., Liakakou, E., Kuipers, H., van der Kooij, Y., Wiermans, V., & Zwart, R. (2019). Final report TKI toeslag project Sludge to Power & Products (S2PP). *TNO PUBLIEK*. https://biobasedeconomy.nl/wp-content/uploads/2020/01/BBE-1708-S2PP-public-report-20190620-signed.pdf

Gujer, W., & Zehnder, A. J. B. (1983). CONVERSION PROCESSES IN ANAEROBIC DIGESTION. *Water science and technology*, *15*(8-9), 127–167. http://iwaponline.com/wst/article-pdf/15/8-9/127/95639/127.pdfbyTECHNISCHEUNIVERSITEITDELFTuser

Guo, X., Wang, X., & Liu, J. (2016). Composition analysis of fractions of extracellular polymeric substances from an activated sludge culture and identification of dominant forces affecting microbial aggregation. *Scientific Reports*, *6*. https://doi.org/10.1038/srep28391

Her, N., Amy, G., Sohn, J., & Gunten, U. (2008). UV absorbance ratio index with size exclusion chromatography (URI-SEC) as an NOM property indicator. *Journal of Water Supply: Research and Technology - AQUA*, *57*(1), 35–44. https://doi.org/10.2166/aqua.2008.029

Hii, K., Baroutian, S., Parthasarathy, R., Gapes, D. J., & Eshtiaghi, N. (2014). A review of wet air oxidation and Thermal Hydrolysis technologies in sludge treatment. https://doi.org/10.1016/j.biortech.2013.12.066

Hodge, J. E. (1953). Dehydrated foods, Chemistry of Browning Reactions in Model Systems. *Journal of Agricultural and Food Chemistry*, *1*(15), 928–943. https://doi.org/10.1021/JF60015A004

Højris, B., & Lund Skovhus, T. (Eds.). (2019). *Microbiological sensors for the drinking water industry*. IWA Publishing. https://doi.org/10.2166/9781780408699

Holliger, C., Alves, M., Andrade, D., Angelidaki, I., Astals, S., Baier, U., Bougrier, C., Buffière, P., Carballa, M., De Wilde, V., Ebertseder, F., Fernández, B., Ficara, E., Fotidis, I., Frigon, J. C., De Laclos, H. F., Ghasimi, D. S., Hack, G., Hartel, M., … Wierinck, I. (2016). Towards a standardization of biomethane potential tests. *Water Science and Technology*, *74*(11), 2515–2522. https://doi.org/10.2166/wst.2016.336

Huguet, A., Vacher, L., Relexans, S., Saubusse, S., Froidefond, J. M., & Parlanti, E. (2009). Properties of fluorescent dissolved organic matter in the Gironde Estuary. *Organic Geochemistry*, *40*(6), 706–719. https://doi.org/10.1016/j.orggeochem.2009.03.002

Hui, Y., Nip, W., Nollet, L., Paliyath, G., & Simpson, B. (2008). *Food biochemistry and food processing*. John Wiley & Sons. https://books.google.com/books?hl=en&lr=&id=Cd4NnJXgzd4C&oi=fnd&pg=PR5&dq=Food+Biochemistry+and+Food+Processing&ots=pupdXGfj4T&sig=n3ME01PaEgOl3nwVATgCS4oZJ_c

Ignatev, A., & Tuhkanen, T. (2019). Step-by-step analysis of drinking water treatment trains using size-exclusion chromatography to fingerprint and track protein-like and humic/fulvic-like fractions of dissolved organic matter. *Environmental Science: Water Research and Technology*, *5*(9), 1568–1581. https://doi.org/10.1039/c9ew00340a

Isaksson, S. (2018). *Biogas production at high ammonia levels: The importance of temperature and trace element supplementation on microbial communities* (Doctoral dissertation).

Jeong, S. Y., Chang, S. W., Ngo, H. H., Guo, W., Nghiem, L. D., Banu, J. R., Jeon, B. H., & Nguyen, D. D. (2019). Influence of thermal hydrolysis pretreatment on physicochemical properties and anaerobic biodegradability of waste activated sludge with different solids content. *Waste Management*, *85*, 214–221. https://doi.org/10.1016/j.wasman.2018.12.026

Jia, X., Zhu, C., Li, M., Xi, B., Wang, L., Yang, X., Xia, X., & Su, J. (2013). A comparison of treatment techniques to enhance fermentative hydrogen production from piggery anaerobic digested residues. *International Journal of Hydrogen Energy*, *38*(21), 8691–8698. https://doi.org/10.1016/j.ijhydene.2013.05.013

Jimenez, J., Vedrenne, F., Denis, C., Mottet, A., Déléris, S., Steyer, J. P., & Cacho Rivero, J. A. (2013). A statistical comparison of protein and carbohydrate characterisation methodology applied on sewage sludge samples. *Water Research*, *47*(5), 1751–1762. https://doi.org/10.1016/j.watres.2012.11.052

Jin, M. Y., Oh, H. J., Shin, K. H., Jang, M. H., Kim, H. W., Choi, B., Lin, Z. Y., Heo, J. S., Oh, J. M., & Chang, K. H. (2020). The response of dissolved organic matter during monsoon and post-monsoon periods in the regulated river for sustainablewater supply. *Sustainability (Switzerland)*, *12*(13). https://doi.org/10.3390/su12135310

Kaiser, H. F. (1960). The Application of Electronic Computers to Factor Analysis. *Educational and Psychological Measurement*, *20*(1), 141–151. https://doi.org/10.1177/001316446002000116

Kirkwood, R. N., Brandon, S. C. E., De Souza Moreira, B., & Deluzio, K. J. (2013). *Searching for Stability as we Age: The PCA-Biplot Approach* (tech. rep. No. 2).

Kroh, L. W. (1994). Caramelisation in food and beverages. *Food chemistry*, *51*(4), 373–379. https://www.sciencedirect.com/science/article/pii/0308814694901880

Kroll, J. H., Donahue, N. M., Jimenez, J. L., Kessler, S. H., Canagaratna, M. R., Wilson, K. R., Altieri, K. E., Mazzoleni, L. R., Wozniak, A. S., Bluhm, H., Mysak, E. R., Smith, J. D., Kolb, C. E., & Worsnop, D. R. (2011). Carbon oxidation state as a metric for describing the chemistry of atmospheric organic aerosol. *Nature Chemistry*, *3*(2), 133–139. https://doi.org/10.1038/nchem.948

Lakowicz, J. R. (2006). Principles of fluorescence spectroscopy. *Principles of Fluorescence Spectroscopy*, 1–954. https://doi.org/10.1007/978-0-387-46312-4

Larsson, T., Wedborg, M., & Turner, D. (2007). Correction of inner-filter effect in fluorescence excitation-emission matrix spectrometry using Raman scatter. *Analytica Chimica Acta*, *583*(2), 357–363. https://doi.org/10.1016/j.aca.2006.09.067

Lawaetz, A. J., & Stedmon, C. A. (2009). Fluorescence Intensity Calibration Using the Raman Scatter Peak of Water. *Applied spectroscopy*, *63*(8), 936–940.

Le, C., Kunacheva, C., & Stuckey, D. C. (2016). "protein" Measurement in Biological Wastewater Treatment Systems: A Critical Evaluation. *Environmental Science and Technology*, *50*(6), 3074–3081. https://doi.org/10.1021/acs.est.5b05261

Liu, F., Barrault, J., De Oliveira Vigier, K., & Jérôme, F. (2012). Dehydration of highly concentrated solutions of fructose to 5-hydroxymethylfurfural in a cheap and sustainable choline chloride/carbon dioxide system. *ChemSusChem*, *5*(7), 1223–1226. https://doi.org/10.1002/cssc.201200186

Liu, X., Wang, Q., Tang, Y., & Pavlostathis, S. G. (2021). A comparative study on biogas production, energy balance, and nutrients conversion with inter-stage hydrothermal treatment of sewage sludge. *Applied Energy*, *288*. https://doi.org/10.1016/j.apenergy.2021.116669

Liu, Y., Li, X., & Kang, X. (2015). Effect of volume ratio on anaerobic co-digestion of thermal hydrolysis of food waste with activated sludge. *International Biodeterioration and Biodegradation*, *102*, 154–158. https://doi.org/10.1016/j.ibiod.2015.02.015

Lü, F., Zhou, Q., Wu, D., Wang, T., Shao, L., & He, P. (2015). Dewaterability of anaerobic digestate from food waste: Relationship with extracellular polymeric substances. *Chemical Engineering Journal*, *262*, 932–938. https://doi.org/10.1016/J.CEJ.2014.10.051

Lucile, F., Cézac, P., Contamine, F., Serin, J. P., Houssin, D., & Arpentinier, P. (2012). Solubility of carbon dioxide in water and aqueous solution containing sodium hydroxide at temperatures from (293.15 to 393.15) K and pressure up to 5 MPa: Experimental measurements. *Journal of Chemical and Engineering Data*, *57*(3), 784–789. https://doi.org/10.1021/je200991x

Mao, C., Feng, Y., Wang, X., & Ren, G. (2015). Review on research achievements of biogas from anaerobic digestion. https://doi.org/10.1016/j.rser.2015.02.032

Martins, S. I., Jongen, W. M., & Van Boekel, M. A. (2000). A review of Maillard reaction in food and implications to kinetic modelling. *Trends in Food Science & Technology*, *11*(9-10), 364–373. https://doi.org/10.1016/S0924-2244(01)00022-X

Martins, S., & van Boekel, M. A. (2003). Melanoidins extinction coefficient in the glucose/glycine Maillard reaction. *Food Chemistry*, *83*(1), 135–142. https://www.sciencedirect.com/science/article/pii/S030881460300219X

Mcknight, D. M., Boyer, E. W., Westerhoff, P. K., Doran, P. T., Kulbe, T., & Andersen, D. T. (2001). *Spectrofluorometric characterization of dissolved organic matter for indication of precursor organic material and aromaticity* (tech. rep. No. 1).

McNaught, A. D. (1997). *Compendium of chemical terminology* (Vol. Vol. 1669). Oxford: Blackwell Science.

Mohsin, G. F., Schmitt, F. J., Kanzler, C., Dirk Epping, J., Flemig, S., & Hornemann, A. (2018). Structural characterization of melanoidin formed from D-glucose and L-alanine

at different temperatures applying FTIR, NMR, EPR, and MALDI-ToF-MS. *Food Chemistry*, *245*, 761–767. https://doi.org/10.1016/j.foodchem.2017.11.115

Monlau, F., Sambusiti, C., Barakat, A., Quéméneur, M., Trably, E., Steyer, J. P., & Carrère, H. (2014). Do furanic and phenolic compounds of lignocellulosic and algae biomass hydrolyzate inhibit anaerobic mixed cultures? A comprehensive review. https://doi.org/10.1016/j.biotechadv.2014.04.007

Mottet, A., Steyer, J. P., Déléris, S., Vedrenne, F., Chauzy, J., & Carrère, H. (2009). Kinetics of thermophilic batch anaerobic digestion of thermal hydrolysed waste activated sludge. *Biochemical Engineering Journal*, *46*(2), 169–175. https://doi.org/10.1016/j.bej.2009.05.003

Nakaya, Y., & Nakashima, S. (2016). In situ IR transmission spectroscopic observation and kinetic analyses of initial stage of the maillard reaction as a simulated formation process of humic substances. *Chemistry Letters*, *45*(10), 1204–1206. https://doi.org/10.1246/cl.160596

Nanou, P., Sebastiani, F., Legé, L. d., Pels, J., & Driessen, W. (2020). PILOTONDERZOEK HYDROTHERMALE BEWERKING VAN ZUIVERINGSSLIB MET TORWASH ®. *STOWA*, *2020-26*. www.stowa.nl

Nativ, P., Gräber, Y., Aviezer, Y., & Lahav, O. (2021). A simple and accurate approach for determining the vfa concentration in anaerobic digestion liquors, relying on two titration points and an external inorganic carbon analysis. *ChemEngineering*, *5*(2). https://doi.org/10.3390/chemengineering5020015

Nazari, L., Yuan, Z., Santoro, D., Sarathy, S., Ho, D., Batstone, D., Xu, C. C., & Ray, M. B. (2017). Low-temperature thermal pre-treatment of municipal wastewater sludge: Process optimization and effects on solubilization and anaerobic degradation. *Water Research*, *113*, 111–123. https://doi.org/10.1016/J.WATRES.2016.11.055

Neyens, E., Baeyens, J., materials, R. D. J. o. h., & 2004, u. (2004). Advanced sludge treatment affects extracellular polymeric substances to improve activated sludge dewatering. *Elsevier*. https://www.sciencedirect.com/science/article/pii/S0304389403004321

Ngo, P. L., Udugama, I. A., Gernaey, K. V., Young, B. R., & Baroutian, S. (2021). Mechanisms, status, and challenges of thermal hydrolysis and advanced thermal hydrolysis processes in sewage sludge treatment. https://doi.org/10.1016/j.chemosphere.2021.130890

Nguyen, T. T., Nam, S. N., Kim, J., & Oh, J. (2020). Photocatalytic degradation of dissolved organic matter under ZnO-catalyzed artificial sunlight irradiation system. *Scientific Reports*, *10*(1). https://doi.org/10.1038/s41598-020-69115-7

Nielsen, H. B., Thygesen, A., Thomsen, A. B., & Schmidt, J. E. (2011). Anaerobic digestion of waste activated sludge-comparison of thermal pretreatments with thermal inter-stage treatments. *Journal of Chemical Technology and Biotechnology*, *86*(2), 238–245. https://doi.org/10.1002/jctb.2509

Nursten, H. E. (2005). *The Maillard reaction : chemistry, biochemistry, and implications*. Royal Society of Chemistry.

O'Brien, J., Nursten, H., Ames, J., & Crabbe, M. (1998). *The Maillard reaction in foods and medicine*. Woodhead Publishing. https://books.google.com/books?hl=en&lr=&id=9-v6f2NlufwC&oi=fnd&pg=PR5&dq=The+Maillard+reaction+in+foods+and+medicine.+In:O%27Brien,+J.,+Nursten,+H.E.,+Crabbe,+M.J.C.,+Ames,+J.M.+(Eds.),+The+Maillard+reaction+infoods+and+medicine.+Woodhead+Publishing&ots=sZTGgGfCEY&sig=9ZGLUJecREd9igd6NhLeZDOV8m4

Park, K. Y., Yu, Y. J., Yun, S. J., & Kweon, J. H. (2019). Natural organic matter removal from algal-rich water and disinfection by-products formation potential reduction by powdered activated carbon adsorption. *Journal of Environmental Management*, *235*, 310–318. https://doi.org/10.1016/j.jenvman.2019.01.080

Park, M., & Snyder, S. A. (2018). Sample handling and data processing for fluorescent excitation-emission matrix (EEM) of dissolved organic matter (DOM). *Chemosphere*, *193*, 530–537. https://doi.org/10.1016/j.chemosphere.2017.11.069

Parkhurst, D., & Appelo, C. (2013). Description of input and examples for PHREEQC version 3: a computer program for speciation, batch-reaction, one-dimensional transport, and inverse geochemical calculations. *Techniques and methods* (p. 497). U.S. Geological Survey. https://pubs.usgs.gov/tm/06/a43/

Penaud, V., Delgenès, J.-P., & Moletta, R. (2000). Characterization of Soluble Molecules from Thermochemically Pretreated Sludge. *Journal of Environmental Engineering*, *126*(5), 397–402. https://doi.org/10.1061/(ASCE)0733-9372(2000)126:5(397)

Peng, D.-Y., & Robinson, D. B. (1976). A New Two-Constant Equation of State. *Industrial and Engineering Chemistry Fundamentals*, *15*, 59–64. https://pubs.acs.org/sharingguidelines

Pilli, S., Yan, S., Tyagi, R. D., & Surampalli, R. Y. (2015). Thermal pretreatment of sewage sludge to enhance anaerobic digestion: A review. https://doi.org/10.1080/10643389.2013.876527

Rao, P., & Pattabiraman, T. N. (1989). *Reevaluation of the Phenol-Sulfuric Acid Reaction for the Estimation of Hexoses and Pentoses* (tech. rep. No. 1).

Rea, J. (2014). *Kinetic Modeling and experimentation of anaerobic digestion (Doctoral dissertation, Massachusetts Institute of Technology)* (Doctoral dissertation). https://dspace.mit.edu/handle/1721.1/92070

Rossiter, D. G. (2014). *Tutorial: Using the R Environment for Statistical Computing An example with the Mercer & Hall wheat yield dataset* (tech. rep.). University of Twente (UT). http://www.css.cornell.edu/faculty/dgr2/_static/files/R_PDF/mhw.pdf

Sapkaite, I., Barrado, E., Fdz-Polanco, F., & Pérez-Elvira, S. I. (2017). Optimization of a thermal hydrolysis process for sludge pre-treatment. *Journal of Environmental Management*, *192*, 25–30. https://doi.org/10.1016/j.jenvman.2017.01.043

Schönberg, A., & Moubacher, R. (1952). The strecker degradation of α-amino acids. *Chemical Reviews*, *50*(2), 261–277. https://doi.org/10.1021/CR60156A002

Seviour, R. J., Mino, T., & Onuki, M. (2003). The microbiology of biological phosphorus removal in activated sludge systems. https://doi.org/10.1016/S0168-6445(03)00021-4

Stedmon, C. A., Markager, S., & Bro, R. (2003). Tracing dissolved organic matter in aquatic environments using a new approach to fluorescence spectroscopy. *Marine Chemistry*, *82*(3-4), 239–254. https://doi.org/10.1016/S0304-4203(03)00072-0

Takashima, M., & Tanaka, Y. (2010). Application of acidic thermal treatment for one- and two-stage anaerobic digestion of sewage sludge. *Water Science and Technology*, *62*(11), 2647–2654. https://doi.org/10.2166/wst.2010.490

Togo, H. (2004). *Advanced free radical reactions for organic synthesis*. https://books.google.com/books?hl=en&lr=&id=M4JNLKQ0pEEC&oi=fnd&pg=PP1&dq=Togo,+H.,+2004.+Advanced+Free+Radical+Reactions+for+Organic+Synthesis.+Elsevier.&ots=S4gWnbx-Sr&sig=ZHO7uMykkmCjsA-tqmYbAI3u26Q

Toutian, V., Barjenbruch, M., Unger, T., Loderer, C., & Remy, C. (2020). Effect of temperature on biogas yield increase and formation of refractory COD during thermal hydrolysis of waste activated sludge. *Water research*, *171*. https://www.sciencedirect.com/science/article/pii/S0043135419311571

Trubetskaya, O. E., Richard, C., Patsaeva, S. V., & Trubetskoj, O. A. (2020). Evaluation of aliphatic/aromatic compounds and fluorophores in dissolved organic matter of contrasting natural waters by SEC-HPLC with multi-wavelength absorbance and fluorescence detections. *Spectrochimica Acta - Part A: Molecular and Biomolecular Spectroscopy*, *238*, 118450. https://doi.org/10.1016/j.saa.2020.118450

Urrea, J. L., García, M., Collado, S., Oulego, P., & Díaz, M. (2018). Sludge hydrothermal treatments. Oxidising atmosphere effects on biopolymers and physical properties. *Journal of Environmental Management*, *206*, 284–290. https://doi.org/10.1016/j.jenvman.2017.10.043

Urrea, J. L., Collado, S., Oulego, P., & Díaz, M. (2016). Effect of wet oxidation on the fingerprints of polymeric substances from an activated sludge. *Water Research*, *105*, 282–290. https://doi.org/10.1016/j.watres.2016.09.004

Van Boekel, M. A. J. S. (2001). Kinetic aspects of the Maillard reaction: a critical review. *Food/Nahrung*, *45*(3), 150–159.

van Lier, J. B., Mahmoud, N., & Zeeman, G. (2020). Anaerobic wastewater treatment. In G. Chen, G. A. Ekama, M. C. M. van Loosdrecht, & D. Brdjanovic (Eds.), *Biological wastewater treatment: Principles, modeling and design*.

Villamiel, M., del Castillo, M., & Corzo, N. (2006). *Food Biochemistry and Food Processing*. Wiley-Blackwell.

Wang, G., Yonghao, L., Deng, J., Kuang, J., & Zhang, Y. (2011). Pretreatment of biomass by torrefaction. *Chinese Science Bulletin*, *56*(14), 1442–1448. https://doi.org/10.1007/s11434-010-4143-y

Wilson, C. A., & Novak, J. T. (2009). Hydrolysis of macromolecular components of primary and secondary wastewater sludge by thermal hydrolytic pretreatment. *Water Research*, *43*(18), 4489–4498. https://doi.org/10.1016/j.watres.2009.07.022

Wu, J., West, L. J., & Stewart, D. I. (2002). *Effect of humic substances on Cu(II) solubility in kaolin-sand soil* (tech. rep.).

Xue, Y., Liu, H., Chen, S., Dichtl, N., Dai, X., & Li, N. (2015). Effects of thermal hydrolysis on organic matter solubilization and anaerobic digestion of high solid sludge. *Chemical Engineering*, *26*, 174–180. https://www.sciencedirect.com/science/article/pii/S138589471401448X?casa_token=3U21x7rvDQcAAAAA:Ya9UlhuK1l7MlwIU2sJtjOvvncvbV5MGCszDxSeYV9MK1T0F4Nqd0-YMhZFpQQRpj7_ErCR4

Yan, W., Xu, H., Lu, D., & Zhou, Y. (2022). Effects of sludge thermal hydrolysis pretreatment on anaerobic digestion and downstream processes: mechanism, challenges and solutions. *Bioresource Technology*, *344*, 126248. https://doi.org/10.1016/j.biortech.2021.126248

Yang, D., Dai, X., Song, L., Dai, L., & Dong, B. (2019). Effects of stepwise thermal hydrolysis and solid-liquid separation on three different sludge organic matter solubilization and biodegradability. *Bioresource Technology*, *290*. https://doi.org/10.1016/j.biortech.2019.121753

Yang, H., Yang, S., Kong, J., Dong, A., & Yu, S. (2015). Obtaining information about protein secondary structures in aqueous solution using Fourier transform IR spectroscopy. *Nature Protocols*, *10*(3), 382–396. https://doi.org/10.1038/nprot.2015.024

Yang, N., Yang, S., & Zheng, X. (2022). Inhibition of Maillard reaction during alkaline thermal hydrolysis of sludge. *Science of the Total Environment*, *814*. https://doi.org/10.1016/j.scitotenv.2021.152497

Yousefifar, A., Baroutian, S., Farid, M., Gapes, D. J., & Young, B. R. (2017). Fundamental mechanisms and reactions in non-catalytic subcritical hydrothermal processes: A review. *Water research, 123*, 607–622. https://www.sciencedirect.com/science/article/pii/S0043135417305456

Yu, B., Luo, J., Xie, H., Yang, H., Chen, S., Liu, J., Zhang, R., & Li, Y. Y. (2021). Species, fractions, and characterization of phosphorus in sewage sludge: A critical review from the perspective of recovery. https://doi.org/10.1016/j.scitotenv.2021.147437

Zepp, R. G., Sheldon, W. M., & Moran, M. A. (2004). Dissolved organic fluorophores in southeastern US coastal waters: Correction method for eliminating Rayleigh and

Raman scattering peaks in excitation-emission matrices. *Marine Chemistry*, *89*(1-4), 15–36. https://doi.org/10.1016/j.marchem.2004.02.006

Zhang, D., Feng, Y., Huang, H., Khunjar, W., & Wang, Z. W. (2020). Recalcitrant dissolved organic nitrogen formation in thermal hydrolysis pretreatment of municipal sludge. *Environment International*, *138*(March), 105629. https://doi.org/10.1016/j.envint.2020.105629

Zhen, G., Lu, X., Kato, H., Zhao, Y., & Li, Y. Y. (2017). Overview of pretreatment strategies for enhancing sewage sludge disintegration and subsequent anaerobic digestion: Current advances, full-scale application and future perspectives. *Renewable and Sustainable Energy Reviews*, *69*, 559–577. https://doi.org/10.1016/J.RSER.2016.11.187

Zhou, S., Zhang, Y., Huang, T., Liu, Y., Fang, K., & Zhang, C. (2019). Microbial aerobic denitrification dominates nitrogen losses from reservoir ecosystem in the spring of Zhoucun reservoir. *Science of the Total Environment*, *651*, 998–1010. https://doi.org/10.1016/j.scitotenv.2018.09.160

Zsolnay, A., Baigar, E., Jimenez, M., Steinweg, B., & Saccomandi, F. (1999). Differentiating with fluorescence spectroscopy the sources of dissolved organic matter in soils subjected to drying. *Chemosphere*, *38*(1), 45–50. https://doi.org/10.1016/S0045-6535(98)00166-0

Appendix A

Records of TH tests on WAS-2

Table A.1: Experiment record of WAS-2-1.

Time [min]	Pressure [bar]	Temperature [°C]
0	11.7	190
1	11.7	190
2	11.7	190
3	11.7	190
4	11.6	189
5	11.6	189
6	11.6	189
7	11.6	189
8	11.6	189
9	11.6	189
10	11.9	190
11	11.9	190
12	12	191
13	12	191
14	12	191
15	12	191
16	12	191
17	12	191
18	12	191
19	11.9	190
20	11.8	189
21	11.8	189
22	11.8	189
23	11.8	189
24	11.8	189
25	11.8	189
26	11.9	190
27	11.9	190
28	12	191
29	12	191
30	12	191

Note: The WAS-2-1 was the hydrothermal experiment carried out in the Parr No. 4600 at 190 °C for 30 min.

Table A.2: Experiment record of WAS-2-2.

Time [min]	Pressure [bar]	Temperature [°C]
0	14.2	190
1	14.3	191
2	14.3	192
3	13.9	193
4	13.9	193
5	11.7	190
6	11.2	189
7	11	188
8	11	187
9	11	187
10	11	187
11	11.5	188
12	11.5	188
13	11.5	188
14	11.5	188
15	11.9	189
16	11.9	189
17	11.8	188
18	11.8	188
19	11.8	188
20	11.8	188
21	12	189
22	12	189
23	12	189
24	12	189
25	12.1	190
26	12.1	190
27	12.1	190
28	12.2	191
29	12.2	191
30	12.2	191

Note: The WAS-2-2 was the hydrothermal experiment conducted with the addition of HAc (approx. 16985 mg HAc/ L WAS-2) in the Parr No. 4600 at 190 °C for 30 min.

Table A.3: Experiment record of WAS-2-3.

Time [min]	Pressure [bar]	Temperature [°C]
0	31	191
1	30.8	192
2	30.5	193
3	30	194
4	29	193
5	28.5	192
6	28.2	191
7	28	190
8	27.9	189
9	27.9	189
10	27.9	189
11	27.9	189
12	27.9	189
13	28.2	190
14	28.2	190
15	28.3	191
16	28.3	191
17	28	192
18	28	192
19	28	192
20	28	192
21	28	192
22	27	191
23	27	191
24	27	191
25	26.5	189
26	26.5	189
27	26.2	188
28	26.2	187
29	26.2	187
30	26.2	187

Note: The WAS-2-3 was the hydrothermal experiment with CO_2 pressurisation (10 bar) in the Parr No. 4600 at 190 °C for 30 min.

Table A.4: Experiment record of WAS-2-4.

Time [min]	Pressure [bar]	Temperature [°C]
0	53.38	191
1	53.38	193
2	53.38	194
3	52.38	195
4	52.38	195
5	51.27	194
6	50.35	193
7	50.35	193
8	50.35	193
9	50.35	193
10	50.35	193
11	50.35	193
12	50.35	192
13	50.35	192
14	50.35	192
15	49.33	191
16	49.33	191
17	48.73	190
18	48.73	190
19	48.32	189
20	48.32	189
21	48.32	189
22	48.43	188
23	48.43	188
24	48.43	188
25	48.43	188
26	48.43	188
27	48.43	188
28	48.43	188
29	48.43	188
30	48.73	189

Note: The WAS-2-4 was the hydrothermal experiment with CO_2 pressurisation (20 bar) in the Parr No. 4600 at 190 °C for 30 min.

Table A.5: Experiment record of WAS-2-5.

Time [min]	Pressure [bar]	Temperature [°C]
0	31.5	191
1	31	192
2	31	192
3	31	192
4	31	192
5	29	191
6	29	192
7	29	192
8	29	192
9	29	192
10	29	192
11	29	192
12	29	192
13	29	192
14	29	192
15	28	191
16	28	191
17	28	191
18	28	190
19	27.9	189
20	27.9	189
21	27.8	188
22	27.8	188
23	27.8	188
24	27	188
25	27	187
26	27	187
27	27	187
28	27	187
29	27.5	188
30	27.5	188

Note: The WAS-2-5 was the hydrothermal experiment with CO_2 pressurisation (10 bar) and addition of HAc (approx. 16985 mg HAc/ L WAS-2) in the Parr No. 4600 at 190 °C for 30 min.

Table A.6: Experiment record of WAS-2-6.

Time [min]	Pressure [bar]	Temperature [°C]
0	49.74	190
1	49.33	191
2	48.93	193
3	48.12	194
4	46.91	193
5	46.91	192
6	46.91	191
7	45.9	190
8	45.09	189
9	45.09	189
10	45.09	189
11	45.09	189
12	45.09	189
13	45.29	190
14	45.29	190
15	45.29	191
16	45.29	191
17	45.29	191
18	45.29	190
19	45.29	189
20	45.29	189
21	45.29	188
22	45.29	188
23	45.29	188
24	45.29	188
25	45.29	189
26	45.29	189
27	45.29	190
28	45.29	190
29	45.29	191
30	45.29	191

Note: The WAS-2-6 was the hydrothermal experiment with CO_2 pressurisation (20 bar) and addition of HAc (approx. 16985 mg HAc/ L WAS-2) in the Parr No. 4600 at 190 °C for 30 min.

Appendix B

BMP tests

Table B.1: Characterisation of inoculum.

Inoculum	pH	TS [%]	VS [%]	Total COD [mg O_2/L]	SCOD [mg O_2/L]
Digestate[1]	7.36 ± 0.02	3.764 ± 0.006	2.684 ± 0.002	41000 ± 300	810 ± 10

[1] Digestate was collected from WWTP Harnaschpolder, Netherlands.

Table B.2: Macronutrient stock solution.

Chemical	Concentration [g/L]
NH_4Cl	170
$CaCl_2 \cdot 2H_2O$	8
$MgSO_4 \cdot 7H_2O$	9

Dose: 6 ml per liter medium.

Table B.3: Micronutrient stock solution.

Chemical	Concentration [mg/L]
$FeCl_3 \cdot 4H_2O$	2000
$CoCl_2 \cdot 6H_2O$	2000
$MnCl_2 \cdot 4H_2O$	500
$CuCl_2 \cdot 2H_2O$	30
$ZnCl_2$	50
HBO_3	50
$(NH_4)_6Mo7O_2 \cdot 4H_2O$	90
$Na_2SeO_3 \cdot 5H_2O$	100
$NiCl_2 \cdot 6H_2O$	50
EDTA	1000
HCl (36% (v/v))	1 [mL/L]
Resazurine	500
Yeast extract	2000

Dose: 0.6 ml per liter medium.

Appendix C

EEM data processing

The overall procedure for EEM data processing is illustrated in **Figure C.1**. First, a three-dimensional Delaunay interpolation method developed by Zepp et al. (2004) was used to remove the Rayleigh and Raman scattering peaks manually. Specifically, scattering peaks on EEM spectra were regionally excised and refilled with the surrounding data points through interpolation. The next step was correcting the inner filter effect caused by self-quenching, where light absorption occurs at both the excitation (Ex) and emission (Em) wavelengths. The inner filter effect can be mitigated through sample pre-dilution or mathematical correction (**Equation C.0.1**) (Lakowicz, 2006; Larsson et al., 2007).

$$F_{corr}\ [A.U.] = F_{obs} \cdot 10^{\frac{Abs_{ex}+Abs_{em}}{2}} \qquad (Eq.\ C.0.1)$$

where:
F_{corr} is the corrected fluorescence intensities;
F_{obs} is the observed fluorescence intensities;
Abs_{ex} is the absorbance at Ex wavelength;
Abs_{em} is the absorbance at Em wavelength.

Once the inner filter effect was reduced, the Raman normalisation was employed to minimise the quantitative dependence of instrument specificity. Different instruments have different detectors and/or photomultipliers, resulting in different scales of fluorescence intensity with arbitrary units [A.U.]. Hence, normalisation methods are often required. Water Raman integration was employed in this study. The wavelength-dependent Raman cross-section of water is a fixed property of water of which the integral varies accordingly with different instruments or instrumental settings; therefore, it can be used for calibration (Lawaetz & Stedmon, 2009). Here, 350 nm Ex wavelength was chosen for water Raman integration since it is widely adopted (Stedmon et al., 2003), which equated to a band spanning from 370.8 to 427.9 nm with a peak appearing at 397.3 nm. To perform the calibration, the F_{corr} was divided by the area of Raman peak (**Equation C.0.2**), which calibrated fluorescence signal to Raman units [R.U.] (M. Park & Snyder, 2018).

$$F_{final}[R.U.] = \frac{F_{corr}}{\int_{\lambda_{em,lower}}^{\lambda_{em,upper}} F_{MQ}(\lambda_{em})} = \frac{F_{corr}}{\int_{427.9nm}^{370.8nm} F_{MQ,ex350nm}(\lambda_{em})} \qquad (Eq.\ C.0.2)$$

where:
F_{final} is the final fluorescence intensity;
F_{MQ} is the fluorescence intensity of Milli-Q water;
$F_{MQ,ex350nm}$ is the fluorescence intensity of Milli-Q water at 350 nm Ex wavelength;
$\lambda_{em,lower}$ is the lower boundary of wavelengths for the Raman peak;
$\lambda_{em,upper}$ is the upper boundary of wavelengths for the Raman peak.
Lastly, fluorescence regional integration (FRI) was performed to quantitatively assess DOM fractions represented by five operationally defined fluorescence regions in **Table C.1**. The

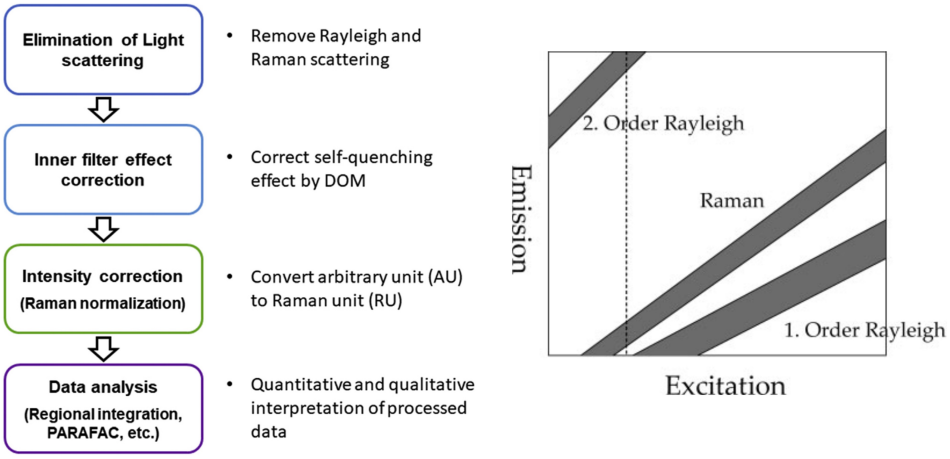

Figure C.1: Procedure for EEM data processing (left) and sketch of the scattering occurring in a fluorescence EEM (right) (Lawaetz & Stedmon, 2009; M. Park & Snyder, 2018).

fluorescence intensity volume beneath region i (ϕ_i) was obtained using **Equation C.0.3**, which then was normalised according to relative regional areas by multiplying the multiplication factor (MF) (**Equation C.0.4**). The MF equals the inverse of the fractional projected Ex-Em area. The percent fluorescence response of fluorescence region i then was calculated by dividing the normalised fluorescence volume beneath region i by total normalised fluorescence volume (**Equation C.0.5**) (Chen et al., 2003).

$$\phi_i = \sum_{\lambda_{ex,i,lower}}^{\lambda_{ex,i,upper}} \sum_{\lambda_{em,i,lower}}^{\lambda_{em,i,upper}} F_{final}(\lambda_{ex}, \lambda_{em}) \Delta\lambda_{ex} \Delta\lambda_{em} \qquad (Eq.\ C.0.3)$$

where:
ϕ_i is the fluorescence volume beneath region i of EEM;
$\lambda_{ex,i}$ is the Ex and Em wavelengths in the EEM region i;
$\lambda_{em,i}$ is the Ex and Em wavelengths in the EEM region i;
The subscripts "lower" and "upper" refer to lower and upper boundaries of EEM region.

$$\phi_{i,n} = MF_i\ \phi_i = \frac{\sum_{\lambda_{ex,lower}}^{\lambda_{ex,upper}} \sum_{\lambda_{em,lower}}^{\lambda_{em,upper}} \Delta\lambda_{ex} \Delta\lambda_{em}}{\sum_{\lambda_{ex,i,lower}}^{\lambda_{ex,i,upper}} \sum_{\lambda_{em,i,lower}}^{\lambda_{em,i,upper}} \Delta\lambda_{ex} \Delta\lambda_{em}}\ \phi_i \qquad (Eq.\ C.0.4)$$

where:
$\phi_{i,n}$ is the normalised fluorescence volume beneath region i of EEM;
MF_i is the multiplication factor of EEM region i.

$$P_{i,n} = \frac{\phi_{i,n}}{\phi_{T,n}} \times 100\% = \frac{\phi_{i,n}}{\sum_{i=1}^{V} \phi_{i,n}} \times 100\% \qquad (Eq.\ C.0.5)$$

where:
$P_{i,n}$ is percent fluorescence response;
$\phi_{T,n}$ is the total normalised fluorescence volume of EEM.

Table C.1: Ex-Em boundaries of five operationally-defined fluorescence regions.

Fluorescence region	Ex boundary [nm]	Em boundary [nm]
I Tyrosine-like aromatic protein	200-250	280-330
II Tryptophan-like aromatic protein	200-250	330-380
III Fulvic acid-like matter	200-250	380-550
IV Soluble microbial byproduct-like matter	250-400	280-380
V Humic acid-like matter	250-400	380-550

Fluorsecence parameters and indices

The Fn(355) (humic-like fluorescence parameter) and Fn(280) (protein-like fluorescence parameter) are the maximum fluorescence intensities of the Em wavelength regions of 440–470 nm at Ex wavelength 355 nm and 340–360 nm at Ex wavelength 280 nm, respectively (Jin et al., 2020). Fluorescence index (FI) is determined as the ratio of fluorescence intensity at the Ex wavelengths of 450 and 500 nm under constant Ex wavelength at 370 nm (Mcknight et al., 2001). Humification index (HIX) is the ratio of two integrated fluorescence regions with Em wavelengths of 435-480 nm and Em 300-345 nm at Ex wavelength 254 nm (Zsolnay et al., 1999). Biological index (BIX) is the fluorescence intensity ratio at Em wavelengths of 380 and 430 nm at Ex wavelength 310 nm (Jin et al., 2020).

Appendix D

Supplementary information for results and discussion

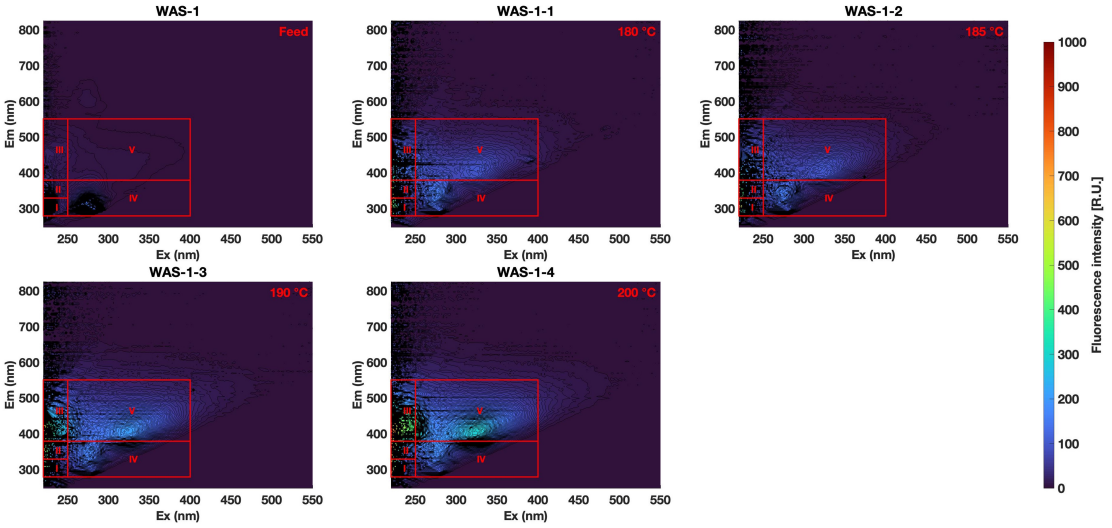

Figure D.1: EEM fluorescence spectra contour of WAS-1 subjecting to thermally-hydrolysed at different temperatures. Horizontal and vertical lines divide EEM spectra into five regions (I-V). Normalised to 1 g DOC/L.

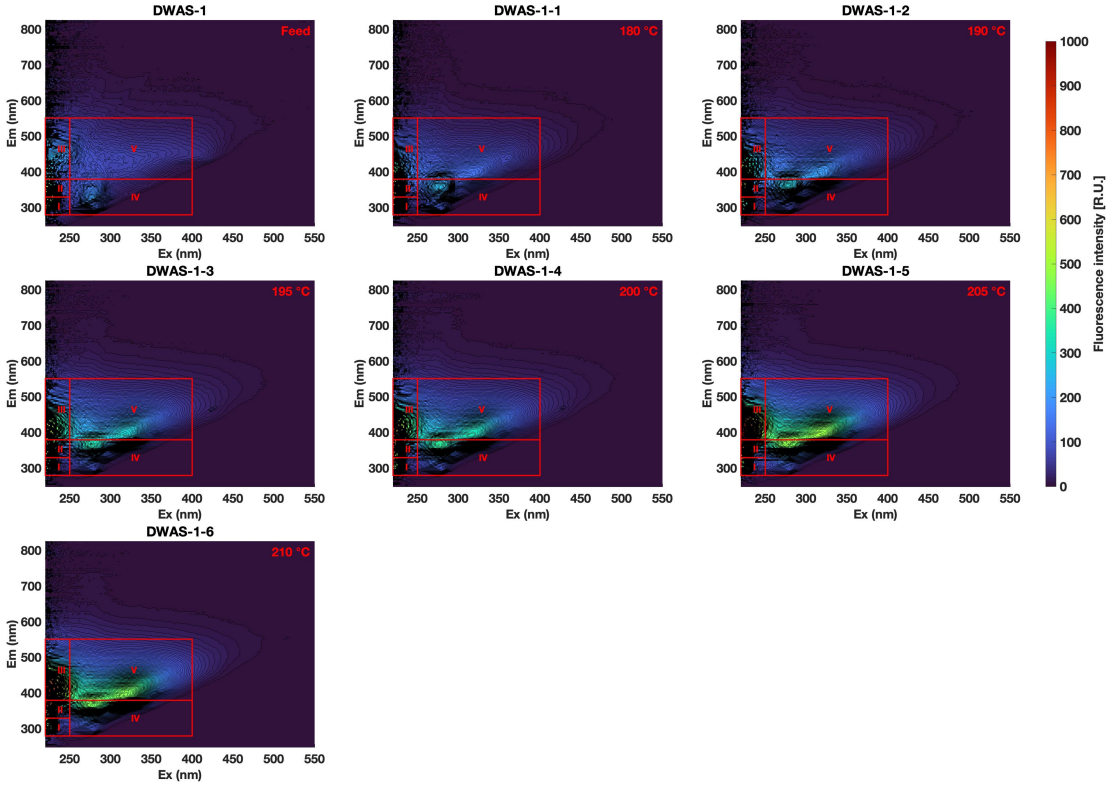

Figure D.2: EEM fluorescence spectra contour of DWAS-1 subjecting to thermal hydrolysis at different temperatures. Horizontal and vertical lines divide EEM spectra into five regions (I-V). Normalised to 1 g DOC/L.

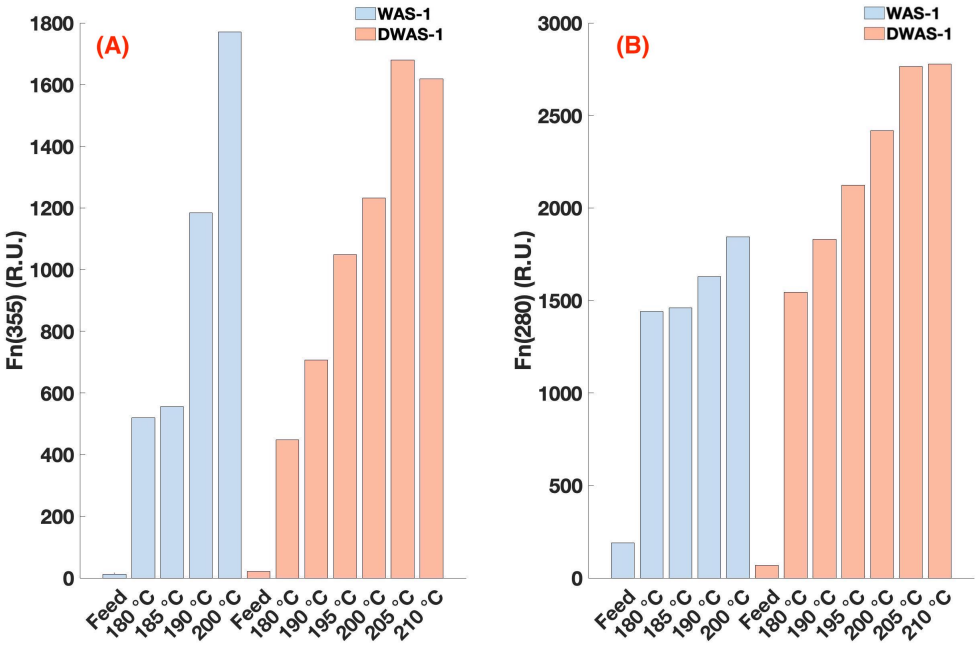

Figure D.3: Effect of reaction temperatures on Fn(355) (A), and Fn(280) (B) of thermally-hydrolysed WAS-1 and DWAS-1.

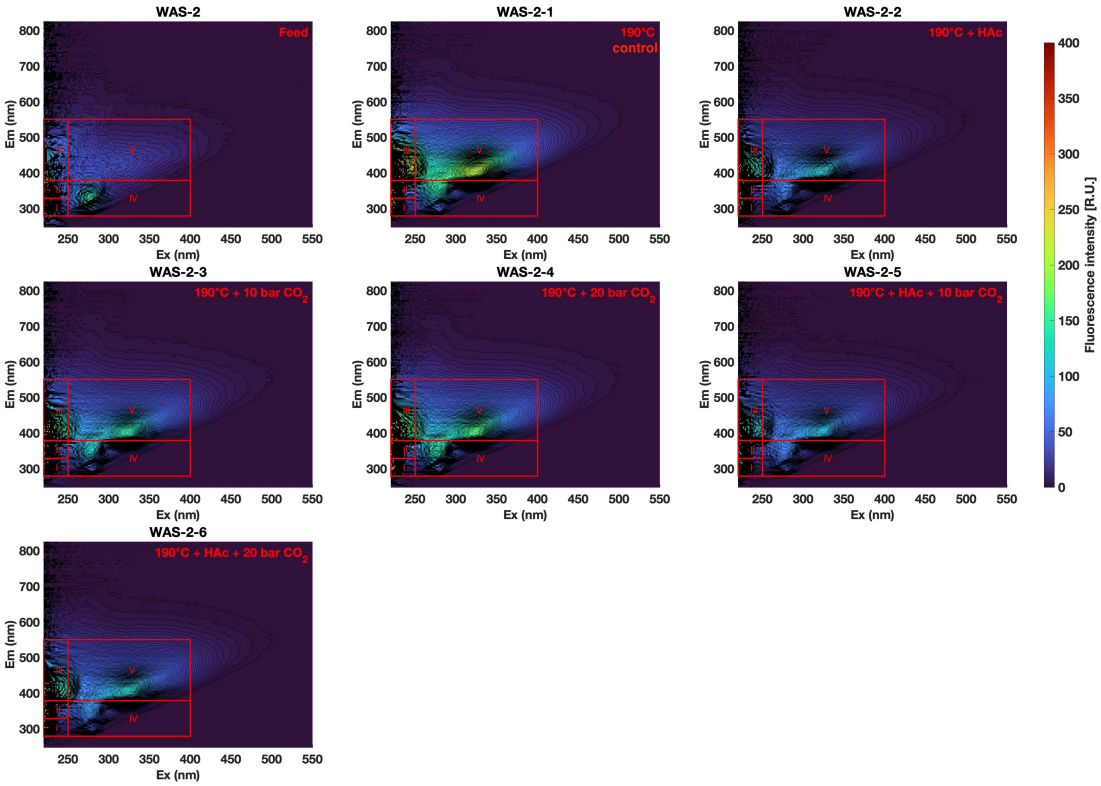

Figure D.4: EEM fluorescence spectra contour of WAS-2 subjecting to thermal hydrolysis with different acidic pretreatments. Horizontal and vertical lines divide EEM spectra into five regions (I-V). Normalised to 1 g DOC/L.

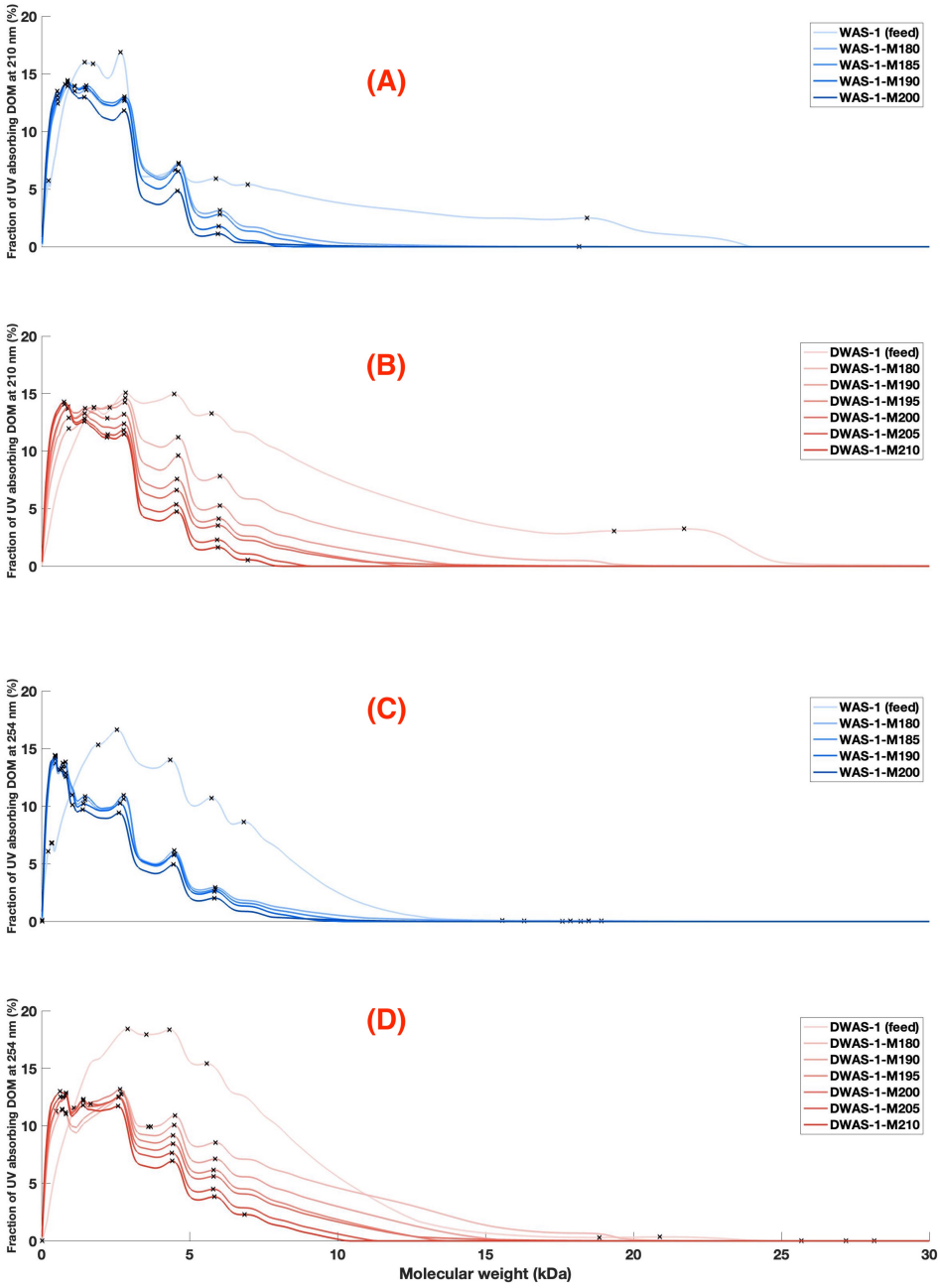

Figure D.5: HPSEC chromatograms with UV absorbance detection at 210 (A and B) and 254 nm (C and D) for WAS-1 and DWAS-1 subjecting to TH at different reaction temperatures.

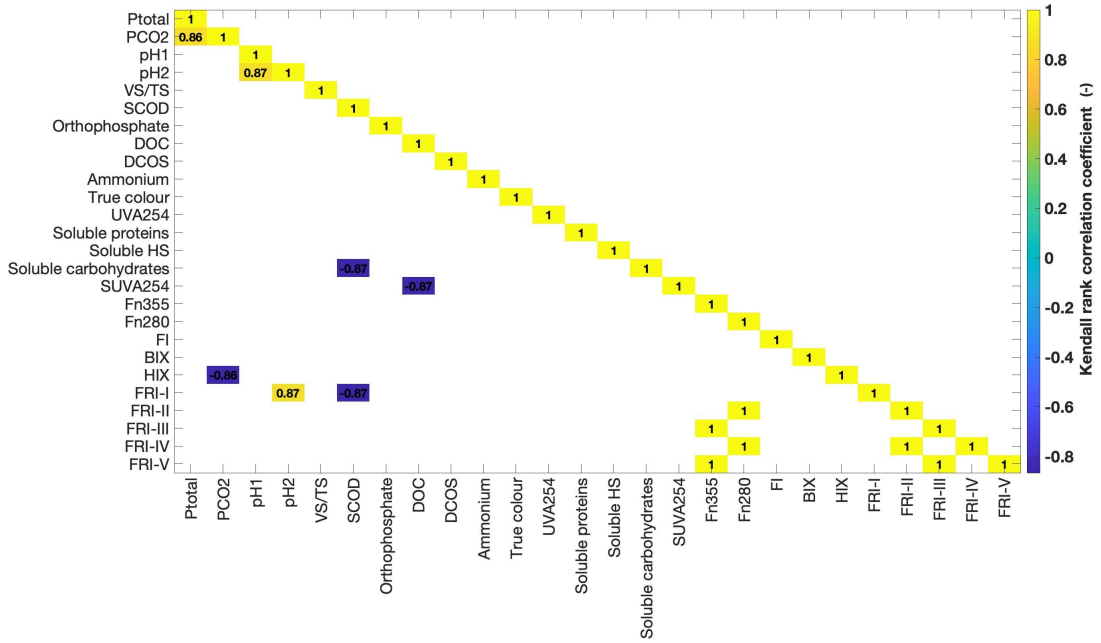

Figure D.6: Heatmap of Kendall rank correlation coefficient for WAS-2 subjecting to TH with different acidic pretreatments. Ptotal is the average total pressure in the reactor headspace during TH. PCO2 is the CO_2 pressure in the reactor headspace (equals the total headspace pressure) before TH. pH1 is the pH value of sample before TH. pH2 is the pH value of sample after TH. Ptotal is the average total pressure in the reactor headspace during TH. PCO2 is the CO_2 pressure in the reactor headspace (equals the total headspace pressure) before TH. pH1 is the pH value of sample before TH. pH2 is the pH value of sample after TH.

Appendix E

PHREEQC Code

```
Database: phreeqc.dat

SOLUTION_MASTER_SPECIES
Acetate Acetate- 1.0 59.05 59.05
Propionate Propionate- 1.0 73.072 73.072
Isobutyrate Isobutyrate- 1.0 87.098 87.098
Butyrate Butyrate- 1.0 87.098 87.098
Isovalerate Isovalerate- 1.0 101.125 101.125
Valerate Valerate- 1.0 101.125 101.125

SOLUTION_SPECIES
Acetate- = Acetate-
        log_k   0
        delta_h 0       kcal
Acetate- + H+ = HAcetate
        log_k   4.76
        delta_h 0       kcal
        -gamma  0       0.06
Propionate- = Propionate-
        log_k 0
H+ + Propionate- = H(Propionate)
        log_k   4.874
        delta_h 0.66    kJ
        -gamma  0       0
Isobutyrate- = Isobutyrate-
        log_k 0
H+ + Isobutyrate- = H(Isobutyrate)
        log_k   4.849
        delta_h 3.2217  kJ
        -gamma  0       0
Butyrate- = Butyrate-
        log_k 0
H+ + Butyrate- = H(Butyrate)
        log_k   4.819
        delta_h 2.8     kJ
        -gamma  0       0
Isovalerate- = Isovalerate-
        log_k 0
H+ + Isovalerate- = H(Isovalerate)
        log_k   4.781
```

```
        delta_h 4.5606   kJ
        -gamma  0        0
Valerate- = Valerate-
        log_k 0
H+ + Valerate- = H(Valerate)
        log_k   4.843
        delta_h 2.887    kJ
        -gamma  0        0
END

Solution 1 WAS-2
-units mg/l
-pH     6.266
-temperature 20.0
N(-3) 179
P       480
Alkalinity 3586.8 as HCO3-
Acetate 61.31422
Propionate 68.84343333
Isobutyrate     14.83258
Butyrate 4.740266667
Isovalerate     41.89739333
Valerate 5.449306667
END

# 20 % (v/v) HAc solution
Solution 2
-units mg/l
-pH     1.77
-temperature 20.0
Acetate 199666.8948
End

# HAc addition
MIX 1
        1       0.919
        2       0.081
SAVE Solution 3
END

# Define the reactor headspace before TH
GAS_PHASE 1 # 10 bar CO2 in headspace before TH
-fixed_volume
-pressure 20
-volume 1.1
-temperature 20.0
CO2(g) 10
H2O(g) 0.0
END

GAS_PHASE 2 #20 bar CO2 in headspace before TH
```

```
-fixed_volume
-pressure 20
-volume 1.1
-temperature 20.0
CO2(g) 20
H2O(g) 0.0
END

GAS_PHASE 3 # No CO2 pressurisation
-fixed_volume
-pressure 1
-volume 1.1
-temperature 20.0
CO2(g)   0.0004
O2(g)    0.209
N2(g)    0.786
H2O(g)   0.005
END

# Cooling at standard atmosphere
GAS_PHASE 4 # Standard atmospheric condition
-fixed_pressure
-pressure 1
-temperature 20.0
CO2(g)   0.0004
O2(g)    0.209
N2(g)    0.786
H2O(g)   0.005
END

Use Solution 1 # or Use Solution 3
EQUILIBRIUM_PHASES
CO2(g) 0.994 # or CO2(g) 1.295
SAVE Solution 4
END

USE solution 4
USE gas_phase 1 # or USE gas_phase 2
REACTION_TEMPERATURE 1 # Thermal hydrolysis
190
INCREMENTAL_REACTIONS True
SAVE Solution 5
END

USE solution 5
USE gas_phase 4
REACTION_TEMPERATURE 1 # Cooling
20
INCREMENTAL_REACTIONS True
SAVE Solution 6
END
```